FINAL REPORT

Synergistic Reductive Dechlorination of 1,1,1-Trichloroethane and Trichloroethene and Aerobic Biodegradation of 1,4-Dioxane - Phase II

SERDP Project ER-2721

MARCH 2021

Bruce Rittmann
Rosa Krajmalnik-Brown
Chen Zhou
Arizona State University

David Friese
APT Water, LLC

Youneng Tang
Florida State University

Distribution Statement A
This document has been cleared for public release

SERDP
DOD ▪ EPA ▪ DOE

This report was prepared under contract to the Department of Defense Strategic Environmental Research and Development Program (SERDP). The publication of this report does not indicate endorsement by the Department of Defense, nor should the contents be construed as reflecting the official policy or position of the Department of Defense. Reference herein to any specific commercial product, process, or service by trade name, trademark, manufacturer, or otherwise, does not necessarily constitute or imply its endorsement, recommendation, or favoring by the Department of Defense.

REPORT DOCUMENTATION PAGE

Form Approved
OMB No. 0704-0188

Public reporting burden for this collection of information is estimated to average 1 hour per response, including the time for reviewing instructions, searching existing data sources, gathering and maintaining the data needed, and completing and reviewing this collection of information. Send comments regarding this burden estimate or any other aspect of this collection of information, including suggestions for reducing this burden to Department of Defense, Washington Headquarters Services, Directorate for Information Operations and Reports (0704-0188), 1215 Jefferson Davis Highway, Suite 1204, Arlington, VA 22202-4302. Respondents should be aware that notwithstanding any other provision of law, no person shall be subject to any penalty for failing to comply with a collection of information if it does not display a currently valid OMB control number. **PLEASE DO NOT RETURN YOUR FORM TO THE ABOVE ADDRESS.**

1. REPORT DATE *(DD-MM-YYYY)*	**2. REPORT TYPE**	**3. DATES COVERED** *(From - To)*
01-08-2022	SERDP Final Report	05-04-2017 – 31-05-2019

4. TITLE AND SUBTITLE
Synergistic Reductive Dechlorination of 1,1,1-Trichloroethane and Trichloroethene and and Aerobic Biodegradation of 1,4-Dioxane - Phase II

5a. CONTRACT NUMBER
W912HQ-17-C-0013

5b. GRANT NUMBER
N/A

5c. PROGRAM ELEMENT NUMBER

6. AUTHOR(S)

Bruce Rittmann, Rosa Krajmalnik-Brown, Chen Zhou: Arizona State University

David Friese: APT Water, LLC

Youneng Tang: Florida State University

5d. PROJECT NUMBER
ER-2721; W74RDV63282715

5e. TASK NUMBER
N/A

5f. WORK UNIT NUMBER
001, 002, 003

7. PERFORMING ORGANIZATION NAME(S) AND ADDRESS(ES)
Arizona State University
660 Mill Ave., Suite 312
Tempe, AZ 84281-3679

Florida State University
874 Traditions Way, Third Floor
Tallahassee, FL 32306-4166

Aptwater, Inc.
1921 Arena Blvd.
Sacramento, CA 95834-3721

8. PERFORMING ORGANIZATION REPORT NUMBER
AWD00031373, GR15155

9. SPONSORING / MONITORING AGENCY NAME(S) AND ADDRESS(ES)
Strategic Environmental Research and Development Program
USACE Humphrey Engr. Ctr Spt Activity
7701 Telegraph Road
Alexandria, VA 22315-3860

10. SPONSOR/MONITOR'S ACRONYM(S)
SERDP

11. SPONSOR/MONITOR'S REPORT NUMBER(S) ER-2721

12. DISTRIBUTION / AVAILABILITY STATEMENT
Open to the public

13. SUPPLEMENTARY NOTES

14. ABSTRACT

1,4-dioxane (1,4-D) is frequently detected as a co-contaminant with chlorinated solvents because of its widespread use as a stabilizer in trichloroethane (TCA) formulations. Phase I of this limited-scope project showed that a H2-based membrane palladium-film reactor (H2-MPfR) converted 1,1,1-trichloroethane (TCA) and trichloroethene (TCE) to ethane by reductive dechlorination. The ethane was then used as a primary substrate to drive biodegradation of 1,4-D in an a O2-based membrane biofilm reactor (O2-MBfR). This report addresses Phase II, which focused on the O2-MBfR.

15. SUBJECT TERMS
Reductive dechlorination of trichloroethane and trichloroethene, mono-oxygenation of 1,4-dioxane, hydrogen-based palladium-film reactor, oxygen-based membrane biofilm reactor

16. SECURITY CLASSIFICATION OF:			**17. LIMITATION OF ABSTRACT**	**18. NUMBER OF PAGES**	**19a. NAME OF RESPONSIBLE PERSON**
a. REPORT	**b. ABSTRACT**	**c. THIS PAGE**			Bruce Rittmann, PhD
UCLASS	UNCLASS	UNCLASS	UNCLASS	99	**19b. TELEPHONE NUMBER** *(include area code)* (480)727-0434

Abstract

Introduction: 1,4-dioxane (1,4-D) is frequently detected as a co-contaminant with chlorinated solvents because of its widespread use as a stabilizer in trichloroethane (TCA) formulations. Phase I of this limited-scope project showed that a H_2-based membrane palladium-film reactor (H_2-MPfR) converted 1,1,1-trichloroethane (TCA) and trichloroethene (TCE) to ethane by reductive dechlorination. The ethane was then used as a primary substrate to drive biodegradation of 1,4-D in an a O_2-based membrane biofilm reactor (O_2-MBfR). This report addresses Phase II, which focused on the O_2-MBfR.

Technical Approach: The specific objectives of Phase II were to: 1) determine the minimum ethane concentration that supports sustained 1,4-dioxane biodegradation and whether that concentration is consistent with environmentally relevant 1,4-D and ethane levels; 2) determine if the minimum ethane concentration is culture-dependent or universal; 3) determine which bacteria are responsible for 1,4-D degradation when using ethane as the primary substrate; 4) use the mathematical model developed in Phase I to interpret the performance of the O_2-MBfR in terms of fundamental principles of microbial ecology and kinetics; and 5) estimate the cost of the O_2-MBfR for reliable operating conditions. The study covered two experimental parts, two modeling simulations, and cost analysis. The first experimental part involved operating four O_2-based MBfRs to assess their capability for long-term removal of 1,4-D, the required ethane input to sustain good removal of 1,4-D, and the microbial ecology of the biofilms. The second experimental part involved batch experiments to quantify the kinetics associated with ethane and 1,4-D biodegradation. One modeling component was directed towards interpreting the batch experiments in terms of quantifying the stoichiometric and kinetic parameters for ethane and 1,4-D biodegradation. The estimated parameters were then used to simulate and interpret the biodegradation of ethane and 1,4-D in the O_2-based MBfR using a biofilm model. The cost analysis was based on the experimental results, along with commercial experience with the MBfR.

Results: The continuous MBfR studies showed that 1,4-D could be biodegraded to below its detection limit (0.5 μg/L) in O_2-MBfRs as long as sufficient ethane was provided a the primary substrate: a ethane:1,4-D mole ratio of ~ 300:1. The experimental results suggest that a two-stage MBfR may be the best strategy to remove 1,4-D from 100 μg/L to < 0.5 μg/L. Analyses of the microbial-community structures showed that diverse bacteria contributed to the biodegradation of ethane and 1,4-D; key genera were *Pseudonocardia, Mycobacterium*, and *Rhodococcus*. The kinetics model clearly captured all major trends for the concentrations of 1,4-D, ethane, oxygen, and biomass in the batch experiments, and the MBfR model, using those parameters, gave simulations consistent with the experimental values in terms of the 1,4-D removal and ethane:1,4-D mole ratios.

To ensure that the platform performs reliably and cost-effectively at the pilot or field scale, research is needed to define the kinetic and stoichiometry parameters for microbial communities capable of biodegrading the low ethane and 1,4-D concentrations relevant to the O_2-MBfR. Those refined parameter will make it possible to predict optimum loading rates to take the 1,4-D concentration to <0.5 μg/L. Essential will be future experiments using actual contaminated groundwater and testing the two-stage platform at the optimum operating conditions at pilot scale.

Benefits: This research contributes to fundamental understanding of the factors controlling biodegradation of 1,4-D and ethane. It also lays the foundation for developing a reliable and cost-effective platform for treating 1,4-D, which is of intense interest to the Department of Defense.

Table of Contents

Abstract ii

Table of Contents iii

List of Tables v

List of Figures vi

List of Appendices vii

List of Acronyms viii

Keywords xi

Acknowledgements xii

Executive Summary 1

1. Objectives 11

2. Background 12

2.1. 1,4-Dioxane contamination 12

2.2. 1,4-Dioxane treatment methods 12

2.3. The Membrane Biofilm Reactor (MBfR) 13

2.4. Modeling 1,4-dioxane biodegradation 13

2.5. Overview of the Phase II Project 13

3. Materials and Methods 15

3.1. Tasks 1 and 2: Biodegradation of 1,4-dioxane in the O_2-based MBfRs 15

3.2. Task 3: Microbial community analysis 16

3.3. Task 4: Experiments and modeling of 1,4-dioxane and ethane biodegradation kinetics 18

3.3.1. Kinetic experiments of 1,4-dioxane and ethane biodegradation 18

3.3.2. Modeling the batch experiments 19

3.3.3. Modeling 1,4-dioxane and ethane biodegradation in the O_2-MBfR 21

3.4. Task 5: Cost analysis 25

4. Results and Discussion 26

4.1. Task 1: Biodegradation of 1,4-D in the O_2-based MBfRs inoculated with a microbial consortium ("WT") from ASU 26

4.2. Task 2: Biodegradation of 1,4-dioxane in the O_2-based MBfRs inoculated with a microbial consortium ("GF") from FSU 31

4.3. Task 3: Microbial community analysis 35

4.3.1. Microbial community structure of the ASU O_2-MBfR biofilms 35

4.3.2. Microbial community structure of the FSU O_2-MBfR biofilms 36

4.3.3. Oxygenase genes in the ASU O_2-MBfR biofilms 40

4.4. Task 4: Modeling evaluation of 1,4-dioxane removal 45

4.4.1. Kinetics of 1,4-dioxane and ethane biodegradation 45

4.4.2. Modeling of ethane and 1,4-dioxane biodegradation in the O_2-MBfR 55

4.5. Task 5: Cost analysis 61

5. Implications for Future Research and Benefits 64

5.1. Minimum required ethane concentrations and their availability at the contaminated sites 64

5.2. Biodegradation kinetics summary and implications for future research 66

5.3. Microbial-community summary and its implications for future research 66

5.4. Cost summary and implications for future research 67

5.5. Summary of future research needs 67

5.6. Future research plan 68

Literature Cited 69

Appendices 77

List of Tables

Table 1: Experimental setup for ethane and 1,4-dioxane kinetic parameter estimation 18

Table 2: Experimental setup for ethane and 1,4-dioxane model evaluation 18

Table 3: Processes and rate matrices for solid biomass species and dissolved chemical species 24

Table 4: Summary of the operating conditions and steady-state results for the O_2-MBfRs at ASU 29

Table 5: Summary of the operating conditions and steady-state results for the O_2-MBfRs at FSU 32

Table 6: Relative abundance of genes encoding functional monooxygenase for 1,4-dioxane co-oxidation of ASU MBfR1 (left) and MBfR2 (right) 42

Table 7: Pearson correlation and 1-tailed significance among substrates fluxes, dominant genera, and monooxygenase-gene relative abundance 44

Table 8: Experimental conditions for the first set of 1,4-D kinetics batch tests 45

Table 9: Experimental setup for the second set of 1,4-dioxane kinetics batch tests 47

Table 10: Best-fit kinetic parameters for degradation of 1,4-dioxane and ethane 50

Table 11: The mean sum of the squares of the relative residuals for the model results and the experimental values 51

Table 12: Summary of simulated performance of the O_2-based MBfRs for the startup and testing stages 56

Table 13: Estimated Capital and Operating Expense for a two-stage O_2-Based MBfR (100 gpm flow, 100 µg 1,4-D/L, 19.9 kg 1,4-dioxane/yr) for the "Optimum Experimental Case" 62

Table 14: Estimated Capital and Operating Expense for a two-stage O_2-Based MBfR (100 gpm flow, 19.9 kg 1,4-dioxane/yr) for the Optimistic Case 63

Table 15: Suggested minimum ethane concentrations for removing various concentrations of 1,4-dioxane in exemplary scenarios. 1 mg/L of ethane = 3.7 mg COD/L. 66

List of Figures

Figure 1: Schematic of the O_2-MBfR (from Luo et al. (2021)) 15

Figure 2: Model components and their interactions for biodegradation of 1,4-D using ethane as the primary substrate in the O_2-MBfR. Note: Descriptions of the parameters used in the figure are provided in Appendix Table A2. 22

Figure 3: The influent (closed circles) and effluent (open circles) concentrations of 1,4-D in the O_2-based MBfRs operated at ASU. The A and B graphs present the data of the separated O_2-MBfR1 and O_2-MBfR2, respectively. The red arrows highlight the time points for re-inoculation and the green arrows the times for biofilm sample collection. The vertical dashed lines indicate the changes of operating stages. The ratio are the ethane:1,4-D (E:D) mole ratios in the influent. 28

Figure 4: Ethane and 1,4-dioxane concentrations in the influent and effluent of the MBfR3 and MBfR4 at FSU. A biomass-enrichment stage of 70 days preceded the startup stage. E:D is the influent ethane:1,4-D mole ratio. Biofilm samples were taken when the MBfRs reached steady states, which are indicated by the upward green arrows. 34

Figure 5: The relative abundances of sequences at the genus level in the biofilms in MBfR1 and MBfR2 at ASU (A) and MBfR3 and MBfR4 at FSU (B). Genera known to biodegrade 1,4-D and ethane are high-lighted in red and blue, respectively. "Others" are sum of species that had relative sequence abundance <1%. 39

Figure 6: Principal component analysis among substrates flux, dominant genera, and the relative abundances of monooxygenase genes. Blue dots represent the flux of ethane and 1,4-D; yellow squares represent the relative abundances of three genera; and green triangles represent the relative-abundance of genes encoding different monooxygenases. 43

Figure 7: Results for the first set of kinetics batch tests with different initial ethane to 1,4-D ratios. 46

Figure 8: Results for the second set of 1,4-dioxane and ethane batch tests with different initial 1,4-dioxane and ethane concentrations. 48

Figure 9: Comparison of modeling simulations and experimentally measured results for 1,4-D and ethane in kinetic batch experiments A – H. The concentrations of ethane and oxygen shown in the graphs are dissolved concentrations. Simulation use the best-fit parameters in Table 10. 53

Figure 10: Model evaluation for 1,4-D and ethane kinetics using experiments D, I, and J, which were not used for parameter fitting. 54

Figure 11: Biofilm thickness during the startup and testing stages of the O_2-MBfRs1&3 and MBfRs2&4. Startup, stage I, stage II, stage IV, and stage were operated by both MBfRs at ASU and FSU. Stage III was operated at FSU only while stage V was operated at ASU only. The E:D ratios are ethane: 1,4-D mole ratios. 55

Figure 12: Comparison of the experimental and modeling results for ethane and 1,4-dioxane biodegradation in the O_2-MBfRs1&3 and O_2-MBfRs2&4 57

Figure 13: Simulated fractions of solid (biomass) species within the biofilm at different ethane-to-1,4-D mole ratios 59

Figure 14: Simulated concentration of the soluble species at different ethane-to-1,4-D mole ratios 60

Figure 15: Co-contamination of TCE and 1,4-dioxane in the groundwater. The yellow dashed line highlights the 300:1 mole ratio. The figure was adapted from Anderson et al., (2012). 65

List of Appendices

Table A 1: Parameters used in the kinetics modeling 77

Table A 2: Model inputs used in the O_2-based MBfR modeling 79

Table A 3: Model outputs of the O_2-based MBfR modeling 83

Table A 4: Shallow metagenomic sample information before and after quality control 85

List of Acronyms

1,4-D	1,4-Dioxane
AGMO	Alkylglycerol Monooxygenase
AOPs	Advanced Oxidation Processes
ARoNITE	Autotrophic Reduction of nitrate treatment
ASU	Arizona State University
ATSDR	Agency for Toxic Substances and Disease Registry
BAP	Biomass Associated Products
BWT	Burrows-Wheeler transform
CAR/PDMS	Carboxen/Polydimethylsiloxane
COC	Contaminants Of Concern
COD	Chemical Oxygen Demand
CPM	Counts Per Million
DCA	Dichloroethane
DCE	Dichoroethene
DNA	Deoxyribonucleic Acid
DO	Dissolved Oxygen
DOB	1,4-dioxane-oxidizing bacteria
DoD	Department of Defense
E:D	Ethane to 1,4-Dioxane ratio
EDCOB	Ethane and 1,4-Dioxane-Co-Oxidizing Bacteria
EOB	Ethane-Oxidizing Bacteria
EPA	Environmental Protection Agency

EPS	Extracellular Polymeric Substances
ESTCP	Environmental Security Technology Certification Program
FORTRAN	Formula Translation computer-programming language
FSU	Florida State University
GC/MS	Gas Chromatography/Mass Spectrometry
GC-FID	Gas Chromatography - Flame Ionization Detector
GC-TCD	Gas Chromatography - Thermal Conductivity Detector
GTDB	Genome Taxonomy Database
HRT	Hydraulic Retention Time
IARC	International Agency for Research on Cancer
IB	Inert Biomass
KEGG	Kyoto Encyclopedia of Genes and Genomes
MBfR	Membrane Biofilm Reactor
MCA	Monochloroethane
MCfR	Membrane Catalytic-film Reactor
MMO	Methane Monooxygenase
MPfR	Membrane Palladium-film Reactor
MSRR	Mean Sum of Squares Relative Residual
MTBE	Methyl Tert-Butyl Ether
NDMA	N-nitrosodimethylamine
NGB	Non-oxidizing Group of Bacteria
NMS	Nitrate Mineral Salts
PCA	Principal Component Analysis

PCBs	Polychlorinated Biphenyls
PCR	Polymerase Chain Reaction
PEST	Model-Independent Parameter Estimation
PFCs	Perfluorinated Chemicals
pMMO	Particulate Methane Monooxygenase
PMO	Propane Monooxygenase
QC	Quality Control
SERDP	Strategic Environmental Research and Development Program
SIM	Selected Ion Monitoring
sMMO	Soluble Methane Monooxygenase
SMPOB	Soluble-Microbial-Products-Oxidizing Bacteria
SON	Statement of Need
SPME	Solid-Phase Micro-Extraction
TCA	Trichloroethane
TCE	Trichloroethene
THF	Tetrahydrofuran
TMO	Toluene Monooxygenase
UAP	Utilization Associated Products
VAN	Vanillate Monooxygenase
VC	Vinyl Chloride

Keywords

1,4-Dioxane, ethane, biodegradation, membrane biofilm reactor, kinetics, modeling, microbial ecology

Acknowledgements

The authors gratefully thank the U.S. Department of Defense's Strategic Environmental Research and Development Program (SERDP) for funding the research through Project ER-2721.

Executive Summary

Introduction

Contamination. 1,4-dioxane (1,4-D) is frequently detected as a co-contaminant with chlorinated solvents, primarily because of its widespread use as a stabilizer in trichloroethane (TCA) formulations. Distinct from TCA and trichloroethene (TCE), 1,4-D is miscible in groundwater and does not adsorb strongly to aquifer solids. As an emerging water contaminant, 1,4-D has attracted significant attention in recent years. According to a national survey completed in 2015 by the U.S. EPA, 1,4-D is detected in 21% of the U.S. public water systems and exceeded the 0.35-µg/L reference level (corresponding to a 10^{-6} cancer risk) at 6.9% of these surveyed sites (Dourson et al., 2017; U.S. EPA, 2018). 1,4-D contamination of water at US DoD sites is common.

Biodegradation. The first species shown to biodegrade 1,4-D and grow on it as a sole electron donor and carbon source is *Pseudonocardia dioxanivorans* CB1190 (Mahendra et al., 2007; Parales et al., 1994). Subsequently, He et al. (2017a) summarized 11 types of bacteria capable of metabolizing 1,4-D and 13 types of bacteria capable of "co-metabolizing" 1,4-D by using tetrahydrofuran (THF), toluene, methane, or propane as the primary growth substrates. Another primary substrate for bacteria that biodegrade 1,4-D is ethane (Luo et al., 2021; Xiong et al., 2020). Previous research by our team showed that ethane has advantages over other primary substrates. On the one hand, ethane resulted in faster kinetics for 1,4-D biodegradation than propane (Xiong et al., 2020). On the other hand, ethane can be generated by reductive dechlorination of co-contaminating TCA and TCE (Lien and Zhang, 2007; Luo et al., 2021).

Reactor. The membrane biofilm reactor (MBfR), an emerging technology for water and wastewater treatment, is based on gas-transfer membranes that supply a dissolved gas to a biofilm formed on the membrane's exterior (Rittmann, 2007; Rittmann, 2018). The gaseous substrate moves across the membrane, while the naturally forming biofilm on the outer surface catalyzes desired reactions (Butler and Boltz, 2014; Rittmann, 2018). The MBfR achieves effective delivery of a gaseous substrate and stable retention of slow-growing bacteria. In the context of biodegrading 1,4-D, the delivered gas is oxygen (O_2), which is required for the initial monooxygenase reactions, as well as for aerobic respiration to support microbial synthesis and maintenance. Figure E1 presents a typical schematic of the O_2-MBfR.

Modeling. Several researchers have studied the kinetics of bacteria that biodegrade 1,4-D (Barajas-Rodriguez and Freedman, 2018; Chen et al., 2016; Mahendra and Alvarez-cohen, 2006; Nam et al., 2016; Sei et al., 2013; Yamamoto et al., 2018). However, information on the kinetic properties of ethanotrophs and bacteria that can co-oxidize ethane and 1,4-D are not reported in the literature. The modeling section of this study, therefore, address estimating kinetic and stoichiometric parameters for 1,4-D and ethane biodegradation in metabolic and co-oxidation conditions. The estimated parameters were then used to simulate and interpret the biodegradation of ethane and 1,4-D in the O_2-based MBfR.

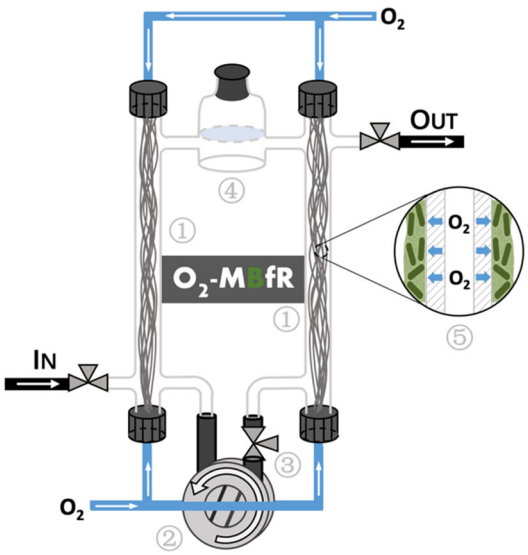

Figure E1: Schematic of the O_2-MBfR (from Luo et al. (2021))

Objectives

The title of the limited scope project is "Synergistic Reductive Dechlorination of 1,1,1-Trichloroethane and Trichloroethene and Aerobic Biodegradation of 1,4-Dioxane". In Phase I of the limited scope project, the research team achieved the following proof of concept: A hydrogen (H_2)-based membrane palladium-film reactor (H_2-MPfR) anaerobically converted 1,1,1-trichloroethane (TCA) and trichloroethylene (TCE) to ethane by reductive dechlorination. The ethane was then utilized as a primary substrate in an O_2-based membrane biofilm reactor (O_2-MBfR) to stimulate 1,4-D-degrading bacteria that removed 1,4-D under aerobic conditions.

From 2019 to 2021, the team carried out the limited-scope project's Phase II, which focused on the second stage of the synergistic platform: Biodegradation of 1,4-D in the O_2-MBfR with ethane as the primary substrate. The overall objective of Phase II was to determine the effects of ethane on 1,4-D biodegradation at environmentally relevant concentrations. Specific objectives of Phase II were to:

1) Determine the minimum ethane concentration that supports sustained 1,4-dioxane biodegradation and whether that concentration is consistent with environmentally relevant 1,4-D and ethane levels.

2) Determine if the minimum ethane concentration is culture-dependent or universal.

3) Determine which bacteria likely are responsible for 1,4-D degradation when using ethane as the primary substrate.

4) Use the model the team developed in Phase I to interpret the performance of the O_2-MBfR in terms of fundamental principles of microbial ecology and kinetics.

5) Estimate the cost of the O_2-MBfR for reliable operating conditions.

Technical Approach

Phase II had two experimental parts. The first experimental part involved operation of O_2-based MBfRs to assess their capability for long-term removal of 1,4-D, the required ethane input

to sustain good removal of 1,4-D, and the microbial ecology of the biofilms. The second experimental part involved batch experiments to develop data to quantify the kinetics associated with ethane and 1,4-D biodegradation.

Phase II also included a modeling part with two components that were linked to each other. One modeling component was directed towards interpreting the batch experiments in terms of quantifying the stoichiometric and kinetic parameters for ethane and 1,4-D biodegradation. The second component applied the modeling principles and parameters from the first component to a biofilm model for the O_2-based MBfR.

Finally, Phase II included a cost analysis that was based on the experimental and modeling results, along with commercial experience with the MBfR.

This report summarizes the methods and results for all aspects of the Phase II project. It also outlines next steps for moving this technology for 1,4-D detoxification forward.

Results and Discussion

Interpretations from the MBfR experiments. Based on long-term continuous operation of four O_2-MBfRs with different influent ethane concentrations over the various stages, we found that an ethane:1,4-D mole ratio of around 300:1 was an optimized condition for input 1,4-D concentrations of 100 µg/L and 10 µg/L. Table E1 lists the details of optimized operating conditions and steady-state results. The findings of the MBfR studies at Arizona State University (ASU) and Florida State University (FSU) suggest that a two-stage MBfR system may be required to remove 1,4-D from 100 µg/L to below the detection limit of 0.5 µg/L, which is close to the health-based reference level of 0.35 µg/L (EPA, 2017). The first stage would remove 1,4-D from 100 µg/L to ~10 µg/L at an ethane to 1,4-dioxane ratio of 300:1. The second stage would remove 1,4-D from ~10 µg/L to < 0.5 µg/L at an ethane:1,4-dioxane ratio of 300:1. With an influent 1,4-D concentration of ~10 µg/L, a one-stage O_2-MBfR could achieve over 95% removal, or effluent 1,4-D ≤ 0.5 µg/L.

Table E1: Operating conditions and steady-state results for the O_2-MBfRs at Arizona State University (ASU) and Florida State University (FSU) having an optimized ethane:1,4-dioxane mole ratio of ~ 300:1.

Optimized conditions		ASU		FSU		Units
		MBfR1	MBfR2	MBfR3	MBfR4	
Operating conditions	HRT	8	4	8	4	hour
	Dioxane influent	100	10	100	10	µg/L
	Dioxane loading	1.4	0.29	1.4	0.29	mg/m^2-day
	Ethane influent	10800	1100	10800	1100	µg/L
	Ethane loading	155	31	155	31	mg/m^2-day
	E/D ratio	300	300	300	300	mole/mole
Steady-state results	Ethane flux	155	31	155	31	mg/m^2-day
	Ethane removal	>99	>99	>99	>99	%
	Dioxane flux	1.0 ± 0.01	0.29	1.3	0.23	mg/m^2-day
	Dioxane removal	73 ± 1.0	>95	89 ± 0.7	79 ± 3.5	%
	Dioxane effluent	26.5 ± 1.0	<0.5	11.0 ± 0.7	2.1 ± 0.4	µg/L

Notes:

- Red Font indicates the concentration is above 0.35 µg/L, a Health Advisory Level by EPA.
- Blue Font indicates the concentration is below our detection limits: 1 µg/L for ethane and 0.5 µg/L for 1,4-D with GC/MS.

Conclusions from the microbial community analysis (ASU). At the genus level, sequences for *Pseudonocardia*, *Mycobacterium, Nocardia*, *Methyloversatilis*, and *Methylibium* were dominant in both ASU MBfRs (MBfRs1&2), and it is likely that the bacteria they represent contributed to the co-oxidation of 1,4-D. The ASU biofilms showed a strong shift from sequences most similar to genera known to do metabolic 1,4-D biodegradation to sequences for genera that carry out co-oxidation. Other less abundant genera in the biofilm, like *Gordonia*, *Bradyrhizobium*, and *Afipia* also have been reported to contribute to 1,4-D co-oxidation (Masuda, 2009; Sei et al., 2013; Tusher et al., 2021). Based on the presence and abundance of monooxygenase-encoding genes, it seems that many monooxygenases -- including toluene monooxygenase (TMO), soluble methane monooxygenase (sMMO), particulate methane monooxygenase (pMMO), and propane monooxygenase (PMO) -- were present in ethane and 1,4-D co-oxidation community. This diversity in monooxygenase genes is consistent with the range of genera and species presented in ethane and 1,4-D co-oxidation when the ethane/1,4-D mole ratio was around 300, which yielded stable and efficient co-oxidation of ethane and 1,4-D.

Conclusions from the microbial community analysis (FSU). The FSU biofilms did not show a clear community shift over time, and the dominant sequences at the genera level for 1,4-D co-oxidation were *Rhodococcus* and *Mycobacterium*. However, the relative abundance of

sequences in the genus *Mycobacterium*, which ranged from 7% to 24% in MBfR3, were smaller than 16% to 38% in MBfR4. Sequences for the less-abundant genera in MBfR3 and MBfR4 were different, which may have been caused by the different influent ethane/1,4-D concentrations and surface loadings. Sequences in the genera *Nocardia, Afipia*, and *Mesorhizobium* were enriched in later stages of MBfR3, while sequences in the genera *Nocardia* and *Gordonia* were enriched in MBfR4. One important finding is that a wide range of bacteria were present in our reactors and most likely capable of co-oxidation of ethane and 1,4-D in the O_2-MBfR.

Comparison between ASU and FSU biofilm communities. Although the 1,4-dioxane removal performances were similar between ASU and FSU teams' O_2-MBfRs, the biofilm communities were dramatically different. The ASU results show a clear transition from abundance of sequences of genera capable of doing metabolic 1,4-D biodegradation to abundance of sequences of genera that are generally active in co-oxidation. In contrast FSU's results did not show a clear community shift, and sequences of genera *Rhodococcus* and *Mycobacterium* were abundant throughout. Taken together, the microbial-community structures support that co-oxidation was important for the biodegradation of 1,4-D, and a wide range of bacteria could contribute to the co-oxidation of ethane and 1,4-D in O_2-MBfRs. The ethane and 1,4-D oxidation kinetics may have caused the community structure differences among the four MBfRs, this requires further research on the specific role of the bacteria sequenced in our O_2-MBfRs.

Kinetics of ethane and 1,4-D co-oxidation. We conducted batch tests with different ethane:1,4-D ratios. We focused on investigating the kinetics of metabolic- versus co-oxidation of 1,4-D. The molar ratio of ethane:1,4-D ranged from 0.1 to 1.0. The enriched culture growing on ethane and 1,4-D was used as the inoculum. Groups A and B, which had 1,4-D as the only substrate with different two initial concentrations, were for 1,4-D metabolism. In the co-oxidation groups C-F, we kept constant the initial 1,4-D concentration (0.1 mM or 8.81 mg/L), but increased the initial ethane concentration from 0.01 to 0.1 mM (0.3 to 3 mg/L). In groups G and H, ethane was the only substrate with two different initial concentrations. Figure E2 shows that all the groups removed over 99% of initial 1,4-D in the first 9 days of batch tests. With relatively lower ethane-to-1,4-D (E/D) ratios in this set of experiments (0.1 to 1), ethane promoted 1,4-D oxidation.

Best-fit kinetic parameters were estimated for 1,4-D and ethane biodegradation. As shown in Figure E2, the model clearly captured all major trends for the concentrations of 1,4-D, ethane, oxygen, and biomass throughout the period of the experiments. Furthermore confirming the validity of the model and parameter is that the parameters for 1,4-D were within the range of values reported in the literature. However, no study has reported the kinetic and stoichiometric parameters for ethane biodegradation. The estimated parameters were evaluated by comparing the model-simulated results with an independent set of experimental values. The parameterized model again captured all the major trends.

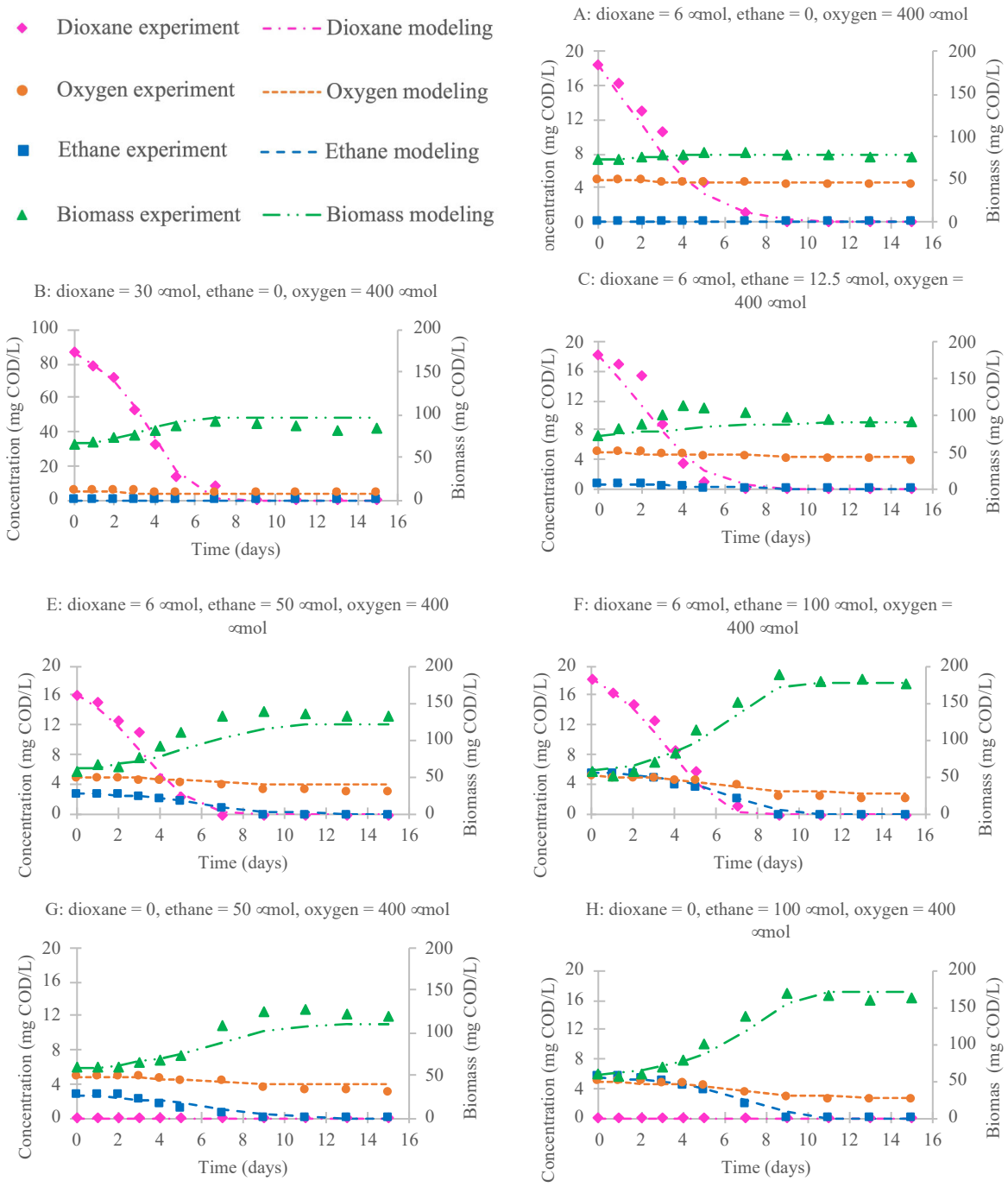

Figure E2: Comparison of modeling and experimentally measured results for selected batch experiments with1,4-D and ethane. The concentrations of ethane and oxygen shown in the graphs are dissolved concentrations. Experiment D was used for model evaluation.

Modeling of ethane and 1,4-D co-oxidation. An MBfR model was used to simulate the operating conditions used in the experiments at ASU and FSU. During the model-testing stages, the 1,4-D influent concentrations were 100 µg/L in MBfRs1&3 and 10 µg/L in MBfRs2&4, while the influent ethane concentrations varied from 0 to 3,600 µg/L. Hydraulic retention times of 8 hours and 4 hours were used for MBfRs1&3 and MBfRs2&4, respectively. The simulated results were consistent with the experimental values in terms of the 1,4-D removal trends at various ethane-to-1,4-D molar ratios; this is shown in Figure E3. The biofilm thickness responded to changes in the influent ethane concentration, particularly for MBfRs1&3, which had the higher influent concentrations of ethane and 1,4-D. Thus, the accumulation of biofilm and the consequent removal capacity for 1,4-D depended on the influent loading of ethane. When the ethane and 1,4-D influent concentrations decreased, the fraction of the active biomass groups decreased, while the fraction of the inert biomass (IB) increased and was almost all of the biomass for no ethane in the influent. These trends reinforce the need to have a sufficient supply of ethane as the primary substrate to support an active biofilm.

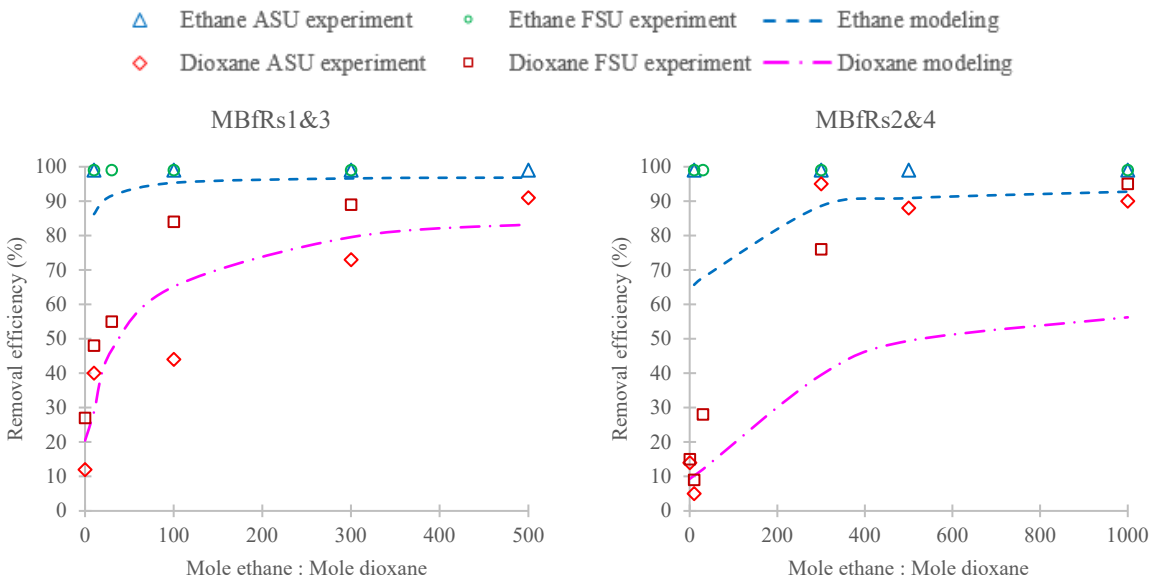

Figure E3: Comparison of the experimental and modeling results for ethane and 1,4-dioxane biodegradation in the O_2-MBfRs1&3 and O_2-MBfRs2&4

Cost analysis. A typical case of 100 gallons/min flow at a 1,4-D concentration of 100 µg/L was chosen as a basis for preliminary design and cost analysis. This flow and concentration provided a 1,4-D loading that was used, along with the experimental MBfR performance data, to determine a system size. At this design loading and applying APTwater's MBfR module containing 170 m^2 membrane area, approximately 226 modules would be required in Stage 1 and 112 modules in Stage 2. The expected capital and operating costs of this system per kg 1,4-D/yr are $181,000 and $11,000 respectively. For an "Optimistic Case" using a five-fold larger design loading, and thus one-fifth required membrane area, approximately 46 full-scale modules would be required in Stage 1 and 22 modules in Stage 2. The estimated capital and operating expenses per kg 1,4-D/yr are $89,200 and $5,400 respectively.

The cost summary was based solely on experimental MBfR performance data corresponding to only one fixed flow rate. Since the flow rate, which is proportional to the 1,4-D loading, is the major factor that determines the costs, finding the maximum flow rate (i.e., maximum loading rate) that gives satisfactory 1,4-D removal is key to reducing costs. Future research should use systematic experiments and modeling to determine a true maximum loading rate.

Implications for Future Research and Benefits

Phase II of the project focused on the 1,4-dioxane-oxidizing O_2-MBfR and determined that the molar ratio of ethane: 1,4-dioxane = ~300:1 is the minimum ratio for removing 1,4-D to below the detection limit of 0.5 µg/L, which is only slightly above the health-based reference level of 0.35 µg/L and below the groundwater and drinking-water guideline levels established by most states. The conclusion is based on >500-day continuous operation of four O_2-MBfRs: Two O_2-MBfRs were operated by the ASU team with a mixed culture and the other two identical O_2-MBfRs were operated by the FSU team with a different mixed culture. One practical implication is that the minimum ethane: 1,4-dioxane ratio does not significantly depend on the inoculum.

The two O_2-MBfRs operated by each team had two different influent 1,4-D concentrations: 100 and 10 µg/L. In the O_2-MBfRs fed with 10 µg/L of 1,4-D, an ethane: 1,4-dioxane ratio of ≥300 was able to remove 1,4-D to below the detection limit in a single-stage reactor. In the O_2-MBfRs fed with 100 µg/L of 1,4-D, an ethane: 1,4-dioxane ratio ≥300 was able to remove 1,4-D to ~10 µg/L in a single-stage reactor. The practical implication is that a two-stage O_2-MBfR may be the best strategy to treat a water containing 100 µg/L of 1,4-D.

We reviewed reported mole ratio range of TCE:1,4-D in the groundwater (Anderson et al., 2012). If TCA also is present, the TCA+TCE:1,4-D ratio will be larger. As shown in Figure E4, the ratio ranges from 1:1 to 1:1000, with many exceeding 1:300. Assuming all TCE is converted to ethane, external ethane addition for these groundwater with high TCE:1,4-dioxane ratios would not be needed, although a preceding MCfR would be required to convert TCE and TCA to ethane. Based on the experimental and modeling results, the suggested ethane concentration to add is 1 mg/L for influent 1,4-dioxane of 10 µg/L or less, and it is computed from the 300:1 mole ratio of higher 1,4-dioxane concentrations: added ethane concentration in mg/L = influent 1,4-dioxane concentration x 0.1. For example, an influent concentration of 100 µg/L requires added ethane of 10 mg/L.

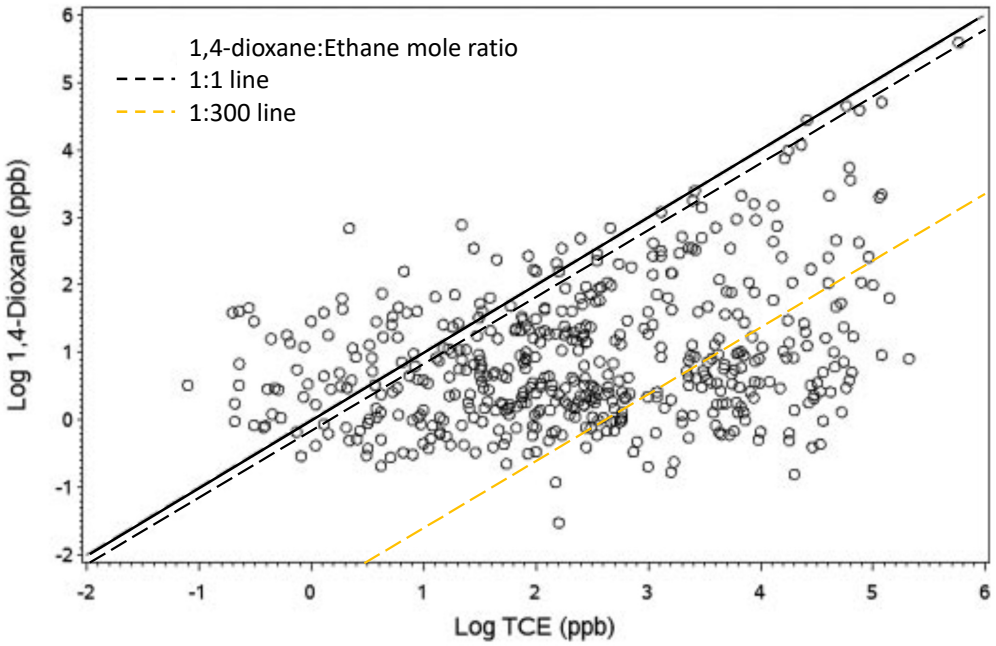

Figure E4: Co-contamination of TCE and 1,4-dioxane in the groundwater. The yellow dashed line highlights the 300:1 mole ratio. Figure adapted from Anderson et al., (2012).

We adapted the MBfR model framework developed in Phase I to simulate the O_2-MBfRs in Phase II. The ethane and 1,4-D degradation kinetic parameters were determined through batch tests combined with kinetics modeling, and then were input into the O_2-MBfR model. The adapted model simulated well all measured trends of 1,4-D and ethane removal in the tested O_2-MBfRs. For example, a higher ethane: 1,4-D ratio led to greater biofilm accumulation and more removal of 1,4-D. However, the model simulations deviated from experimental MBfR results for low influent concentration of 1,4-D, which also corresponded to lower influent concentration of ethane. The model simulated less 1,4-D removal than occurred experimentally in MBfRs2&4. This deviation may be explained by significant differences in the microbial communities between MBfRs2&4, which had low ethane and 1,4-D concentrations, and the batch kinetic experiments based on cultures enriched with and tested with higher concentrations.

We uncovered the following fundamental and practical knowledge gaps that need to be filled to ensure that the platform performs reliably and cost-effectively at the pilot or field scale:

1) The kinetics of 1,4-D and ethane biodegradation at relatively high concentrations were well-determined in Phase II, but our experimental results in the O_2-MBfR, combined with modeling results, suggest that continual enrichment with low concentrations altered the microbial community in ways that affected the kinetic and stoichiometry parameters. Determining the kinetic and stoichiometry parameters for microbial communities truly representative of MBfR biofilms is necessary to ensure that model prediction are relevant and accurate for an O_2-MBfR.

2) Inputting the most reliable parameters into the already developed O_2-MBfR model will allow us to optimize design and operating strategies in advance of a pilot study. For example, we can evaluate how a pilot-scale system will respond to changes in flow rate and influent

concentrations, and then determine the maximum 1,4-D loading rate that gives the effluent of 1,4-D below 0.5 μg/L.

3) Because synthetic groundwater was used in Phases I and II, any impacts of real-world groundwater chemistry is unknown. A platform demonstration with actual contaminated groundwater is needed to ensure the reliable performance of the platform. It is better to test this using a laboratory-scale two-stage platform at the maximum 1,4-D loading rate determined by the model.

4) When the above three knowledge gaps are filled, we will be ready to design, build, and operate a pilot-scale reactor in cooperation with SERDP/ESTCP and APTwater, LLC.

To address the knowledge gaps, we envision a two-phases project. The first phase will focus on addressing the first three knowledge gaps. The following three tasks are proposed to address the three knowledge gaps, respectively.

Task 1 (in the first eight months): Determine the kinetic and stoichiometry parameters for microbial communities truly representative of O_2-MBfR biofilms. The methods are similar to Phase II batch experiments and modeling, but the ethane and 1,4-D concentrations used in the batch tests will be much lower (at μg/L level).

Task 2 (in the second eight months): Use the kinetic and stoichiometry parameters determined in Task 1 to predict (using the existing model of the O_2-MBfR biofilm) the maximum 1,4-D loading rate that gives an effluent 1,4-D concentration of <0.5 μg/L.

Task 3 (in the third eight months): Use the maximum flow rate determined in Task 2 to test the two-stage platform fed with a real groundwater. The two-stage platform includes a H_2-based MPfR to reduce TCE and 1,1,1-TCA to ethane, followed by an O2-based MBfR to co-oxidize ethane and 1,4-D.

The second phase research, lasting for an additional two years, will adapt of the APTwater's H_2-based MBfR modules to become an H_2-MPfR (first stage) and O_2-based MBfR (second stage). The two-stage platform will be evaluated at a field site using at the optimum operating conditions predicted by the model.

1. Objectives

From 2017 to 2018, our research team completed Phase I of a limited-scope project (ER-2721) in response to Strategic Environmental Research and Development Program (SERDP)'s 2017 Statement of Need (SON): "Proposals focused on the common DoD contaminants of concern (COCs) are of most interest. These include: chlorinated and non-chlorinated volatile organic compounds (VOCs), polychlorinated biphenyls (PCBs), metals, perchlorate, 1,4-dioxane (1,4-D), perfluorinated chemicals (PFCs), N-nitrosodimethylamine (NDMA) and munitions constituents." This report is for a follow up second year of limited scope project ER-2721.

The title of the limited scope project is "Synergistic Reductive Dechlorination of 1,1,1-Trichloroethane and Trichloroethene and Aerobic Biodegradation of 1,4-Dioxane." In Phase 1 of the limited scope project, the research team achieved the following proof of concept: A hydrogen (H_2)-based membrane catalyst-film reactor (H_2-MCfR) anaerobically converted 1,1,1-trichloroethane (TCA) and trichloroethylene (TCE) to ethane by reductive dechlorination. The ethane was then utilized as a primary substrate in an O_2-based membrane biofilm reactor (O_2-MBfR) to stimulate 1,4-D-degrading bacteria that removed 1,4-D under aerobic conditions.

From 2019 to 2021, the team carried out the limited-scope project's Phase II, which focused on the second stage of the synergistic platform: Biodegradation of 1,4-D in the O_2-MBfR with ethane as the primary substrate. The overall objective of Phase II is to determine the effects of ethane on 1,4-D biodegradation at environmentally relevant concentrations. Specific objectives of Phase II are to:

1) Determine the minimum ethane concentration that supports sustained 1,4-D biodegradation and whether that concentration is consistent with environmentally relevant 1,4-D and ethane levels.

2) Determine if the minimum ethane concentration is culture-dependent or universal.

3) Determine which bacteria likely are responsible for 1,4-D degradation when using ethane as the primary substrate.

4) Use the model the team developed in Phase I to interpret the performance of the O_2-MBfR in terms of fundamental principles of microbial ecology and kinetics.

5) Estimate the cost of the O_2-MBfR for reliable operating conditions.

Achieving these specific objectives is essential to 1) uncovering the fundamentals of ethane-enhanced 1,4-D biodegradation and 2) further testing of the two-stage synergistic with real-world groundwater. Both Phases of this project meet the ultimate goal of the SON: "The ultimate goal is to develop methods that can be used in series or in parallel to address the DoD's most commonly found COCs in commingled (or co-existing) plumes. In particular, cost-effective methods are needed to stimulate degradation processes likely to have a positive effect on other processes." This reports summarizes findings from Phase II.

2. Background

2.1. 1,4-Dioxane contamination

1,4-dioxane (1,4-D) is frequently detected as a co-contaminant with chlorinated solvents, primarily because of its widespread use as a stabilizer in trichloroethane (TCA) formulations. Furthermore, trichloroethene (TCE) was used at many of the same industrial sites with TCA, which led to co-contaminations of 1,4-D, TCA, TCE, and their degradation products (e.g., dichoroethene (DCE), dichloroethane (DCA), vinyl chloride (VC), and monochloroethane (MCA)) (Adamson et al., 2015; Anderson et al., 2012; Karges et al., 2018). Distinct from TCA and TCE, 1,4-D is miscible in groundwater and does not adsorb strongly to aquifer solids. Toxicological studies suggest that 1,4-D has carcinogenic potential (Stickney et al., 2003; U.S. EPA, 2018), and 1,4-D is classified as a probable human carcinogen by the U.S. EPA, the International Agency for Research on Cancer (IARC), and the Agency for Toxic Substances and Disease Registry (ATSDR).

As an emerging water contaminant, 1,4-D has attracted significant attention in recent years. According to a national survey completed in 2015 by the U.S. EPA, 1,4-D is detected in 21% of the U.S. public water systems and exceeds the 0.35-μg/L reference level (corresponding to a 10^{-6} cancer risk) at 6.9% of these surveyed sites (Dourson et al., 2017; U.S. EPA, 2018). 1,4-D contamination of water at US DoD sites is common. While the US EPA put 1,4-D in its third unregulated-contaminant monitoring rule, more than 30 states in the US have established guidelines and standards for 1,4-D, some as low as 0.25 μg/L in drinking water and groundwater (Miao et al., 2020; Suthersan et al., 2016).

2.2. 1,4-Dioxane treatment methods

The distinct chemical properties of 1,4-D, such as high solubility and low sorbability, make conventional physiochemical treatment processes, such as activated carbon adsorption and air stripping, ineffective (Scheutz et al., 2011). Advanced oxidation processes (AOPs, e.g., O_3/H_2O_2 and UV/TiO_2) are able to achieve fast removal of 1,4-D, but are hampered by incomplete removal and high cost (Choi et al., 2010; Miao et al., 2020; Suthersan et al., 2016). Compared to the physical and chemical treatment method, biodegradation has the advantages of low cost and potential to have complete mineralization.

Because of its cyclic ether structure, 1,4-D is more stable to biodegradation than most organic compounds (e.g., alcohols, aldehydes, and carboxylic acids). However, 1,4-D can be biodegraded by certain bacterial species. The first species shown to biodegrade 1,4-D and grow on it as a sole electron donor and carbon source is *Pseudonocardia dioxanivorans* CB1190 (Mahendra et al., 2007; Parales et al., 1994). Subsequently, other bacteria were found able to oxidize 1,4-D, e.g., *Acinetobacter baumannii*, *Rhodococcus aetherivorans*, and *Afipia* sp. strain D1 (Huang et al., 2014; Inoue et al., 2016; Isaka et al., 2016). The key common feature for these 1,4-D-biodegrading bacteria is that they utilize a monooxygenase to initiate biodegradation. He et al. (2017a) summarized 11 types of bacteria capable of metabolizing 1,4-D and 13 types of bacteria capable of co-metabolizing 1,4-D by using tetrahydrofuran (THF), toluene, methane, or propane as the primary growth substrates. Barajas-Rodriguez and Freedman (2018) reported a significant difference between metabolic and co-metabolic oxidation with propane as the primary substate when removing a low concentration of 1,4-D. They showed that the half-maximum-rate

coefficients for 1,4-D for the co-metabolic propanotrophs (a mixed enriched culture ENV487) were one-half to one-quarter of those for *Pseudonocardia dioxanivorans* CB1190.

Another primary substrate for bacteria that biodegrade 1,4-D is ethane (Luo et al., 2021; Xiong et al., 2020). Previous research by our team showed that ethane has advantages over other primary substrates. On the one hand, ethane resulted in faster kinetics for 1,4-D biodegradation than propane (Xiong et al., 2020). On the other hand, ethane can be generated by reductive dechlorination of co-contaminating TCA and TCE (Lien and Zhang, 2007; Luo et al., 2021).

2.3. The Membrane Biofilm Reactor (MBfR)

The membrane biofilm reactor (MBfR), an emerging technology for water and wastewater treatment, is based on using gas-transfer membranes that supply a dissolved gas to a biofilm that accumuilated on the membranes' exterior (Rittmann, 2007; Rittmann, 2018). The gaseous substrate moves across the membrane, while the naturally forming biofilm on the outer surface catalyzes desired reactions (Butler and Boltz, 2014; Rittmann, 2018). The MBfR achieves effective delivery of a gaseous substrate and stable retention of slow-growing bacteria. In the context of biodegrading 1,4-D, the delivered gas is oxygen (O_2), which is required for the initial monooxygenase reactions, as well as for aerobic respiration to support microbial synthesis and maintenance.

2.4. Modeling 1,4-dioxane biodegradation

Multispecies one-dimensional biofilm models that are based on the biofilm growth dynamics, microbial kinetics, and conservation principles (Wang and Zhang, 2010) can be utilized to gain insights into how various scenarios and operating conditions affect contaminant-removal performances in MBfRs (Tang et al., 2013a, 2013c, 2012a, 2012b). They are widely used for making qualitative and quantitative interpretations of experimental results and providing theoretical guidance for reactor operation and design (Tang et al., 2013c; Wang and Zhang, 2010). Successful modeling of a biofilm reactor requires selecting appropriate kinetic parameters that incorporate the physical, chemical, and biological processes (Wang and Zhang, 2010; Zhang et al., 2017).

Several researchers have studied the kinetics of bacteria that biodegrade 1,4-D (Barajas-Rodriguez and Freedman, 2018; Chen et al., 2016; Mahendra and Alvarez-cohen, 2006; Nam et al., 2016; Sei et al., 2013; Yamamoto et al., 2018). However, information on the kinetic properties of ethanotrophs and bacteria that can co-oxidize ethane and 1,4-D are not reported in the literature. The modeling section of this study, therefore, address estimating kinetic and stoichiometric parameters for 1,4-D and ethane biodegradation in metabolic and co-oxidation conditions. The estimated parameters are then used to simulate and interpret the biodegradation of ethane and 1,4-D in the O_2-based MBfR.

2.5. Overview of the Phase II Project

This report summarizes the results of Phase 2 of a SERDP seed project (ER-2721). In Phase I, our team documented that a H_2-based membrane palladium-film reactor (MPfR) could

completely reduce TCE and TCA to ethane, an O_2-based MBfR could monooxygenate and mineralize 1,4-D when supplied with sufficient ethane, and the MPfR and MBfR could be linked in series to completely remove TCA, TCE, and 1,4-D. Phase II focuses on the O_2-based MBfR for 1,4-D removal.

Phase II had two experimental parts. The first experimental part involved operation of O_2-based MBfRs to assess their capability for long-term removal of 1,4-D, the required ethane input to sustain good removal of 1,4-D, and the microbial ecology of the biofilms. The second experimental part involved batch experiments to develop data to quantify the kinetics associated with ethane and 1,4-D biodegradation.

Phase II also included a modeling part with two components that were linked to each other. One modeling component was directed towards interpreting the batch experiments in terms of quantifying the stoichiometric and kinetic parameters for ethane and 1,4-D biodegradation. The second component applied the modeling principles and parameters from the first component to a biofilm model for the O_2-based MBfR.

Finally, Phase II included a cost analysis that was based on the experimental and modeling results, along with commercial experience with the MBfR.

This report summarizes the methods and results for all aspects of the Phase II project. It also outlines next steps for moving this technology for 1,4-D detoxification forward.

3. Materials and Methods

3.1. Tasks 1 and 2: Biodegradation of 1,4-dioxane in the O_2-based MBfRs

Figure 1 is a schematic of the bench-scale O_2-MBfR. Continuous-mode biodegradation of 1,4-D was performed in four O_2-based hollow-fiber membrane biofilm reactors (O_2-MBfRs), two at Arizona State University (ASU) and two at Florida State University (FSU). The MBfRs had a total working volume of 90 mL (70-mL medium and 20-mL headspace) and contained two bundles of 32 hollow-fiber membranes (composite gas-transfer membrane, 280 μm OD, 180 μm ID, wall thickness 50 μm, length 26 cm, total surface area 0.0146 m^2; Model MHF 200TL Mitsubishi Rayon Co., Ltd, Tokyo, Japan) in two glass tubes (6-mm internal diameter and 27-cm length). O_2 gas (>99.9%) was supplied to the end of fiber bundles at pressures controlled by a pressure regulator set at 3 psig (1.2 atm absolute pressure).

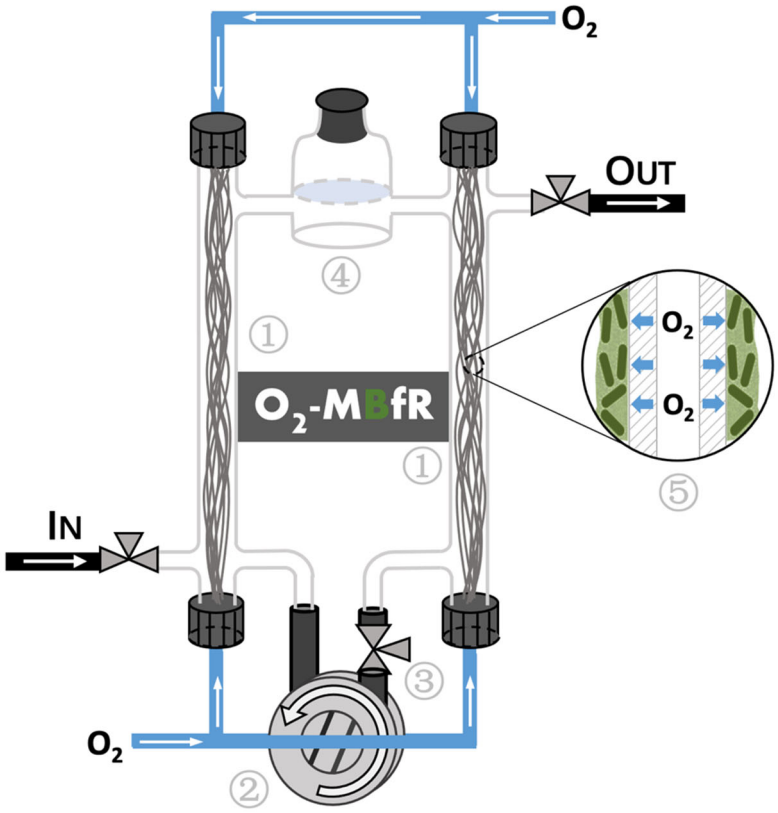

Figure 1: Schematic of the O_2-MBfR (from Luo et al. (2021))

A modified nitrate mineral solution (NMS) was used for O_2-MBfRs, as well as for the kinetic tests in serum bottles. The components of the NMS were: 11.76 KNO_3, 1.28 Na_2SO_4, 0.15 $MgCl_2$, 0.07 $CaCl_2$, 0.08 $FeSO_4$, 3.9 KH_2PO_4, 6.1 K_2HPO_4, 0.002 $ZnCl_2$, 0.002 H_3BO_3, 0.002 $MnCl_2$, 0.004 $CoCl_2$, 0.004 Na_2MoO_4, 0.01 $CuCl_2$, 0.01 $NiCl_2$, and 0.01 Na_2WO_4 (units are mmole/L). The pH of the medium was adjusted to ~7.2 using H_2SO_4 and NaOH. To supply ethane, gas bags containing ethane and nitrogen (N_2) were connected to the bottles containing the synthetic medium

and 1,4-D. The amounts of ethane added were calculated based on Henry's law and the exact gas and liquid volumes (Sander, 2015; Yu et al., 2017).

To measure the ethane and oxygen concentrations during continuous operation of the O_2-MBfR (and also the batch kinetic tests), we collected 100-μL gas sample from the headspace of the reactors and serum bottles. Then, the aqueous-phase ethane and O_2 concentrations were calculated based on Henry's law. The ethane concentrations in the gas samples were measured by using gas chromatography (GC) equipped with flame ionization detection (FID) and a column of "Rt-QSPLOT column 30m×0.53mm×10 mm (Restek®, Bellefonte, PA)." The detection limit of aqueous ethane was ~1 μg/L. The O_2 concentration was measured by using GC equipped with a thermal conductivity detector (TCD) and a column of "1010 plot Capillary column 30m× 0.53mm×10 mm (Carboxen®, Bellefonte, PA)". The detection limit of O_2 by GC-TCD was ~30 μg/L. The chemical oxygen demand (COD) was measured using low range (3-150 mg/L) COD digestion vial (HACH®, US).

The concentrations of 1,4-D were measured using Hewlett-Packard gas chromatography/mass spectrometry (GC/MS) (GC 5890 series II; MSD 5971A) in the selected ion monitoring (SIM) mode. Quantification was based on standard method 6040-E: Solid-Phase Microextraction (SPME) with GC/MS (APHA, 2012). 10-mL liquid samples from the influent and effluent bottles were transferred into 20-ml vials with dioxane-d8 as an internal standard. The vials were then sealed and magnetically stirred at 400 rpm and 65°C for 20 minutes. A SPME-fiber assembly (Carboxen/Polydimethylsiloxane (CAR/PDMS) df 75 μm) was inserted to extract the 1,4-D from the samples. After extraction, the fiber was thermally desorbed for 8 min in the GC/MS with an injector and detector temperatures at 225°C and 280°C, respectively. An initial oven temperature of 40°C was maintained for 2 minutes and then increased at a rate of 15°C/min to 225°C (Xiong et al., 2019). The detection limit of the GC/MS for 1,4-D measurement was 0.5 μg/L.

3.2. Task 3: Microbial community analysis

DNA extraction and sequencing. When the effluent concentrations of all substrates were stable for at least three consecutive sampling dates (standard deviation <5%), O_2-MBfR operation was considered to be at steady state. We collected the biofilm samples of all the O_2-MBfRs at steady state of each stage for the microbial community analysis. We pulled out a bundle of fibers and used sterilized tweezers to grip the biofilm on the fibers. The collected biofilm (about 0.5 mL) was put into sterilized centrifuge tube (two samples for each reactor). After centrifuging the samples at 10,000 rpm for 10 min and removing the supernatant, the biofilm pellet was stored in a -80°C refrigerator. A QIAGEN (USA) DNeasy® PowerBiofilm kit was used to extract the DNA from all biofilm pellets when all the stages were finished. The extracted DNA samples were stored in the -80°C refrigerator before sequencing. All the extracted DNA samples were sent to CosmosID Inc. (MD, US) for shallow metagenomic sequencing. All the samples were quantified using Varioskan and Qubit 4 fluorometer with Qubit™ dsDNA HS Assay Kit (Thermofisher Scientific). DNA libraries were prepared using the Nextera XT DNA Library Preparation Kit. Genomic DNA was fragmented using a proportional amount of Illumina Nextera XT fragmentation enzyme. Combinatory dual indexes were added to each sample followed by 12 cycles of PCR (polymerase chain reaction) to construct libraries. DNA libraries were purified

using AMpure magnetic Beads (Beckman Coulter) and eluted in QIAGEN EB buffer. DNA libraries were prepared using the Illumina Nextera XT library preparation kit. Library quantity was assessed with Qubit (ThermoFisher). Libraries were then sequenced on an Illumina NextSeq 550 2x150bp.

Sequences quality control. After sequencing, all DNA sequencing reads were trimmed to remove low-quality bases (sequence length < 60 bp; quality score < 30) by using the "Trimmomatic" tool (Bolger et al., 2014). The detailed quality of the DNA sequencing reads before and after quality control (QC) for each sample is listed in the Appendices Table A4.

Taxonomic classification for community structure. In order to relate DNA sequences to a specific genus and species, we aligned our DNA reads to the genome taxonomy database (GTDB) to identify bacteria taxonomy and functions (Chaumeil et al., 2020; Parks et al., 2020). The alignment was accomplished by using the "Kaiju" microbial classification engine (Menzel et al., 2016). The "Kaiju" system used the BWT (Burrows-Wheeler transform) change to align all samples' DNA-sequence reads to the database of all complete bacterial genomes (Manzini, 2001). The relative abundance (%) of specific taxa was calculated by reads mapped to specific classification category divided by the total reads (after quality control) of each sample.

Functional genes assignment and abundance. To investigate the relative abundance of functional genes, we used the "UProC" toolbox to classify all samples' DNA sequencing reads based on the KEGG (Kyoto Encyclopedia of Genes and Genomes) database (Meinicke, 2015). The "UProC" toolbox translated the DNA reads into amino acids sequences. Then, we compared the translated reads with oligopeptides at the protein-level and used the "Mosaic Matching Score" to identity the best-matched protein family (Meinicke et al., 2014). All the relative abundance of functional category is presented as counts per million (CPM). CPM reported here are calculated in a similar way to the transcripts per million calculation method introduced by Wagner et al. (2012).

3.3. Task 4: Experiments and modeling of 1,4-dioxane and ethane biodegradation kinetics

3.3.1. Kinetic experiments of 1,4-dioxane and ethane biodegradation

Kinetic batch experiments were performed with different combinations of ethane and 1,4-D; Table 1 summarizes all the experimental conditions. The study focused on investigating the kinetic differences between biodegradation of 1,4-D by bacteria that could utilize only 1,4-D and other bacteria that could utilize ethane and 1,4-D. Thus, the molar ratios of ethane to 1,4-D ranged from 0 to 1.0. An enriched culture grown on ethane and 1,4-D as substrates was used as the inoculum for all the batch experiments. Groups A and B, which had 1,4-D as the only substrate with two initial concentrations, 0.1 mM (8.8 mg/L) and 0.5 mM (44 mg/L), were for 1,4-D-only metabolism. Groups C-F had an initial 1,4-D concentration of 0.1 mM (8.8 mg/L), but increased the initial ethane concentration from 0.01 to 0.1 mM (0.9 to 8.8 mg/L). This set was used to evaluate the kinetics for bacteria that used ethane and 1,4-D together. In groups G and H, ethane was the only substrate, with two different initial concentrations, 0.05 mM and 0.1 mM (4.4 and 8.8 mg/L). Another set of experiment, summarized in Table 2 for experiments D, I, and J, was used for independent evaluation of the estimated parameters from the results of experiments in Table 1.

Table 1: Experimental setup for ethane and 1,4-dioxane kinetic parameter estimation

Exp. No.	Initial biomass (mg COD/L)	Volume of Ethane (mL)	Volume of Oxygen (mL)	1,4-dioxane amount (µmole)	Ethane amount (µmole)	Oxygen amount (µmole)
A	70	0	10	6	0	400
B	70	0	10	30	0	400
C	70	0.313	10	6	10	400
E	70	1.25	10	6	50	400
F	70	2.5	10	6	100	400
G	70	1.25	10	0	50	400
H	70	2.5	10	0	100	400

Note: The molecular weights are 30.07 g/mol for ethane and 88.11 g/mol for 1,4-D. The serum bottles have a medium volume of 100 mL and a headspace of 60 mL.

Table 2: Experimental setup for ethane and 1,4-dioxane model evaluation

Exp. No.	Initial biomass (mg COD/L)	Volume of Ethane (mL)	Volume of Oxygen (mL)	1,4-dioxane amount (µmole)	Ethane amount (µmole)	Oxygen amount (µmole)
D	70	0.625	10	6	30	400
I	30	0	10	30	0	400
J	50	6	100	0	240	4000

Note: The molecular weights are 30.07 g/mol for ethane and 88.11 g/mol for 1,4-D.

3.3.2. Modeling the batch experiments

The following stoichiometric equations for the biodegradation of ethane and 1,4-D were used to determine the amount of oxygen required for complete oxidation of ethane and 1,4-D (Strand et al., 1990):

$$C_2H_6 + 2.1\ O_2 + 0.2\ NO_3^- + \ 0.2\ H^+ = 0.2\ C_5H_7O_2N + \ CO_2 + 2.4\ H_2O$$

$$C_4H_8O_2 + 3\ O_2 + 0.3\ NO_3^- + \ 0.3\ H^+ = 0.3\ C_5H_7O_2N + 2.57CO_2 + 3.14H_2O$$

The total mass of ethane or O_2 in the serum bottles was the sum of their gaseous and liquid phases; this is represented by the mass balance of Equation 1. Because the mass transfer rate of the gases from the headspace to the liquid was much faster than the biodegradation kinetics, we considered the concentrations in the gaseous and liquid phases to be in equilibrium (Yu et al., 2017) according to Equation 2. Replacing S_G of Equation 1 using Equation 2 leads to Equation 3.

$$\boldsymbol{M_T = \rho V_s = \ S_L V_L + \ S_G\, V_G} \tag{1}$$

$$\boldsymbol{K_H = \ \frac{S_L}{S_G}} \tag{2}$$

$$\boldsymbol{M_T = S_L\ \left(V_L + \frac{V_G}{K_H}\right)} \tag{3}$$

The parameters used in Equations 1 – 3 are described in Appendix Table A1.

Five groups of bacteria – namely 1,4-D-oxidizing bacteria (DOB), ethane-oxidizing bacteria (EOB), ethane- and 1,4-dioxane-co-oxidizing bacteria (EDCOB), inert biomass (IB), and bacteria not involved in the oxidation of ethane or 1,4-D (NGB) – are considered to be present in the serum bottles of the experiments. In the model, ethane is oxidized by EOB and EDCOB, while 1,4-D is oxidized by DOB and EDCOB. The four-biomass groups decay to produce inert biomass (IB).

The kinetic equations for the degradation of 1,4-D, ethane, and oxygen are expressed by Equations 4 to 6, respectively. Equation 4 shows the rate of change in the concentration of 1,4-D being oxidized by DOB and EDCOB. Similarly, Equation 5 describes the rate of change in the total mass of ethane by EOB and EDCOB. Equation 6 describes the rate of change in the total mass of oxygen for oxidizing 1,4-D and/or ethane by DOB, EOB, EDCOB. It also includes the oxygen demand for endogenous respiration of the four active biomass groups: DOB, EOB, EDCOB, and NGB.

1,4-Dioxane oxidation by DOB and EDCOB:

$$\boldsymbol{\frac{dS_d}{dt} = -\ X_d\ q_d \left[\frac{S_d}{K_d + S_d}\right]\left[\frac{S_{oL}}{K_o + S_{oL}}\right] - \ X_c\ q_{dc}\left[\frac{S_d}{K_{dc}\left(1+\frac{S_{eL}}{K_{ie}}\right) + S_d}\right]\left[\frac{S_{oL}}{K_o + S_{oL}}\right]} \tag{4}$$

Ethane oxidation by EOB and EDCOB:

$$\frac{dM_{eT}}{dt} = \frac{dS_{eL}}{dt}\left(V_L + \frac{V_G}{K_{He}}\right) = -X_e\ q_e\left[\frac{S_{eL}}{K_e + S_{eL}}\right]\left[\frac{S_{oL}}{K_o + S_{oL}}\right]V_L - X_c\ q_{ec}\left[\frac{S_{eL}}{K_{ec}\left(1+\frac{S_d}{K_{id}}\right)+S_{eL}}\right]\left[\frac{S_{oL}}{K_o+S_{oL}}\right]V_L \quad (5)$$

Oxygen consumption by DOB, EOB, EDCOB, and NGB:

$$\frac{dM_{oT}}{dt} = \frac{dS_{oL}}{dt}\left(V_L + \frac{V_G}{K_{Ho}}\right) = -(1-Y_d)\,X_d\,q_d\left[\frac{S_d}{K_d+S_d}\right]\left[\frac{S_{oL}}{K_o+S_{oL}}\right]V_L - (1-Y_d)\,X_c\,q_{dc}\left[\frac{S_d}{K_{dc}\left(1+\frac{S_{eL}}{K_{ie}}\right)+S_d}\right]\left[\frac{S_{oL}}{K_o+S_{oL}}\right]V_L$$

$$-(1-Y_e)X_e q_e\left[\frac{S_{eL}}{K_e+S_{eL}}\right]\left[\frac{S_{oL}}{K_o+S_{oL}}\right]V_L - (1-Y_e)X_c\,q_{ec}\left[\frac{S_{eL}}{K_{ec}\left(1+\frac{S_d}{K_{id}}\right)+S_{eL}}\right]\left[\frac{S_{oL}}{K_o+S_{oL}}\right]V_L$$

$$-0.8\,(p_d\,X_d + p_e\,X_e + p_c\,X_c + p_n\,X_n)\left[\frac{S_{oL}}{K_o+S_{oL}}\right]V_L \quad (6)$$

The parameters used in Equations 4 – 6 are described in Appendix Table A1.

The rates of change in the biomass concentrations are described using dual-substrate Monod kinetics for growth, electron-acceptor Monod kinetics for endogenous respiration, and first-order losses by decay (Equations 7 to 11). The total biomass concentrations were determined by summing the biomass concentrations of the five groups of bacteria after considering the biomass growth, endogenous respiration, and biomass decay (Equation 12).

$$\frac{dX_d}{dt} = Y_d\ X_d\ q_d\left[\frac{S_d}{K_d+S_d}\right]\left[\frac{S_{oL}}{K_o+S_{oL}}\right] - p_d\,X_d\left[\frac{S_{oL}}{K_o+S_{oL}}\right] - b_d\,X_d \quad (7)$$

$$\frac{dX_e}{dt} = Y_e\,X_e\ q_e\left[\frac{S_{eL}}{K_e+S_{eL}}\right]\left[\frac{S_{oL}}{K_o+S_{oL}}\right] - p_e\,X_e\left[\frac{S_{oL}}{K_o+S_{oL}}\right] - b_e\,X_e \quad (8)$$

$$\frac{dX_c}{dt} = Y_d\,X_c q_{dc}\left[\frac{S_d}{K_{dc}\left(1+\frac{S_{eL}}{K_{ie}}\right)+S_d}\right]\left[\frac{S_{oL}}{K_o+S_{oL}}\right] + Y_e X_c\,q_{ec}\left[\frac{S_{eL}}{K_{ec}\left(1+\frac{S_d}{K_{id}}\right)+S_{eL}}\right]\left[\frac{S_{oL}}{K_o+S_{oL}}\right] - p_c\,X_c\left[\frac{S_{oL}}{K_o+S_{oL}}\right] - b_c X_c \quad (9)$$

$$\frac{dX_n}{dt} = -p_n\,X_n\left[\frac{S_{oL}}{K_o+S_{oL}}\right] - b_n\,X_n \quad (10)$$

$$\frac{dX_b}{dt} = 0.2\,(p_d\,X_d + p_e\,X_e + p_c\,X_c + p_n\,X_n)\left[\frac{S_{oL}}{K_o+S_{oL}}\right] + (b_d\,X_d + b_e X_e + b_c X_c + b_n X_n) \quad (11)$$

$$X = X_d + X_e + X_c + X_n + X_b \quad (12)$$

The parameters used in Equations 7 – 12 are described in Appendix Table A1.

The initially measured concentrations of biomass and various chemicals were used as the initial conditions for Equations 4-12. The parameters for biodegradation -- including Y_d, Y_e, q_d, q_e, q_{dc}, q_{ec}, K_d, K_e, K_{dc}, K_{ec}, K_{id}, K_{ie}, K_o, p_d, p_e, p_c, p_n, b_d, b_e, b_c, b_n, f_d, f_e, f_c, f_n, and f_b -- were determined by best-fitting the experimental and model simulated chemical and biomass concentrations using Equations 4 to 12. The model was coded in FORTRAN, and model-independent parameter estimation (PEST) was used to estimate the model parameters based on the experimental results

(PEST, 2019). The mean sum of squared relative residuals (MSRR) was used to determine the goodness of fit between the model results and all experimentally measured values (Equation 13).

$$\boldsymbol{MSRR} = \frac{1}{N}\left\{\sum_{i=0}^{n}\left[\frac{S_{d,i}^{m} - S_{d,i}^{e}}{S_{d,i}^{e}}\right]^{2} + \sum_{i=0}^{n}\left[\frac{S_{e,i}^{m} - S_{e,i}^{e}}{S_{e,i}^{e}}\right]^{2} + \sum_{i=0}^{n}\left[\frac{S_{o,i}^{m} - S_{o,i}^{e}}{S_{o,i}^{e}}\right]^{2} + \sum_{i=0}^{n}\left[\frac{X_{i}^{m} - X_{i}^{e}}{X_{i}^{e}}\right]^{2}\right\} \quad (13)$$

The parameters used in Equation 13 are described in Appendix Table A1.

The accuracy of the estimated parameters was then evaluated by comparing the simulated results with an independent set of experimental values, i.e., in Table 2.

3.3.3. Modeling 1,4-dioxane and ethane biodegradation in the O_2-MBfR

A one-dimensional model comprised of five dissolved chemical species and six solid biomass species was developed to simulate the biodegradation of 1,4-dioxane and ethane in an O_2-MBfR. The chemical species considered are oxygen gas (O_2), ethane (C_2H_6), 1,4-dioxane ($C_4H_8O_2$), utilization associated products (UAP), and biomass associated products (BAP). The six biomass groups include ethane-oxidizing bacteria (EOB), 1,4-D-oxidizing bacteria (DOB), ethane- and 1,4-D-co-oxidizing bacteria (EDCOB), extracellular polymeric substances (EPS), soluble microbial products oxidizing bacteria (SMPOB), and inert biomass (IB). A conceptual model, summarized in Figure 2, represents the interaction processes of the chemical species and the biomass species in the O_2-MBfR. The biofilm uses ethane (C_2H_6) and 1,4-D ($C_4H_8O_2$) as electron donors and energy and carbon sources and oxygen gas (O_2) as an electron acceptor. Four groups of bacteria -- EOB, DOB, EDCOB, and SMPOB -- are involved in the oxidation/reduction reactions. The figure further illustrates that EOB and EDCOB compete for ethane, DOB and EDCOB compete for 1,4-D, and all the four groups of bacteria compete for the electron acceptor (O_2). Finally, the active biomass that comprise of EOBs, DOBs, EDCOBs, and SMPOBs decay to produce inert biomass (IB), a non-biodegradable biomass.

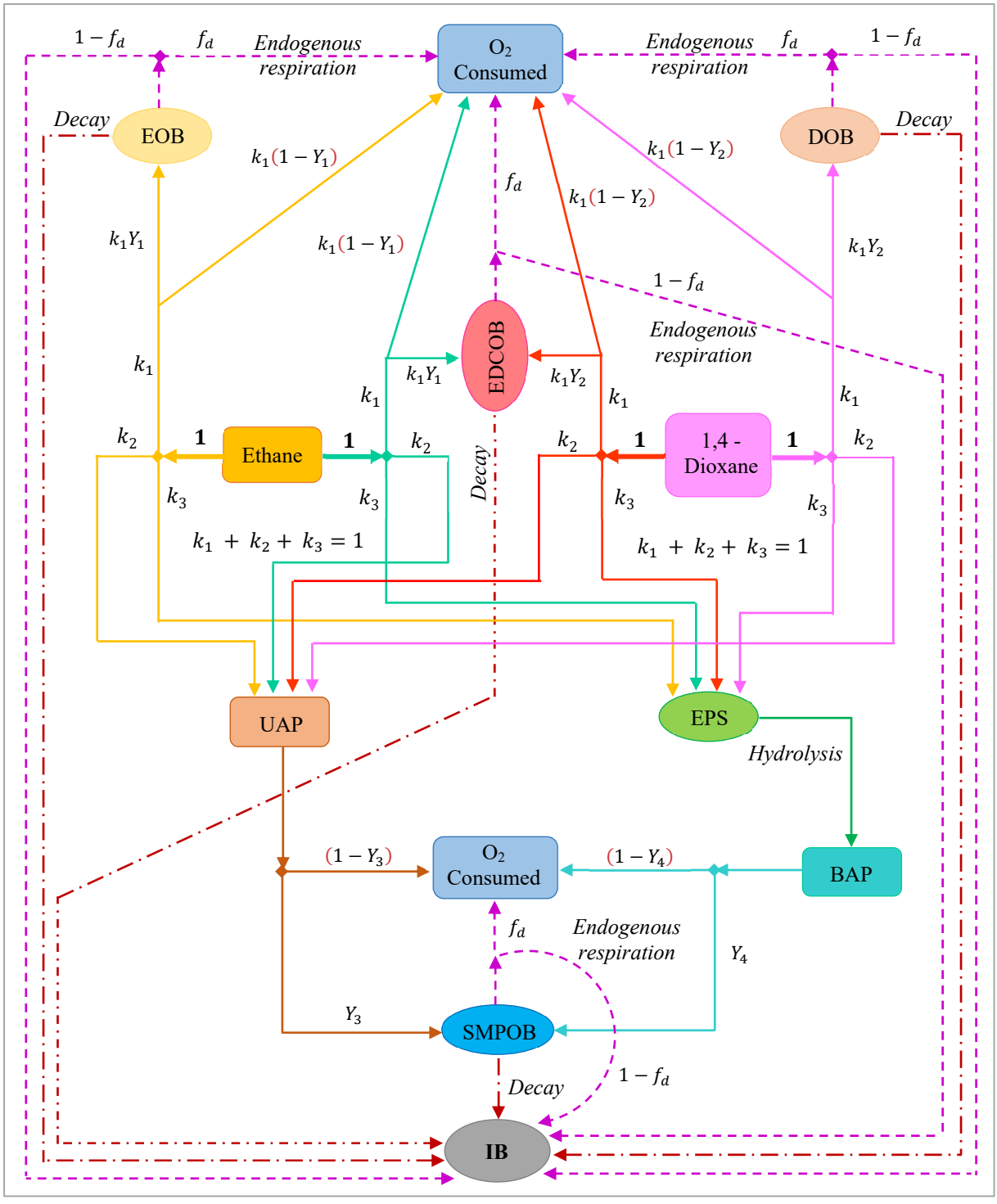

Figure 2: Model components and their interactions for biodegradation of 1,4-D using ethane as the primary substrate in the O_2-MBfR. Note: Descriptions of the parameters used in the figure are provided in Appendix Table A2.

The governing equations for the mass-balance of solid biomass species in the biofilm and the diffusion and reaction of the dissolved chemical species are described in the Phase I final report, ER-2721 (Rittmann et al., 2019). They are also available at Wang et al. (2020), Tang & Valocchi (2013), and Tang, Zhao, et al. (2012a). Calculation of the reaction rates of the dissolved chemical species (R_i) and specific growth rates of the solid biomass species (μ_j) are summarized in Table 3. Model inputs and outputs, including constants and operating parameters of the O_2-based MBfR, are defined in Appendix Tables A2 and A3. The governing equations for the solid biomass species and the dissolved chemical species were solved using numerical methods by discretizing the biofilm into 50 sections. Initial conditions were set by assuming the biofilm thickness (L_f), fraction of solid species (f_j), dissolved species concentration in the biofilm (S_{fi}), and dissolved species concentration in the bulk water (S_{bi}). Using the initial conditions and a time step *dt* of *1 day*, the governing equations were implemented by finite-difference method. The equations were parametrized and programmed using FORTRAN to simulate the O_2-MBfR performance under various operating conditions.

Table 3: Processes and rate matrices for solid biomass species and dissolved chemical species

Process (pr)		*Coefficient of biomass species j in process pr (η_{jpr})*						*Coefficient of chemical species i in process pr (η_{ipr})*					*Conversion rate in process pr (C_{Rpr})*
		EOB (*j=1*)	DOB (*j=2*)	EDCOB (*j=3*)	EPS (*j=4*)	SMPOB (*j=5*)	IB (*j=6*)	O_2 (*i=1*)	Ethane (*i=2*)	1,4-Dioxane (*i=3*)	UAP (*i=4*)	BAP (*i=5*)	
EOB	Growth on ethane *(pr=1)*	k_1Y_1			k_3			$-k_1(1-Y_1)$	-1		k_2		C_{R1}
	Endogenous respiration *(pr=2)*	-1					$(1-f_d)$	$-f_d$					C_{R2}
	Decay *(pr=3)*	-1					1						$b_1f_1X_f$
DOB	Growth on 1,4-dioxane *(pr=4)*		k_1Y_2		k_3			$-k_1(1-Y_2)$		-1	k_2		C_{R4}
	Endogenous respiration *(pr=5)*		-1				$(1-f_d)$	$-f_d$					C_{R5}
	Decay *(pr=6)*		-1				1						$b_2f_2X_f$
EDCOB	Growth on ethane *(pr=7)*			k_1Y_1	k_3			$-k_1(1-Y_1)$	-1		k_2		C_{R7}
	Growth on 1,4-dioxane *(pr=8)*			k_1Y_2	k_3			$-k_1(1-Y_2)$		-1	k_2		C_{R8}
	Endogenous respiration *(pr=9)*			-1			$(1-f_d)$	$-f_d$					C_{R9}
	Decay *(pr=10)*			-1			1						$b_3f_3X_f$
EPS	Hydrolysis *(pr=11)*				-1							1	$K_{hyd}f_4X_f$
SMPOB	Growth on UAP *(pr=12)*					Y_3		$-(1-Y_3)$			-1		C_{R12}
	Growth on BAP *(pr=13)*					Y_4		$-(1-Y_4)$				-1	C_{R13}
	Endogenous respiration *(pr=14)*					-1	$(1-f_d)$	$-f_d$					C_{R14}
	Decay *(pr=15)*					-1	1						$b_5f_5X_f$
Summed conversion rate		Summed specific growth rate of biomass species *j*			$\mu_j = \frac{\sum_{pr}(\eta_{jpr}\, C_{Rpr})}{f_j\, X_f}$			Summed reaction rate of chemical species *i*			$R_i = \sum_{pr}(\eta_{ipr}\, C_{Rpr})$		

$$C_{R1} = \hat{q}_1 f_1 X_f \left[\frac{S_{f1}}{K_{11}+S_{f1}}\right]\left[\frac{S_{f2}}{K_{21}+S_{f2}}\right] \qquad C_{R4} = \hat{q}_4 f_2 X_f \left[\frac{S_{f1}}{K_{14}+S_{f1}}\right]\left[\frac{S_{f3}}{K_{34}+S_{f3}}\right]$$

$$C_{R7} = \hat{q}_7 f_3 X_f \left[\frac{S_{f1}}{K_{17}+S_{f1}}\right]\left[\frac{S_{f2}}{K_{27}\left(1+\frac{S_{f3}}{K_{37i}}\right)+S_{f2}}\right] \qquad C_{R8} = \hat{q}_8 f_3 X_f \left[\frac{S_{f1}}{K_{18}+S_{f1}}\right]\left[\frac{S_{f3}}{K_{38}\left(1+\frac{S_{f2}}{K_{28i}}\right)+S_{f3}}\right]$$

$$C_{R12} = \hat{q}_{12} f_5 X_f \left[\frac{S_{f1}}{K_{1-12}+S_{f1}}\right]\left[\frac{S_{f4}}{K_{4-12}+S_{f4}}\right] \qquad C_{R13} = \hat{q}_{13} f_5 X_f \left[\frac{S_{f1}}{K_{1-13}+S_{f1}}\right]\left[\frac{S_{f5}}{K_{5-13}+S_{f5}}\right]$$

$$C_{R2} = p_1 f_1 X_f \left[\frac{S_{f1}}{K_{12}+S_{f1}}\right] \qquad C_{R5} = p_2 f_2 X_f \left[\frac{S_{f1}}{K_{15}+S_{f1}}\right] \qquad C_{R9} = p_3 f_3 X_f \left[\frac{S_{f1}}{K_{19}+S_{f1}}\right] \qquad C_{R14} = p_5 f_5 X_f \left[\frac{S_{f1}}{K_{1-14}+S_{f1}}\right]$$

Note: $K_{i\text{-}pr}$ represents the half-maximum-rate concentration of species *i* in process *pr*.

3.4. Task 5: Cost analysis

A full-scale MBfR system can be designed by determining the amount of membrane surface area required to achieve the desired contaminant removal. A typical case of 100 gallons/min flow at a 1,4-D concentration of 100 μg/L was chosen as a basis for preliminary design and cost analysis. This flow and concentration provide a 1,4-D loading that can be used, along with the experimental MBfR performance data (i.e., the maximum loading that can still achieve the target removal in each stage) to determine a system size. APTwater, LLC has developed and installed commercial-scale H_2-based MBfRs for nitrate treatment (called ARoNITE, where ARo stands for Autotrophic Reduction of). From this experience, APTwater has programs for equipment sizing and capital and operating cost estimation for the hydrogen-based MBfR systems. These design programs were modified for the use of O_2 in place of H_2 to estimate the capital and operating cost of the required-size O_2-based MBfR.

4. Results and Discussion

4.1. Task 1: Biodegradation of 1,4-D in the O_2-based MBfRs inoculated with a microbial consortium ("WT") from ASU

Table 4 lists the steady-state operation and performance of all the stages for the two O_2-MBfRs operated by ASU. Both reactors were operated in the continuous mode in the initial biofilm-enrichment stage with high substrates concentrations and an HRT of 12 hours. The 1,4-D influent concentration was set as 0.5 mM (44 mg/L), and ethane was at concentration of about 1.2 mM (36 mg/L). Once at least 99% removal of 1,4-D was achieved in both reactors, we lowered the 1,4-D and ethane concentrations.

In the start-up stage, the two O_2-MBfRs were operated in continuous mode with an HRT of 12 hours. The 1,4-D influent concentration was 0.011 mM (1 mg/L), and the ethane concentration was 1.2 mM (36 mg/L). The ethane to 1,4-D mole ratio was about 100.

After start-up, the influent 1,4-D and ethane concentrations for MBfR1 were reduced to 0.1 mg/L and 0.36 mg/L (1.1 μM and 12.0 μM), respectively, in Stage I. The influent 1,4-D and ethane concentrations for MBfR2 were $1/10^{th}$ of those for MBfR1. The HRTs of MBfR1 and MBfR2 were 8 hours and 4 hours, respectively. Figure 3 shows that the 1,4-D removal was initially 94%, but gradually decreased to 40%, reaching steady state after 20 days in MBfR1. In MBfR2, the 1,4-D removal was 90-99% during the beginning 20 days, but then the removal sharply decreased to about 5% and reached steady state for another 20 days as well. The effluent concentrations of ethane were below the detection limit of the GC-FID (1 μg/L) in both MBfRs. These results indicate that the biofilms still were capable of degrading 1,4-D immediately after the sudden drop of surface loading (to $1/10^{th}$ in MBfR1 and $1/100^{th}$ in MBfR2 for dioxane and to $1/67^{th}$ for MBfR1 and $1/335^{th}$ for MBfR2 for ethane), but 1,4-D removal steadily decreased because the decreased supply of the primary electron donor (ethane) led to a steady loss of biomass. This underscores the importance of a sufficient supply of ethane to sustain 1,4-D biodegradation.

In Stage II, influent concentration of ethane was increased to 10 times that of Stage I in both reactors. The effluent 1,4-D concentration of MBfR1 decreased from 60 to about 16 μg/L in the first three weeks, but then it increased again to about 50 μg/L on day 175. For MBfR2, the effluent concentration did not have a significant decrease in stage II. The sharp increase of the effluent 1,4-D concentration in MBfR1 was caused by the physical loss of biomass during biomass collection on Day 130. To accelerate recovery of the biofilm, we re-inoculated both reactors with the enriched culture from the serum bottles on Day 188. After reinoculation, the effluent concentration of 1,4-D decreased, especially in MBR2. In the last month of Stage II, the effluent 1,4-D from MBfR1 and MBfR2 stabilized at 55 μg/L and 1 μg/L (detection limit: 0.5 μg/L), respectively, which corresponds to 44% and 90% removal, respectively.

In Stage III, the mole ratio of ethane to 1,4-D was 300:1 for both MBfRs. After 60-days operation, the 1,4-D removal ratios in MBfR1 and MBfR2 gradually reached steady state, 73 ± 1.0% and > 95%, respectively. The 1,4-D fluxes for the two reactors were 1.0 and 0.29 mg/m^2-day, respectively. In Stage IV, the mole ratio of ethane to 1,4-D was 500:1 for both MBfRs. During the first 30 days of stage IV, the 1,4-D removal ratios in MBfR1 and MBfR2 decreased from 73% and >95% to 60% and 0%, respectively. These losses of 1,4-D concentration were due

to disruption from biofilm sampling, because we had to remove a significant fraction of the biomass for microbial analysis. To speed up recovery of both reactors, we reinoculated 10 mL of the 1,4-D and ethane-enriched culture (with biomass of ~100 mg COD/L). Four months after reinoculation, the removal of 1,4-D in MBfR1 gradually increased from 40% to 91% at steady-state; the removal of 1,4-D in MBfR2 gradually increased from 0% to >94% and reached steady-state on day 500. We collected biofilm samples of MBfR2 on day-505 and observed that the removal decreased to 70% after collection.

In stage V, both reactors were operated for 1,4-D removal with no ethane supply. The effluent 1,4-D concentrations rapidly increased to 94.7 μg/L in MBfR1 and to 9.5 μg/L in MBfR2. The results of these experiments clearly emphasize the importance of ethane as a primary substrate for the biodegradation of 1,4-D.

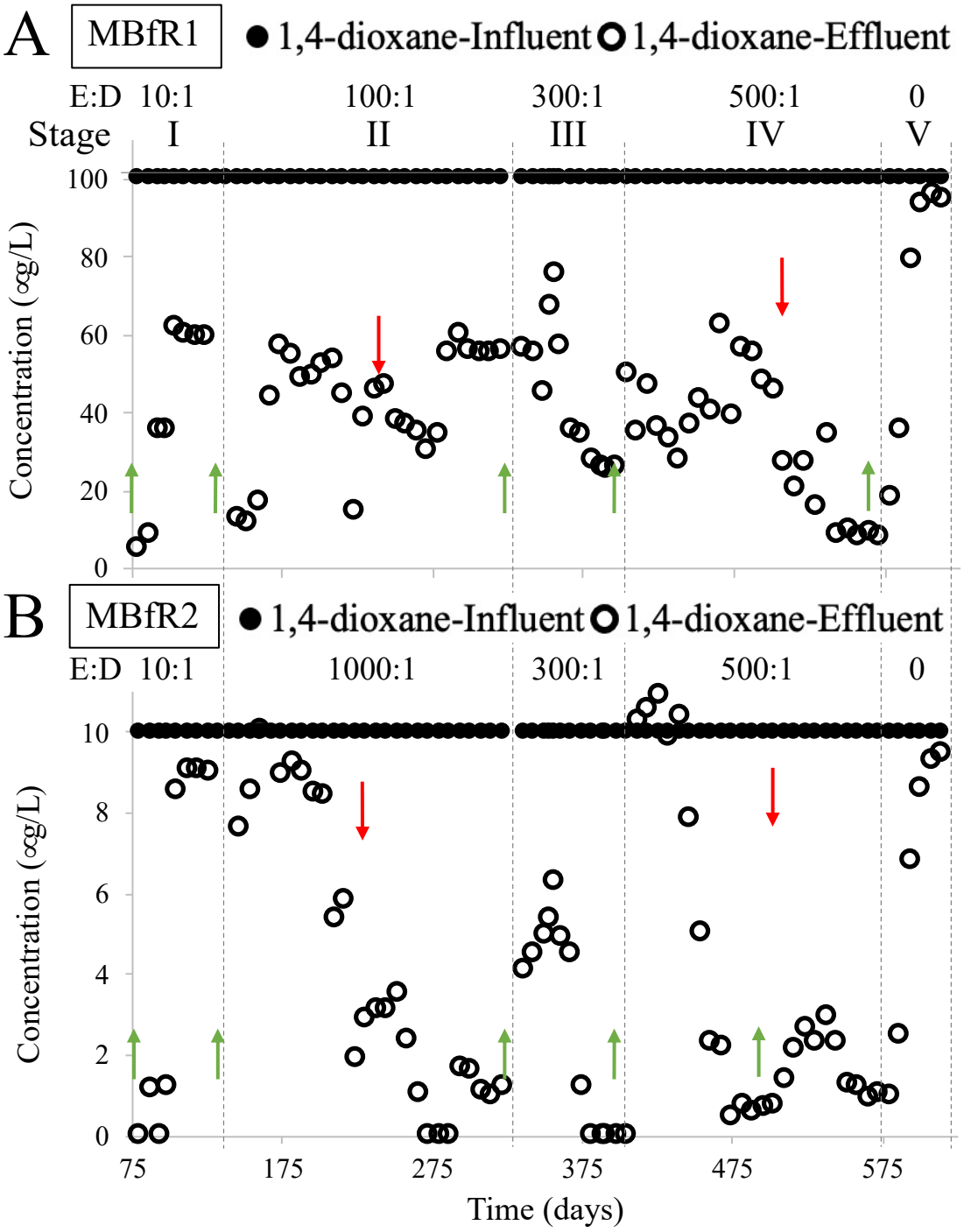

Figure 3: The influent (closed circles) and effluent (open circles) concentrations of 1,4-D in the O_2-based MBfRs operated at ASU. The A and B graphs present the data of the separated O_2-MBfR1 and O_2-MBfR2, respectively. The red arrows highlight the time points for re-inoculation and the green arrows the times for biofilm sample collection. The vertical dashed lines indicate the changes of operating stages. The ratio are the ethane:1,4-D (E:D) mole ratios in the influent.

Table 4: Summary of the operating conditions and steady-state results for the O_2-MBfRs at ASU

Stages		Parameter	MBfR1	MBfR2	Unit
Enrichment	Operational conditions	HRT	12	12	hour
		Dioxane influent	44000	44000	µg/L
		Dioxane loading	421	421	mg/m^2-day
		Ethane influent	36000	36000	µg/L
		Ethane loading	345	345	mg/m^2-day
		E/D ratio	2.4	2.4	mole/mole
	Steady-state results	Ethane flux	345	345	mg/m^2-day
		Ethane removal	>99	>99	%
		Dioxane flux	398 ± 3	398 ± 2	mg/m^2-day
		Dioxane removal	94.5 ± 0.7	94.7 ± 0.5	%
		Dioxane effluent	2400 ± 30	2300 ± 20	µg/L
Start-up	Operational conditions	HRT	12	12	hour
		Dioxane influent	1000	1000	µg/L
		Dioxane loading	10	10	mg/m^2-day
		Ethane influent	36000	36000	µg/L
		Ethane loading	345	345	mg/m^2-day
		E/D ratio	100	100	mole/mole
	Steady-state results	Ethane flux	345	345	mg/m^2-day
		Ethane removal	>99	>99	%
		Dioxane flux	10	10	mg/m^2-day
		Dioxane removal	>99	>99	%
		Dioxane effluent	<10	<10	µg/L
I	Operational conditions	HRT	8	4	hour
		Dioxane influent	100	10	µg/L
		Dioxane loading	1.4	0.29	mg/m^2-day
		Ethane influent	360	36	µg/L
		Ethane loading	5.17	1.03	mg/m^2-day
		E/D ratio	10	10	mole/mole
	Steady-state results	Ethane flux	5.17	1.03	mg/m^2-day
		Ethane removal	>99	>99	%
		Dioxane flux	0.56	0.0145	mg/m^2-day
		Dioxane removal	40 ± 1.3	5 ± 0.4	%
		Dioxane effluent	60.2 ± 1.3	9.05 ± 0.04	µg/L
II	Operational conditions	HRT	8	4	hour
		Dioxane influent	100	10	µg/L
		Dioxane loading	1.4	0.29	mg/m^2-day
		Ethane influent	3600	3600	µg/L
		Ethane loading	51.7	103	mg/m^2-day
		E/D ratio	100	1000	mole/mole
		Ethane flux	51.7	3	mg/m^2-day

Stages		Parameter	MBfR1	MBfR2	Unit
	Steady-state results	Ethane removal	>99	>99	%
		Dioxane flux	0.62	0.29	mg/m^2-day
		Dioxane removal	44 ± 1.6	90 ± 6.3	%
		Dioxane effluent	56.4 ± 2.0	0.81 ± 0.71	µg/L
III	Operational conditions	HRT	8	4	hour
		Dioxane influent	100	10	µg/L
		Dioxane loading	1.4	0.29	mg/m^2-day
		Ethane influent	10800	1100	µg/L
		Ethane loading	155	31	mg/m^2-day
		E/D ratio	300	300	mole/mole
	Steady-state results	Ethane flux	155	31	mg/m^2-day
		Ethane removal	>99	>99	%
		Dioxane flux	1.0 ± 0.01	0.29	mg/m^2-day
		Dioxane removal	73 ± 1.0	>95	%
		Dioxane effluent	26.5 ± 1.0	<0.5	µg/L
IV	Operational conditions	HRT	8	4	hour
		Dioxane influent	100	10	µg/L
		Dioxane loading	1.4	0.29	mg/m^2-day
		Ethane influent	18000	1830	µg/L
		Ethane loading	258	52	mg/m^2-day
		E/D ratio	500	500	mole/mole
	Steady-state results	Ethane flux	258	52	mg/m^2-day
		Ethane removal	>99	>99	%
		Dioxane flux	1.3 ± 0.01	0.26 ± 0.005	mg/m^2-day
		Dioxane removal	91 ± 0.9	88 ± 1.9	%
		Dioxane effluent	9.1 ± 0.9	1.1 ± 0.2	µg/L
V	Operating conditions	HRT	8.0	4.0	hour
		Dioxane influent	100	10	µg/L
		Dioxane loading	1.4	0.29	mg/m^2-day
		Ethane influent	0	0	µg/L
		Ethane loading	0	0	mg/m^2-day
		E/D ratio	0	0	mole/mole
	Steady-state results	Ethane flux	0	0	mg/m^2-day
		Ethane removal	-	-	%
		Dioxane flux	0.39	0.043	mg/m^2-day
		Dioxane removal	5.3 ± 1.1	8.8 ± 2.3	%
		Dioxane effluent	95 ± 1.1	9.1 ± 0.3	µg/L

Notes:

- Red Font indicates the concentration is above 0.35 µg/L, a Health Advisory Level by EPA.
- Blue Font indicates the concentration is below our detection limits: 10 µg/L for 1,4-dioxane and 1 µg/L for ethane with GC-FID, and 0.5 µg/L for 1,4-dioxane with GC/MS.

4.2. Task 2: Biodegradation of 1,4-dioxane in the O_2-based MBfRs inoculated with a microbial consortium ("GF") from FSU

Table 5 summarizes the operating conditions and the steady-state results of the MBfRs 3 and 4 at FSU during enrichment, start-up, and Stages I to V. From Stage I to V, the 1,4-D concentration was constant at ~100 μg/L in MBfR3, and ~10 μg/L in MBfR4, but the ethane:14-D mass ratio varied from 0:1 to108:1 in MBfR3 (corresponding to mole ratios of 0:1 to 300:1), and from 0:1 to 360:1 in MBfR4 (corresponding to mole ratio of 0:1 to 1000:1). Figure 4 presents the ethane and 1,4-D concentrations in the influent and effluent of the two O_2-MBfRs. The operating strategy for the MBfRs at FSU generally mirrored the strategy for the ASU MBfRs except for one thing: While ASU evaluated an ethane:1,4-D mass ratio of 180:1 (corresponding to a molar ratio of 500:1) in Stage IV, FSU evaluated an ethane:1,4-D mass ratio of 11:1 (corresponding to a molar ratio of 30:1) in Stage III.

In Stage I, the molar ratios of ethane to 1,4-D were maintained at 10:1 for both reactors. At steady state, the removal efficiencies of 1,4-D were 48% in MBfR3 and 9% in MBfR4. In Stage II, the molar ratios of ethane to 1,4-D were increased to 100:1 and 1000:1 for MBfR3 and O_2-MBfR4, respectively. The effluent 1,4-D concentrations gradually decreased to ~ 16 μg/L in O_2-MBfR3 and to < 0.5 μg/L (below the detection limit of the GC/MS) in MBfR4. The effluent ethane was below detection limit of 1 μg/L in both reactors. In stage III, the molar ratios of ethane to 1,4-D were decreased to 30:1 for both reactors to examine if the promotional effects of ethane would decline with less input ethane. The removal efficiencies of 1,4-D then decreased to about 55% in MBfR3 and 28% in MBfR4 at steady state. When the molar ratios of ethane to 1,4-D were increased to 300:1 in stage IV, the removal efficiencies of 1,4-D improved to 89% in MBfR3 and 76% in MBfR4.

In stage V, both reactors were operated for 1,4-D removal with no ethane supply. The effluent 1,4-D concentrations rapidly increased to 73 μg/L in O_2-MBfR3 and to 8.5 μg/L in O_2-MBfR4. The results of these experiments clearly emphasize the importance of ethane as a primary substrate for the biodegradation of 1,4-D.

Table 5: Summary of the operating conditions and steady-state results for the O_2-MBfRs at FSU

Stages		Parameter	O_2-MBfR3	O_2-MBfR4	Unit
Enrichment	Operating conditions	HRT	8.0	8.0	hour
		Dioxane influent	36000	36000	µg/L
		Dioxane loading	520	520	mg/m^2-day
		Ethane influent	36000	36000	µg/L
		Ethane loading	520	520	mg/m^2-day
		E/D ratio	3	3	mole/mole
	Steady-state results	Ethane flux	520	520	mg/m^2-day
		Ethane removal	>99	>99	%
		Dioxane flux	72	76	mg/m^2-day
		Dioxane removal	14 ± 1.4	15 ± 1.8	%
		Dioxane effluent	31000 ± 360	31000 ± 870	µg/L
Start-up	Operating conditions	HRT	8.0	8.0	hour
		Dioxane influent	1000	1000	µg/L
		Dioxane loading	14	14	mg/m^2-day
		Ethane influent	36000	36000	µg/L
		Ethane loading	520	520	mg/m^2-day
		E/D ratio	100	100	mole/mole
	Steady-state results	Ethane flux	520	520	mg/m^2-day
		Ethane removal	>99	>99	%
		Dioxane flux	8	10	mg/m^2-day
		Dioxane removal	53 ± 1.3	72 ± 4.0	%
		Dioxane effluent	480 ± 10	280 ± 40	µg/L
I	Operating conditions	HRT	8.0	4.0	hour
		Dioxane influent	100	10	µg/L
		Dioxane loading	1.4	0.29	mg/m^2-day
		Ethane influent	360	36	µg/L
		Ethane loading	5.2	1.0	mg/m^2-day
		E/D ratio	10	10	mole/mole
	Steady-state results	Ethane flux	5.2	1.0	mg/m^2-day
		Ethane removal	>99	>99	%
		Dioxane flux	0.56	0.015	mg/m^2-day
		Dioxane removal	48 ± 0.8	9 ± 1.9	%
		Dioxane effluent	52 ± 0.8	10 ± 0.3	µg/L
II	Operating conditions	HRT	8.0	4.0	hour
		Dioxane influent	100	10	µg/L
		Dioxane loading	1.4	0.29	mg/m^2-day
		Ethane influent	3600	3600	µg/L
		Ethane loading	52	100	mg/m^2-day
		E/D ratio	100	1000	mole/mole

Stages		Parameter	O_2-MBfR3	O_2-MBfR4	Unit
	Steady-state results	Ethane flux	52	100	mg/m^2-day
		Ethane removal	>99	>99	%
		Dioxane flux	1.2	0.28	mg/m^2-day
		Dioxane removal	84 ± 4.0	> 95	%
		Dioxane effluent	16 ± 1.0	< 0.5	µg/L
III	Operating conditions	HRT	8.0	4.0	hour
		Dioxane influent	100	10	µg/L
		Dioxane loading	1.4	0.29	mg/m^2-day
		Ethane influent	1100	110	µg/L
		Ethane loading	16	3.2	mg/m^2-day
		E/D ratio	30	30	mole/mole
	Steady-state results	Ethane flux	16	3.2	mg/m^2-day
		Ethane removal	>99	>99	%
		Dioxane flux	0.79	0.08	mg/m^2-day
		Dioxane removal	55 ± 1.4	28 ± 1.4	%
		Dioxane effluent	45 ± 1.4	7.2 ± 1.0	µg/L
IV	Operating conditions	HRT	8.0	4.0	hour
		Dioxane influent	100	10	µg/L
		Dioxane loading	1.4	0.29	mg/m^2-day
		Ethane influent	10800	1100	µg/L
		Ethane loading	155	31	mg/m^2-day
		E/D ratio	300	300	mole/mole
	Steady-state results	Ethane flux	155	31	mg/m^2-day
		Ethane removal	>99	>99	%
		Dioxane flux	1.3	0.23	mg/m^2-day
		Dioxane removal	89 ± 0.7	79 ± 3.5	%
		Dioxane effluent	11 ± 0.7	2.1 ± 0.4	µg/L
V	Operating conditions	HRT	8.0	4.0	hour
		Dioxane influent	100	10	µg/L
		Dioxane loading	1.4	0.29	mg/m^2-day
		Ethane influent	0	0	µg/L
		Ethane loading	0	0	mg/m^2-day
		E/D ratio	0	0	mole/mole
	Steady-state results	Ethane flux	0	0	mg/m^2-day
		Ethane removal	-	-	%
		Dioxane flux	0.39	0.043	mg/m^2-day
		Dioxane removal	27 ± 0.5	15 ± 2.8	%
		Dioxane effluent	73 ± 0.5	8.5 ± 0.1	µg/L

Notes: Red Font indicates that the 1.4-dioxane effluent concentrations are above the health-based reference level of 0.35 µg/L. Blue Font indicates that the concentrations are below the FSU GC/MS detection limit of 0.5 µg/L for 1,4-dioxane or GC-FID detection limit of 1 µg/L for ethane.

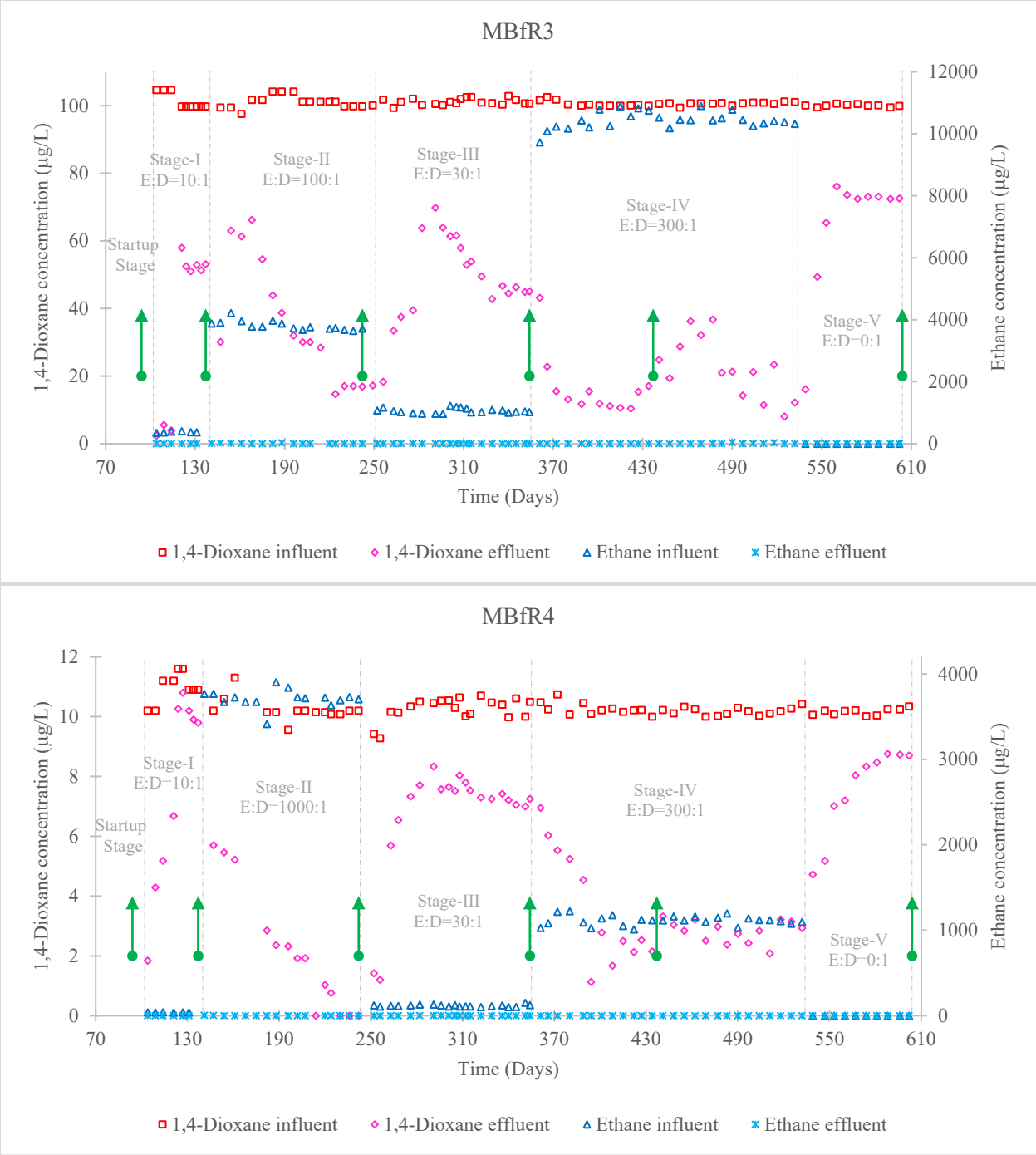

Figure 4: Ethane and 1,4-dioxane concentrations in the influent and effluent of the MBfR3 and MBfR4 at FSU. A biomass-enrichment stage of 70 days preceded the startup stage. E:D is the influent ethane:1,4-D mole ratio. Biofilm samples were taken when the MBfRs reached steady states, which are indicated by the upward green arrows.

Interpretations of the results from the MBfR experiments. Based on long-term continuous operation of the four O_2-MBfRs with different influent ethane concentrations over the various stages, we interpret that an ethane:1,4-D mole ratio of around 300:1 is close to an optimized

condition for input 1,4-D concentrations of 100 µg/L and 10 µg/L. The findings of the MBfR studies at ASU and FSU also suggest that a two-stage MBfR system may be required to remove 1,4-D from 100 µg/L to below the detection limit of 0.5 µg/L, which is close to the health-based reference level of 0.35 µg/L (EPA, 2017). The first stage would remove 1,4-D from 100 µg/L to ~10 µg/L at an ethane to 1,4-dioxane ratio of 300:1. The second stage would remove 1,4-D from ~10 µg/L to < 0.5 µg/L at an ethane:1,4-dioxane ratio of 300:1. With an influent 1,4-D concentration of ~10 µg/L, a one-stage O_2-MBfR could achieve over 95% removal, or effluent 1,4-D ≤ 0.5 µg/L.

4.3. Task 3: Microbial community analysis

4.3.1. Microbial community structure of the ASU O_2-MBfR biofilms

Enrichment and start-up stage. Based on the results of shallow metagenomic sequencing, Figure 5A summarizes the community structures of biofilm at the genus level for ASU O_2-MBfRs in the different stages. The dominant sequences at the genus level in MBfR1 and MBfR2 during the enrichment stage (E:D = 2.4), the start-up stage (E:D = 100), and stage I (E:D = 10) were most similar to *Pseudonocardia. Pseudonocardia* are known to grow with 1,4-D as the only carbon source and electron donor (Mahendra and Alvarez-Cohen, 2005; Sales et al., 2013). The dominant sequences for species within genera *Pseudonocardia* in the biofilm were most similar to *P. dioxanivorans,* which occupied over 90% of the sequences of the genera *Pseudonocardia* in the enrichment and start-up stages. The tetrahydrofuran/dioxane monooxygenase is the functional enzyme that *P. dioxanivorans* uses to oxidize 1,4-D (Li et al., 2013; Mahendra and Alvarez-cohen, 2006).

***Mycobacterium* was the dominant genus in the operating stages.** The relative abundance of sequences in the genera *Mycobacterium* gradually increased through the stages and eventually dominated the biofilm communities (from ~1% to >50%) of both reactors in stages II (E:D = 100), III (E:D = 300) and IV (E:D = 500). Based on the sequences, the dominant species within the *Mycobacterium* genus were *M. rhodesiae*, *M. mageritense*, and *M. paragordonae*. *Mycobacterium* has genes that encode for ethane and 1,4-D monooxygenases, which suggests that *Mycobacteria* may have been the dominant bacteria utilizing ethane as the primary substrate while also oxidizing 1,4-D via mono-oxygenation. Recently, the species *M. dioxanotrophicus* PH-06 was reported to use 1,4-D as a sole source of carbon and electrons, and the functional gene is a Group-6 soluble di-iron monooxygenase (*prmA*) (Deng et al., 2018a; He et al., 2017b, 2017a); however, we did not detect sequences for this species in our samples.

Less abundant genera that increased in the operating stages. The relative abundance of sequences of *Methyloversatilis* gradually increased through the stages and eventually became a significant fraction of the sequences (from <1% to >10%) of biofilms of MBfR1 in stage III and IV. Although, the genus *Methyloversatilis* has not been reported to oxidize 1,4-dioxane, it was able to oxidize ethane and had high expression of propane monooxygenase encoding gene (*prmA*) (Miao et al., 2021; Rochman, 2016). The relative-abundance changes and reported properties suggest that genus *Methyloversatilis* could have contributed to the co-oxidation of ethane and 1,4-D in MBfR1.

For MBfR2, the relative abundance of sequences of the genus *Nocardia* greatly increased from <1% in start-up to > 35% in stage I. Although the relative abundance gradually decreased to ~10% in stages, sequences in the genus *Nocardia* were the second most dominant sequences at the genus level in the operation stages of MBfR2. The genus *Nocardia* has been commonly detected in other 1,4-dioxane biodegradation communities (Masuda, 2009; Picone et al., 2020; Ramalingam and Cupples, 2020).

The relative abundance of sequences for genus *Methylibium* gradually increased through the stages and eventually became a significant fraction of the sequences (from <1% to ~5%) of biofilms of both reactors in stages II and III. The dominant sequence at the species level within genera *Methylibium* was *M. petroleiphilum,* which was previously reported as the dominant species in activated sludge reactors exposed to 1,4-D (Shin et al., 2010). Nakatsu et al. (2006) reported biodegradation of methyl tert-butyl ether (MTBE, a similar ether structure to 1,4-D) by *M. petroleiphilum*, which suggests it has the potential for 1,4-D biodegradation. Whole-genome sequencing of *M. petroleiphilum* strain PM1 indicated that its genome contains genes encoding for two toluene/benzene monooxygenase (TMO) pathways, a putative propane monooxygenase pathway (PMO), and a soluble methane monooxygenase (sMMO) (Kane et al., 2007). Sequences of *Methylibium* also were the only dominant genera (21%) in the sequences from the ethane-enriched culture in serum bottles for kinetic batch tests (reported below). Other less-abundant genera in biofilm community, like *Gordonia*, *Bradyrhizobium*, and *Afipia*, in the community also have been reported to contribute to 1,4-D co-oxidation (Masuda, 2009; Sei et al., 2013; Tusher et al., 2021).

Comparison between MBfR1 and MBfR2. The trends of abundances of sequences in the genera *Pseudonocardia* and *Mycobacterium* were similar in both MBfRs. However, the less-abundant genera in MBfR1 and MBfR2 were different, which may have been caused by the different influent ethane/1,4-D concentrations and surface loadings. Sequences for the genera *Methyloversatilis and Methylibium* were enriched in later stages of MBfR1, while sequences for genera *Nocardia* and *Gordonia* were enriched in MBfR2. The ethane and 1,4-D oxidation kinetics may have caused the community-structure differences between MBfR1 and MBfR2; this suggests that further research on these four genera and their possible contribution to ethane and 1,4-D oxidation is warranted.

A shift of the dominant sequences from *Pseudonocardia* to *Mycobacterium* and other genera supports that the removal of 1,4-D may have shifted to co-oxidation, since only *M. dioxanotrophicus* PH-06 is known to be able to grow on 1,4-D alone. Another explanation is that the relatively low 1,4-D influent (and even lower effluent) concentration selectively enriched for bacteria with enzymes having a lower half-maximum-rate concentration for 1,4-D. Perhaps *Mycobacterium* has the lowest half-maximum-rate concentration. This is another promising topic for future research.

4.3.2. Microbial community structure of the FSU O_2-MBfR biofilms

Dominant genera in all stages. Based on shallow metagenomic sequencing results, Figure 5B summarizes the abundances of sequences at the genus level in the biofilm in different stages for the FSU O_2-MBfRs. The first dominant sequences in MBfR3 and MBfR4 at the genus level

during all stages was *Rhodococcus*. Two species (*R. aetherivorans* JCM 14343^T and *R. ruber* 219) have been reported to metabolically biodegrade 1,4-D as the sole carbon and energy source (Bernhardt and Diekmann, 1991; Inoue et al., 2016), while other *Rhodococcus* species could co-metabolically degrade 1,4-D with primary substrates such as isobutane, THF, and propane (Murnane et al., 2021; Rolston et al., 2019). The species *R. erythropolis* and *R. rhodochrous* also were able to grow on ethane (Gou et al., 2006; Taquino, 2001). Therefore, the dominant *Rhodococcus* genus may have contributed to metabolic oxidation and co-oxidation of ethane/1,4-D in the FSU biofilm communities.

Potential 1,4-D degraders in the biofilm communities. The second dominant sequences were for the genus *Mycobacterium*. The genus *Mycobacterium* was the dominant genera in the inoculum (>55%) and still dominant in MBfR4, ranging from 26% to 51%. *Mycobacterium* has potential for ethane and 1,4-D co-oxidation, as discussed in section 4.3.1. In MBfR3, the relative abundance of genus *Mycobacterium* ranged from 7% to 24%. The high relative abundance suggested that the genus *Mycobacterium* could play important roles in the co-oxidation of ethane and 1,4-D. For MBfR3 and MBfR4, the relative abundance of sequences in the genus *Nocardia* greatly increased, from ~3% to 10~30%, starting from stage III (E:D = 30). The genus *Nocardia* was commonly detected in the 1,4-dioxane degradation communities (Masuda, 2009; Picone et al., 2020; Ramalingam and Cupples, 2020). The methane monooxygenases present in *Nocardia* also suggests the potential for ethane and 1,4-D co-oxidation. Other less abundant genera present in the biofilm (*Gordonia*, *Afipia*, and *Bradyrhizobium*) also are reported able to do 1,4-D co-oxidation (Kim et al., 2020; Sei et al., 2013; Yanık-Yıldırım and Vardar-Schara, 2014). Interestingly, all genera discussed in this paragraph were also found in the ASU MBfRs.

Comparison between MBfR3 and MBfR4. The trends of sequences in the genera *Rhodococcus* and *Mycobacterium* relative abundances were similar in both MBfRs. However, the relative abundance of sequences in the genus *Mycobacterium*, which ranged from 7% to 24% in MBfR3, were smaller than the 16% to 38% in MBfR4. Furthermore, sequences for the less-abundant genera in MBfR3 and MBfR4 were different, probably caused by the different influent ethane/1,4-D concentrations and surface loadings. Sequences in the genera *Nocardia, Afipia*, and *Mesorhizobium* were enriched in later stages of MBfR3, while genera *Nocardia* and *Gordonia* were enriched in MBfR4; this trend is similar to that in MBfR2 at ASU.

Comparison between ASU and FSU biofilm communities. Although the 1,4-D removal performances were similar between ASU and FSU teams' O_2-MBfRs, the biofilm communities were dramatically different. The ASU results show a clear transition from genera doing metabolic 1,4-D biodegradation to genera active in co-oxidation. In contrast, FSU's results did not show a clear community shift, since genera *Rhodococcus* and *Mycobacterium* were important throughout. Other potential 1,4-D-degrading genera were found in the FSU and ASU MBfRs, including *Mycobacterium*, *Gordonia*, *Bradyrhizobium*, *Afipia*, and *Nocardia*.

Taken together, the microbial-community structures support that co-oxidation was important for the biodegradation of 1,4-D, and a wide range of bacteria could contribute to the co-oxidation of ethane and 1,4-D in the O_2-MBfRs. Differences in ethane- and 1,4-D-oxidation kinetics may have caused the community-structure differences among the four MBfRs; a potent direction for further research is on these ethane- and 1,4-D-co-oxidizing bacteria.

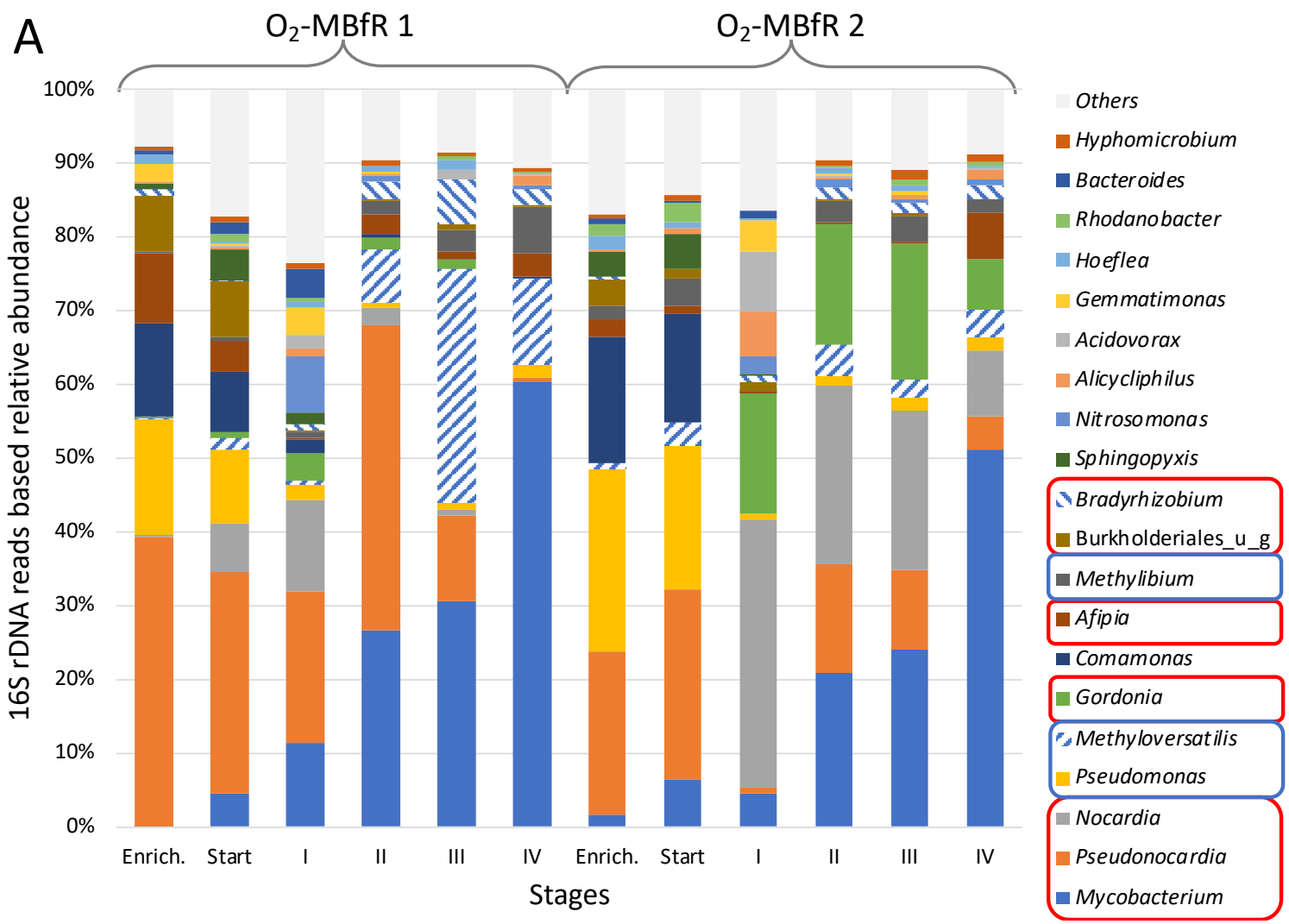
A
O2-MBfR 1
O2-MBfR 2
16S rDNA reads based relative abundance
100%
90%
80%
70%
60%
50%
40%
30%
20%
10%
0%
Enrich.
Start
I
II
III
IV
Enrich.
Start
I
II
III
IV
Stages
Others
Hyphomicrobium
Bacteroides
Rhodanobacter
Hoeflea
Gemmatimonas
Acidovorax
Alicycliphilus
Nitrosomonas
Sphingopyxis
Bradyrhizobium
Burkholderiales_u_g
Methylibium
Afipia
Comamonas
Gordonia
Methyloversatilis
Pseudomonas
Nocardia
Pseudonocardia
Mycobacterium

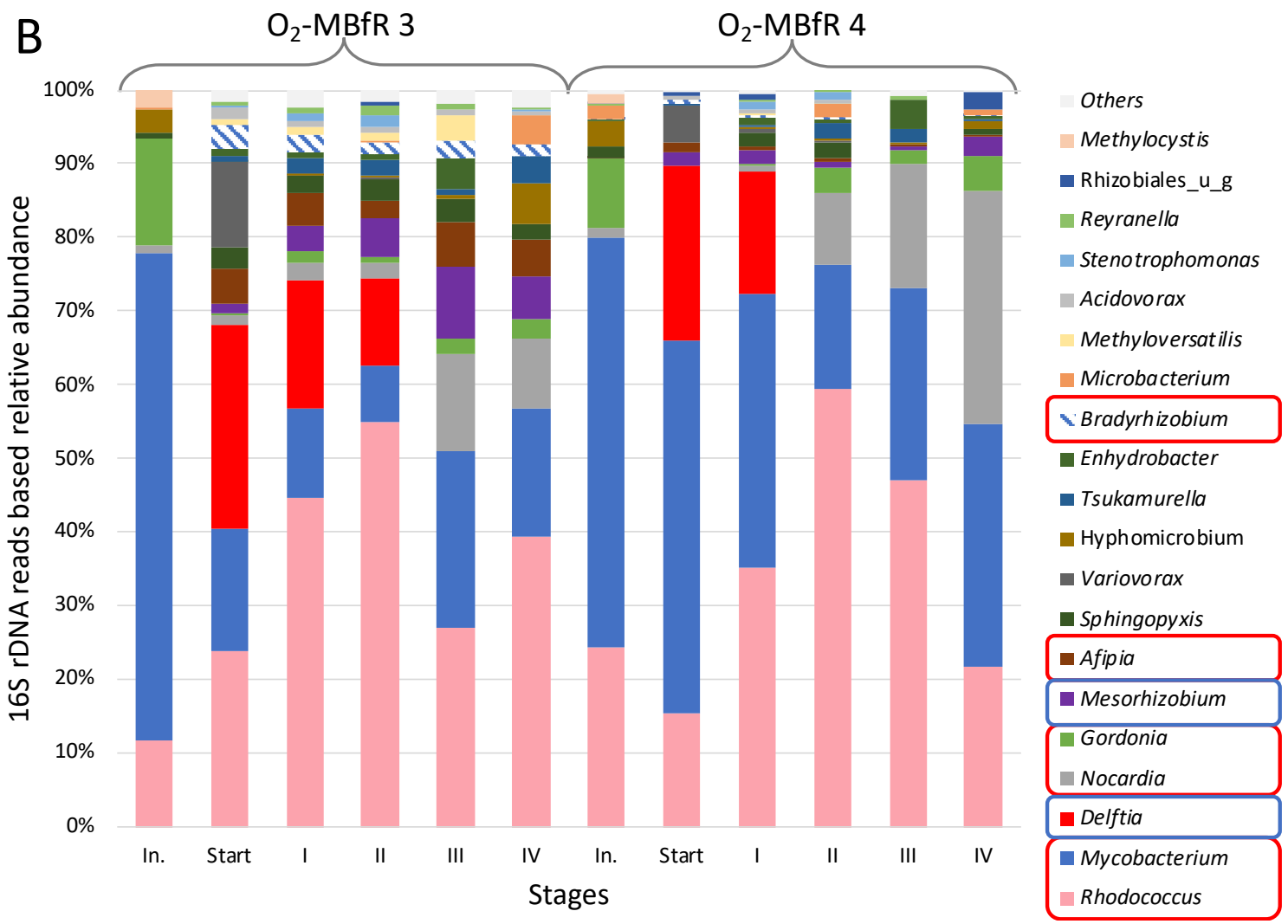

Figure 5: The relative abundances of sequences at the genus level in the biofilms in MBfR1 and MBfR2 at ASU (A) and MBfR3 and MBfR4 at FSU (B). Genera known to biodegrade 1,4-D and ethane are high-lighted in red and blue, respectively. "Others" are sum of species that had relative sequence abundance <1%.

4.3.3. Oxygenase genes in the ASU O_2-MBfR biofilms

Important monooxygenase genes. Based on the shallow metagenomic sequencing results of ASU MBfR1 and MBfR2, Table 6 lists the relative abundances of genes encoding monooxygenases that may be active in 1,4-D co-oxidation. The relative abundances are presented with units of counts per million (CPM) and highlighted with the color scale from green to yellow to red indicating increasing abundance. The genes encoding toluene/benzene monooxygenase (TMO) showed a clear trend in MBfR1: generally, a higher ethane/1,4-D mole ratio increased the abundance of TMO through the stages. A trend of TMO abundance in MBfR2 was not clear, which may have been caused by the 5-fold lower surface loading of ethane and 1,4-D. Various studies reported that TMOs were able to degrade 1,4-D by co-oxidation: e.g., group-1 toluene monooxygenases of *Burkholderia cepacia* G4, group-2 toluene monooxygenases of *Azoarcus* sp. DD4, *Pseudomonas mendocina* KR1, *Pseudomonas pickettii* PKO1, and *Burkholderia cepacia* AA1 (Deng et al., 2020, 2018b; Li et al., 2020; Ma et al., 2021; Mahendra and Alvarez-cohen, 2006).

The relative abundances of genes encoding particulate methane monooxygenase (pMMO) and soluble methane monooxygenase (sMMO) greatly increased when the MBfRs were fed with higher influent ethane concentrations. pMMO and sMMO have been reported to oxidize ethane, while only sMMO is known to oxidize 1,4-D (Mahendra and Alvarez-cohen, 2006; Oh et al., 2019; Redmond et al., 2010; Wilkinson et al., 1996). The relative abundances of genes encoding propane monooxygenase (PMO) had similar trends to TMO genes in the MBfR1, but its abundances gradually decreased through stages in MBfR2. Various studies reported that PMO can contribute to ethane and 1,4-D oxidation (Mahendra and Alvarez-cohen, 2006; Redmond et al., 2010; Xu et al., 2005; Zou et al., 2021). The trends suggest that PMO was a key monooxygenase for ethane and 1,4-D co-oxidation in MBfR1, while TMO and sMMO may have dominated 1,4-D co-oxidation in MBfR2.

Other monooxygenases. In addition to TMO, pMMO, sMMO, and PMO, other monooxygenases were detected by shallow metagenomic sequencing: e.g., vanillate monooxygenase (VAN) and alkylglycerol monooxygenase (AGMO). The relative abundances of these monooxygenase-encoding genes had similar trends to TMO and PMO in both MBfRs. These monooxygenases have not been reported to oxidize ethane or 1,4-D. However, some of these monooxygenases were reported to oxidize short alkyl ethers, which had similar chemical structures to 1,4-D and 1,4-D oxidation intermediates (Buswell and Eriksson, 1988; Watschinger et al., 2010). Therefore, these monooxygenases may have contributed to the co-oxidation of 1,4-D in MBfR.

Correlation among ethane/1,4-dioxane flux, community structure, and monooxygenase genes. Figure 6 is a principal component analysis (PCA) of ethane and 1,4-D fluxes, relative abundances of three dominant genera, and monooxygenase-encoding genes. Table 7 lists Pearson correlation coefficients and 1-tail significances among these factors in the PCA. The close relationships among *Methylibium*, TMO, PMO, pMMO, and VAN, and whole genomes available information, suggest that bacteria in the *Methylibium* genus may have contained these monooxygenases and been key contributors to the co-oxidation of ethane and 1,4-D. The whole-genome sequencing reported for *Methylibium* sp. proved that some *Methylibium* species have the monooxygenase for co-oxidation of ethane and 1,4-D (Kane et al., 2007; Szabó et al., 2015). The

close relationship between *Mycobacterium* and sMMO also suggests that *Mycobacterium* may have contained sMMO that was active for ethane and 1,4-D co-oxidation, which is consistent with previous reports on *Mycobacterium* (Coleman et al., 2011; Kotani et al., 2006; Martin et al., 2014).

Conclusions from the microbial community analysis. *Pseudonocardia*, *Mycobacterium,* and *Methylibium* were three dominant sequences at the genera level in both ASU MBfRs, and it is likely that they contributed to the co-oxidation of 1,4-D. Although 1,4-D removals were similar between ASU and FSU MBfRs, the biofilm communities were dramatically different. The ASU biofilms showed a strong shift from sequences in the genera known to do metabolic 1,4-D biodegradation to those from genera that carry out co-oxidation. The FSU biofilms did not show a clear community shift over time, and the dominant sequences for genera that can do 1,4-D co-oxidation were *Rhodococcus* and *Mycobacterium*. One important finding is that a wide range of bacteria were present in our reactors and possibly involved in co-oxidation of ethane and 1,4-D in the O_2-MBfR.

Based on the abundance of monooxygenase-encoding genes, it seems that many monooxygenases -- including TMO, sMMO, pMMO, and PMO -- were present and possibly active in ethane and 1,4-D co-oxidation. This diversity in monooxygenase genes is consistent with the range of genera and species active in ethane and 1,4-D co-oxidation when the ethane/1,4-D mole ratio was around 300, which yielded stable and efficient co-oxidation of ethane and 1,4-D.

Table 6: Relative abundance of genes encoding functional monooxygenase for 1,4-dioxane co-oxidation of ASU MBfR1 (left) and MBfR2 (right)

Enzyme	Function	Gene	Ethane	Enrich.	Start	I	II	III	IV	Enrich.	Start	I	II	III	IV
TMO	phenol/toluene 2-monooxygenase (NADH) P4/A4	*tomA4*	195.6	24.2	0.0	0.0	7.5	68.8	149.6	36.0	77.4	21.3	28.0	28.1	27.5
	henol/toluene 2-monooxygenase (NADH) P3/A3	*tomA3*	138.2	12.5	14.4	16.0	26.0	47.0	133.2	38.7	47.2	28.8	56.7	31.3	37.2
	phenol/toluene 2-monooxygenase (NADH) P1/A1	*tomA1*	138.3	12.8	15.9	8.9	19.5	64.5	125.4	36.5	58.2	13.5	40.7	28.4	36.6
	phenol/toluene 2-monooxygenase (NADH) P0/A0	*tomA0*	186.2	13.6	0.0	0.0	6.0	35.8	70.3	53.4	39.9	31.7	26.2	19.4	15.0
	phenol/toluene 2-monooxygenase (NADH) P5/A5	*tomA5*	67.3	25.9	10.6	13.0	13.0	34.0	93.1	38.1	22.3	17.2	47.1	13.0	32.0
	phenol/toluene 2-monooxygenase (NADH) P2/A2	*tomA2*	98.4	14.6	6.4	5.1	7.7	20.5	60.5	26.3	27.6	35.0	17.8	13.4	12.9
	toluene monooxygenase system protein A	*tmoA*	26.3	23.3	34.4	24.3	15.4	11.4	4.2	10.9	11.5	5.0	32.8	5.3	6.2
	toluene monooxygenase system protein B	*tmoB*	0.0	59.3	1.9	6.8	26.6	1.1	0.0	18.7	21.8	0.0	21.3	0.0	3.1
	toluene monooxygenase system ferredoxin subunit	*tmoC*	28.1	40.5	15.0	5.9	14.6	16.9	0.0	15.2	3.6	0.0	1.5	6.3	4.6
	toluene monooxygenase system protein E	*tmoE*	2.4	21.5	14.6	11.9	15.3	6.4	5.0	16.0	13.1	0.0	14.5	10.7	7.5
	toluene monooxygenase system protein D	*tmoD*	0.0	37.8	1.5	0.0	20.4	4.1	0.0	27.8	10.3	0.0	2.3	0.0	2.3
	toluene monooxygenase electron transfer	*tmoF*	7.8	0.0	0.0	0.0	1.0	6.2	6.0	0.0	0.0	0.0	3.8	5.2	6.7
pMMO	methane/ammonia monooxygenase subunit C	*pmoC*	103.6	0.0	0.0	12.5	15.4	35.6	72.9	21.4	25.3	0.0	25.9	7.5	19.0
	methane/ammonia monooxygenase subunit B	*pmoB*	82.6	0.0	0.0	11.8	7.9	35.5	54.8	14.0	17.8	1.4	19.8	8.3	22.4
	methane/ammonia monooxygenase subunit A	*pmoA*	89.4	0.0	4.7	8.5	13.0	32.0	49.7	18.6	17.7	0.0	14.7	7.1	18.7
sMMO	methane monooxygenase component A alpha	*mmoX*	10.9	0.0	0.0	0.0	13.3	33.2	11.5	3.5	13.2	3.6	14.2	19.3	23.9
	methane monooxygenase component D	*mmoD*	0.0	0.0	0.0	0.0	0.0	35.4	5.0	0.0	0.0	0.0	16.8	12.9	34.9
	methane monooxygenase component C	*mmoC*	6.1	0.0	2.5	0.0	6.3	14.3	16.8	0.0	3.1	0.0	15.3	11.9	14.0
	methane monooxygenase component A beta	*mmoY*	2.7	0.0	3.4	0.0	7.3	28.6	9.5	0.0	2.4	0.0	8.0	6.1	13.3
	methane monooxygenase component A gamma	*mmoZ*	5.5	0.0	0.0	0.0	3.7	19.3	9.2	0.0	4.3	0.0	1.4	9.5	21.1
	methane monooxygenase regulatory protein B	*mmoB*	0.0	0.0	0.0	1.9	3.9	7.4	4.9	0.0	0.0	0.0	5.6	11.1	14.6
PMO	propane monooxygenase coupling protein	*prmD*	124.5	26.0	5.3	0.0	11.0	28.4	82.8	29.5	57.9	10.7	23.8	26.7	16.1
	propane 2-monooxygenase small subunit	*prmC*	71.2	16.4	14.6	10.8	9.4	20.8	54.6	24.8	30.6	6.7	27.0	26.7	18.8
	propane 2-monooxygenase large subunit	*prmA*	64.4	21.3	9.6	4.6	7.2	28.4	51.0	40.3	39.3	3.5	21.4	14.3	16.0
	propane monooxygenase reductase component	*prmB*	54.0	16.7	14.0	8.9	6.9	17.1	45.2	35.0	20.3	2.9	17.9	9.6	11.6
Other MOs	4-hydroxyacetophenone monooxygenase	*hapE*	201.7	53.3	73.9	92.9	140.1	263.4	220.3	65.8	106.5	84.1	190.7	197.4	202.9
	cyclohexanone monooxygenase	*chnB*	225.6	72.3	87.0	86.2	160.0	214.5	216.5	78.8	139.5	69.9	185.7	140.3	138.4
	nitronate monooxygenase	*ncd2*	82.9	129.6	41.9	50.0	91.3	163.9	116.0	136.1	56.2	163.8	97.3	104.4	148.6
	vanillate monooxygenase ferredoxin subunit (VAN)	*vanB*	301.9	96.6	57.6	41.3	57.9	102.4	199.9	79.2	91.8	35.8	77.2	64.9	79.6
	alkanesulfonate monooxygenase	*ssuD*	111.4	79.2	75.9	24.0	58.0	102.6	91.0	65.3	85.0	112.7	83.2	28.3	44.3
	long-chain alkane monooxygenase	*ladA*	32.0	83.1	54.1	44.7	71.1	110.0	78.1	59.8	57.3	9.0	73.9	66.0	85.8
	alkylglycerol monooxygenase (AGMO)	*AGMO*	77.4	62.7	87.9	56.0	29.5	44.3	41.5	70.7	79.1	99.9	26.0	35.7	43.3
	Unit: CPM, Count Per Million	Color gradient		0.0	30.0	60.0	90.0	120.0	150.0	180.0	210.0	240.0	270.0	300.0	

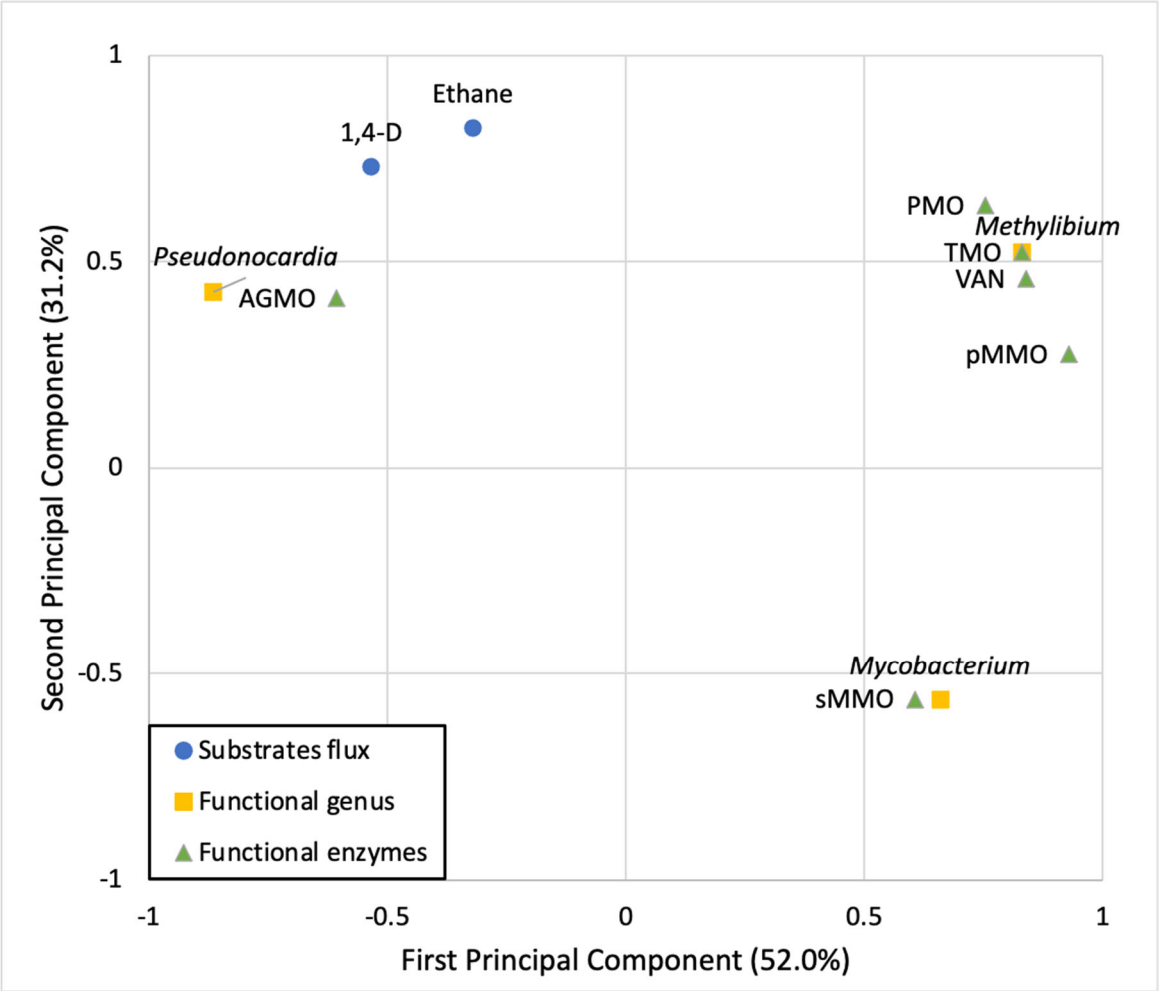

Figure 6: Principal component analysis among substrates flux, dominant genera, and the relative abundances of monooxygenase genes. Blue dots represent the flux of ethane and 1,4-D; yellow squares represent the relative abundances of three genera; and green triangles represent the relative-abundance of genes encoding different monooxygenases.

Table 7: Pearson correlation and 1-tailed significance among substrates fluxes, dominant genera, and monooxygenase-gene relative abundance

	1,4-D	Ethane	*My.*	*Me.*	*P.*	TMO	pMMO	sMMO	PMO	VAN	AGMO
1,4-D		0.000	0.068	0.401	0.006	0.393	0.216	0.074	0.473	0.446	0.086
Ethane	0.947		0.098	0.400	0.038	0.416	0.367	0.103	0.270	0.325	0.198
Mycobacterium	-0.574	-0.511		0.299	0.020	0.295	0.137	0.000	0.405	0.220	0.060
Methylibium	-0.107	0.107	0.221		0.107	0.000	0.001	0.304	0.000	0.002	0.313
Pseudonocardia	0.825	0.660	-0.732	-0.494		0.109	0.034	0.040	0.170	0.080	0.015
TMO	-0.115	0.090	0.227	0.990	-0.489		0.000	0.314	0.000	0.001	0.342
pMMO	-0.326	-0.144	0.440	0.917	-0.673	0.943		0.181	0.003	0.001	0.187
sMMO	-0.562	-0.500	0.964	0.216	-0.650	0.205	0.374		0.410	0.296	0.099
PMO	0.029	0.256	0.102	0.986	-0.389	0.969	0.856	0.096		0.002	0.344
VAN	-0.058	0.192	0.320	0.880	-0.548	0.892	0.894	0.226	0.886		0.118
AGMO	0.536	0.350	-0.595	-0.205	0.755	-0.172	-0.365	-0.509	-0.169	-0.474	
Color scale	-1.0	-0.8	-0.6	-0.4	-0.2	0.0	0.2	0.4	0.6	0.8	1.0

Note: the correlation with 1 tailed significance <0.01 is highlighted with yellow; significance 0.01<X<0.05 is highlighted with green; "*My.*" stands for *Mycobacterium*; "*Me.*" stands for *Methylibium*; "*P.*" stands for *Pseudonocardia*.

4.4. Task 4: Modeling evaluation of 1,4-dioxane removal

4.4.1. Kinetics of 1,4-dioxane and ethane biodegradation

We conducted batch tests with different ethane and 1,4-D concentrations in serum bottles using the ethane- and 1,4-D-enriched mixed culture as the inoculum (condition details are listed in Table 8). Figure 7 presents the results according to a decreasing ethane-to-1,4-D mole ratio from 100:1 in A to 0:1 in E. F had no 1,4-D. High ethane had a significant inhibition effect on 1,4-D biodegradation. In group A, where the initial Ethane/1,4-D mole ratio was 100 (or aqueous concentration mole ratio about 6.1), 1,4-D was not oxidized at all throughout the 22 days batch test. In group B, where the initial Ethane/1,4-D mole ratio was 50 (or aqueous concentration ratio about 3.1), 1,4-D was slowly oxidized, with average removal rate of 1.93 μM/d. In groups C and D, a lower ethane/1,4-D mole ratio led to higher 1,4-D removal rate (C: 5.5 μM/d and D: 11.2 μM/d). When ethane was absent in group E, the enriched culture reached the highest 1,4-D removal rate of 23.9 μM/d. When the ethane-to-oxygen mole ratio was the same (e.g., 10:20 in groups B and F), ethane removal rates were similar whether or not 1,4-D was present (group B; 0.013 mmol/d per bottle) or absent (group F; 0.012 mmol/d per bottle); this indicates no inhibition of 12 mg/L 1,4-D on ethane oxidation, even though high ethane inhibited 1,4-D biodegradation.

Table 8: Experimental conditions for the first set of 1,4-D kinetics batch tests

No.	Initial biomass (mg COD/L)	Volume of Ethane (mL)	Volume of Oxygen (mL)	Initial ethane concentration (mM)	Initial oxygen concentration (mM)	Initial 1,4-D concentration (mM)	Ethane amount (mmole)	1,4-D amount (μmole)	Ethane/1,4-D Conc. mole ratio
A	40	20	10	0.83	0.125	0.136	0.83	8.16	6.1
B	40	10	10	0.42	0.125	0.136	0.42	8.16	3.1
C	40	5	10	0.21	0.125	0.136	0.21	8.16	1.5
D	40	2.5	10	0.10	0.125	0.136	0.10	8.16	0.8
E	40	0	10	0.00	0.125	0.136	0.00	8.16	0.0
F	40	10	10	0.42	0.125	0	0.42	0	NA

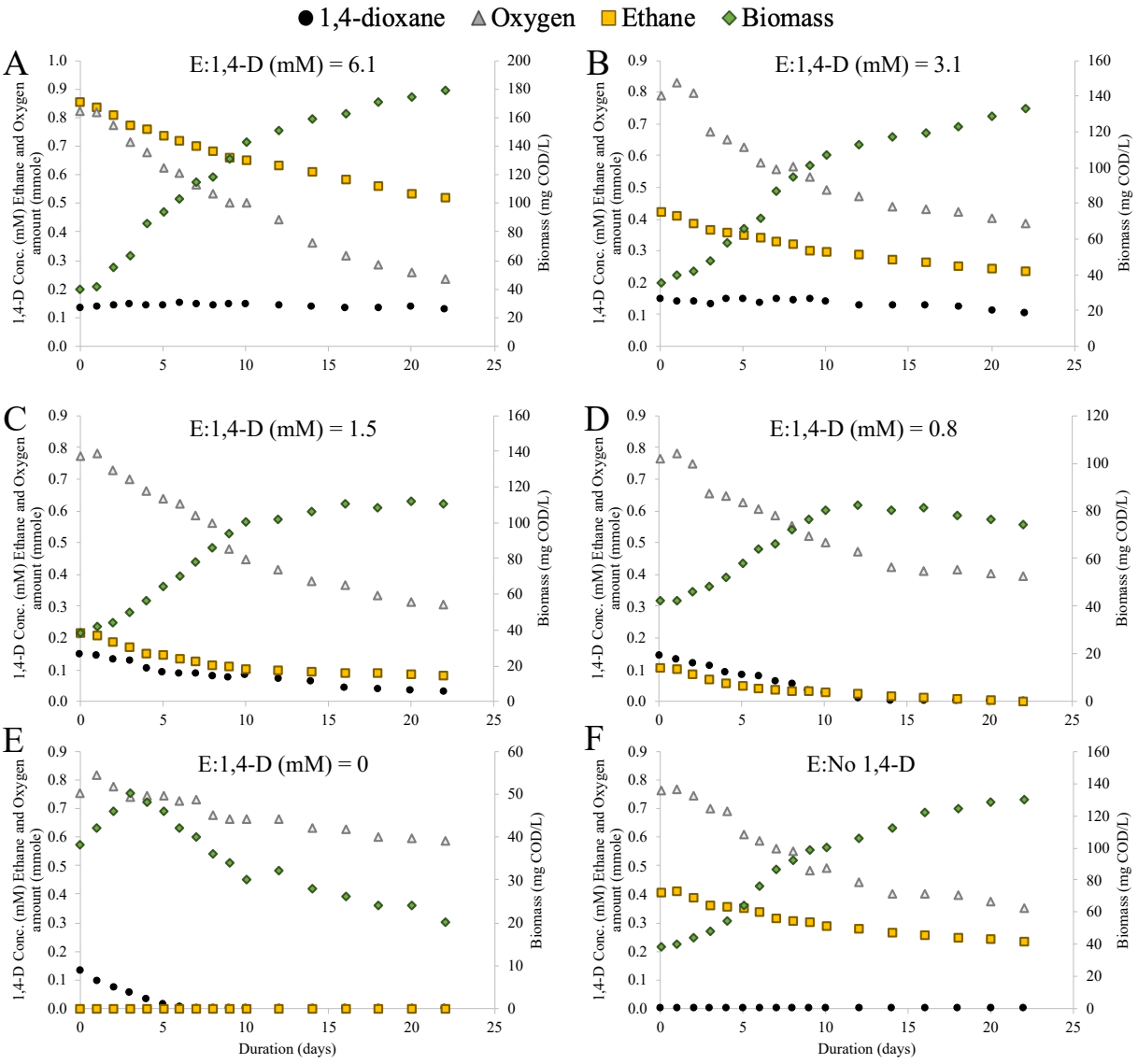

Figure 7: Results for the first set of kinetics batch tests with different initial ethane to 1,4-D ratios.

Inhibition by high ethane could be the case if the monooxygenase for ethane also was the functional enzyme for oxidizing 1,4-D in this enriched culture. Since ethane may have a competitive advantage as the substrate for the enzyme, 1,4-D oxidation would be inhibited competitively when the ethane/1,4-D ratio is high. For the context of the O_2-MBfR, even though the ethane/1,4-D loading ratio was high in the influent, the actual ethane concentration in the MBfR was low enough (usually < 0.03 μM) that competitive inhibition was not relevant. Mechanistically, the batch test results suggest that inhibition role of ethane on biotransformation of 1,4-D should be considered when modeling ethane as a primary electron donor to stimulate 1,4-D monooxygenases, but it may not be important in MBfR operation.

We conducted the second set of batch tests with ethane:1,4-D ratios that were much lower than those in the first set of batch experiments; the concentrations are more directly relevant to the

conditions in the MBfRs. The experimental details are listed in Table 9, and the results are summarized in Figure 8. We focused on investigating the kinetics of metabolic- versus co-oxidation of 1,4-D. The molar ratio of ethane:1,4-D ranged from 0.1 to 1.0. The enriched culture growing on ethane and 1,4-D was used as the inoculum. Groups A and B, which had 1,4-D as the only substrate with different two initial concentrations, were for 1,4-D metabolism. In the co-oxidation groups C-F, we kept constant the initial 1,4-D concentration (0.1 mM), but increased the initial ethane concentration from 0.01 to 0.1 mM. In groups G and H, ethane was the only substrate with two different initial concentrations. Figure 8 shows that all the groups removed over 99% of initial 1,4-D in the first 9 days of batch tests. With relatively lower ethane-to-1,4-D (E/D) ratios in this set of experiments (0.1 to 1), compared to the first set of batch tests (0 to 6.1, Table 8), ethane promoted 1,4-D oxidation. Thus, the lower concentrations mitigated ethane inhibition of 1,4-D biodegradation, as was seen in the first set of experiments.

In group A and B, 0.1 and 0.5 mM 1,4-D were consumed in about 9 days, with corresponding growth of biomass (as particulate COD). In groups C to E, which had an ethane initial concentration smaller than 1,4-D concentration, the removal rates of 1,4-D were faster than group A (without ethane). In group F, which had an ethane initial concentration equal to 1,4-D concentration, the 1,4-D removal was slower than group A. Comparing the results of group E/G and F/H, the ethane removal rates were not affected by the 0.1 mM 1,4-D.

Table 9: Experimental setup for the second set of 1,4-dioxane kinetics batch tests

Expt. No.	Initial biomass (mg COD/L)	Volume of Ethane (mL)	Initial ethane concentration (mM)	Initial 1,4-D concentration (mM)	Ethane amount (mmole)	1,4-D amount (μmole)	Ethane/1,4-D mole ratio	Ethane/1,4-D Conc. ratio
A	70	0	0.00	0.1	0.00	6	0	0.0
B	70	0	0.00	0.5	0.00	30	0	0.0
C	70	0.313	0.01	0.1	0.01	6	2	0.1
D	70	0.625	0.03	0.1	0.03	6	4	0.3
E	70	1.25	0.05	0.1	0.05	6	9	0.5
F	70	2.5	0.10	0.1	0.10	6	17	1.0
G	70	1.25	0.05	0	0.05	0	N.A.	N.A.
H	70	2.5	0.10	0	0.10	0	N.A.	N.A.

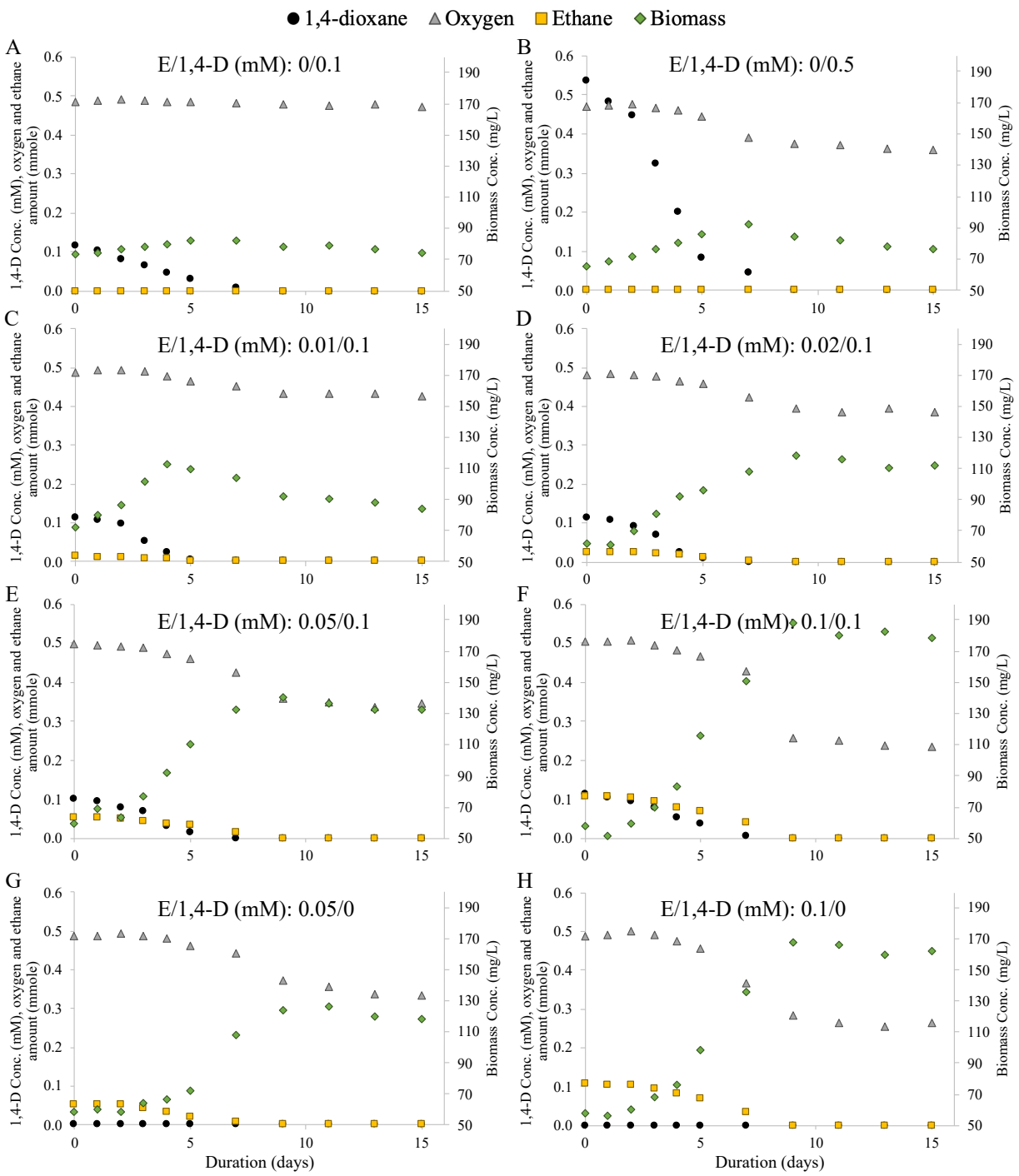

Figure 8: Results for the second set of 1,4-dioxane and ethane batch tests with different initial 1,4-dioxane and ethane concentrations.

Seven of the second set of experiments shown in Figure 8 were used for estimating the kinetic parameters of 1,4-D and ethane (experiment D used for model evaluation). The best-fit parameters in Table 10 lead to good correspondence with experimental values, and Table 11 shows that the MSRR values ranged from 0.01 to 0.20. As we show below, the model with the best-fit

parameters represented well the trends for all measured parameters. Furthermore confirming the validity of the model and parameters is that the parameters for 1,4-D were within the range of values reported in the literature (Barajas-Rodriguez and Freedman, 2018; Chen et al., 2016; Mahendra and Alvarez-cohen, 2006; Nam et al., 2016; Sei et al., 2013; Yamamoto et al., 2018). However, no previous study has reported the kinetic and stoichiometric parameters for ethane biodegradation. We now interpret the meaning of all the parameters for 1,4-D and ethane.

The biomass yield of 1,4-D (y_d) and ethane (y_e) are 0.39 mg COD/mg COD and 0.50 mg COD/mg COD, respectively. The values of y_d for 1,4-D reported in the literature are in the range of 0.07 mg COD/mg COD for *Pseudonocardia dioxanivorans* CB1190 (Mahendra and Alvarez-Cohen, 2006) to 0.45 mg COD/mg COD for Enrichment culture-FS (Nam et al., 2016). The value of y_e for ethane obtained in this study (0.50 mg COD/mg COD) is similar to the biomass yields of propane, 0.56 mg COD/mg COD and 0.61 mg COD/mg COD for *Rhodococcus ruber* ENV425 and propanotrophic mixed culture ENV487, respectively (Barajas-Rodriguez and Freedman, 2018). The maximum specific 1,4-D utilization rate of DOB and EDCOB were estimated as 2.00 mg COD/(mg COD · d) and 2.14 mg COD/(mg COD · d), respectively. These results lie within the range of values available in the literature: 0.87 mg COD/(mg COD · d) for ENV425 and 2.11 to 33.90 mg COD/(mg COD · d) for CB1190 (Barajas-Rodriguez and Freedman, 2018; Mahendra and Alvarez-Cohen, 2006). Of high importance is the 1,4-D had a y_d value, which means that it supported biomass synthesis; this further supports that 1,4-D was biodegraded via co-oxidation.

Our values of the half-maximum-rate concentrations (~25 mg COD/L for 1,4-D for EDCOB and DOB) fall within the wide range of values that have been reported: a minimum value of 3.25 mg COD/L for ENV487 and a maximum of 600 mg COD/L for *Pseudonocardia benzenivorans* B5 (Barajas-Rodriguez and Freedman, 2018; Mahendra and Alvarez-cohen, 2006). The variability of the kinetic parameters among the different studies is attributed to the different culture type, parameter estimation method, and the experimental approach followed (Barajas-Rodriguez and Freedman, 2018). The values for ethane (~1.5 mg COD/L) are much smaller and consistent with the mono-oxygenase be targeted to ethane.

The results of the inhibition coefficients imply that ethane had about 6.5-fold more inhibition on 1,4-D than 1,4-D had on ethane. Among the active biomass groups, DOB showed the highest decay coefficient and endogenous respiration rate, followed by EOB and EDCOB. Since NGB were not involved in the oxidation of ethane and 1,4-D, their biomass decay coefficient and endogenous respiration rate were the lowest compared to the active biomass groups. The initial percentages of the biomass types indicate that about 10% of the biomass was involved in the degradation of ethane and 1,4-D (i.e., EDCOB, DOB, and EOB). Almost 50% was inert biomass, which reflects the long cultivation time, which accentuates decay processes. NGB were almost 42%, which occurs because the bacteria active in biodegrading ethane and 1,4-D release organic matter (decay products and soluble microbial products) that support the growth of a wide-array of bacteria.

Table 10: Best-fit kinetic parameters for degradation of 1,4-dioxane and ethane

S. No.	*Parameter*	*Symbol*	Estimated values	*Unit*
1	Biomass yield of 1,4-dioxane	y_d	0.39	mg_{COD}/mg_{COD}
2	Biomass yield of ethane	y_e	0.50	
3	Maximum specific 1,4-dioxane utilization rate of DOB	q_d	2.00	$mg_{COD}/(mg_{COD}$ d)
4	Maximum specific ethane utilization rate of EOB	q_e	1.39	
5	Maximum specific 1,4-dioxane utilization rate of EDCOB	q_{dc}	2.14	
6	Maximum specific ethane utilization rate of EDCOB	q_{ec}	1.39	
7	Half-maximum-rate concentrations of DOB for 1,4-dioxane	K_d	25.00	mg_{COD}/L
8	Half-maximum-rate concentrations of EOB for ethane	K_e	1.48	
9	Half-maximum-rate concentrations of EDCOB for 1,4-dioxane	K_{dc}	24.90	
10	Half-maximum-rate concentrations of EDCOB for ethane	K_{ec}	1.45	
11	Inhibition coefficient of 1,4-dioxane on ethane	K_{ide}	21.00	
12	Inhibition coefficient of ethane on 1,4-dioxane	K_{ied}	3.21	
13	Half-maximum-rate concentrations for oxygen	K_o	1.39	
14	Endogenous respiration rate of DOB	p_d	0.012	1/d
15	Endogenous respiration rate of EOB	p_e	0.009	
16	Endogenous respiration rate of EDCOB	p_c	0.008	
17	Endogenous respiration rate NGB	p_n	0.007	
18	Biomass decay coefficient of DOB	b_d	0.05	1/d
19	Biomass decay coefficient of EOB	b_e	0.04	
20	Biomass decay coefficient of EDCOB	b_c	0.04	
21	Biomass decay coefficient of NGB	b_n	0.001	
22	Initial percentage of DOB	f_d	0.09	%
23	Initial percentage of EOB	f_e	3.04	
24	Initial percentage of EDCOB	f_c	6.31	
25	Initial percentage of NGB	fn	41.69	
26	Initial percentage of IB	fb	49.10	

Table 11: The mean sum of the squares of the relative residuals for the model results and the experimental values

Experiment	A	B	C	E	F	G	H
MSRR	0.01	0.03	0.20	0.01	0.03	0.10	0.01

Figure 9 provides graphical comparisons of the model simulations and the experimentally measured data for the experiments used in the parameter estimation. The model clearly captured all major trends for the concentrations of 1,4-D, ethane, oxygen, and biomass throughout the period of the experiments. The time-series variations of the biomass-species concentration also matched with the substrate consumptions.

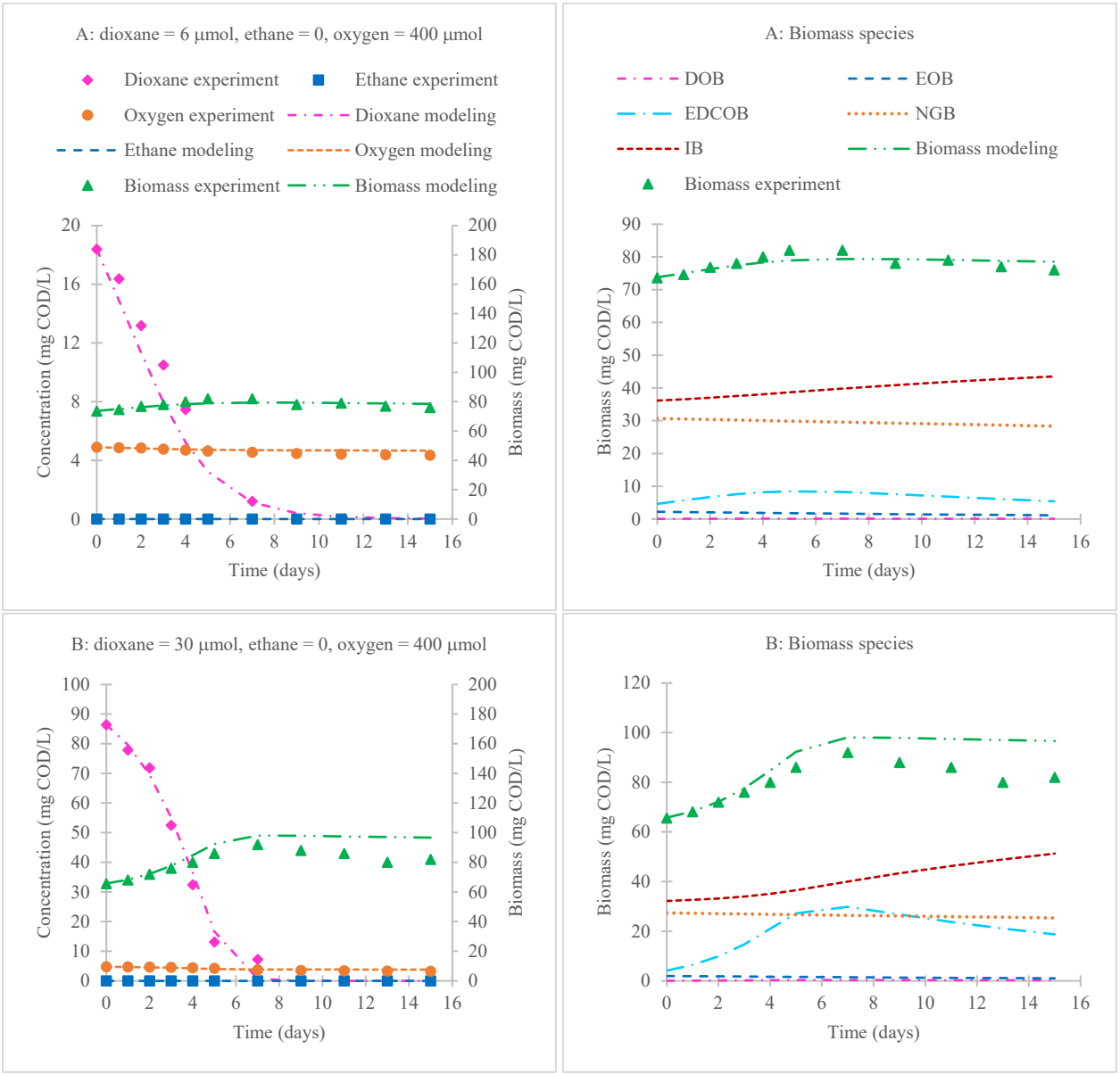

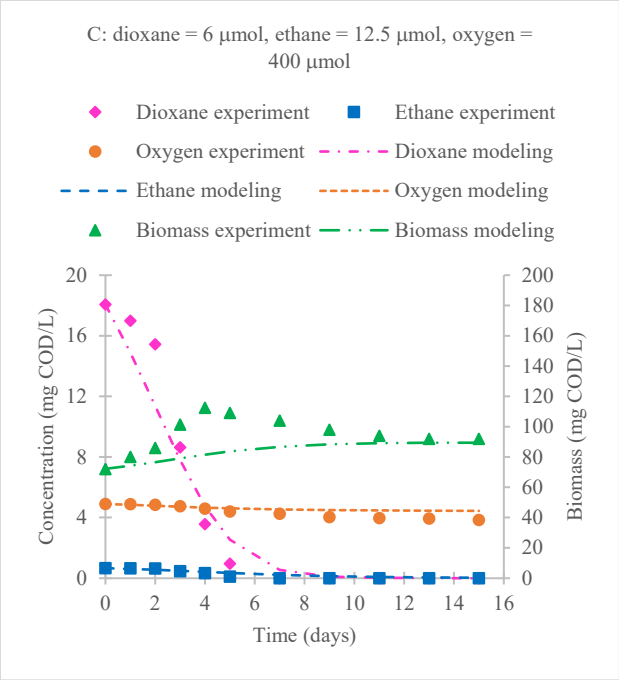
C: dioxane = 6 µmol, ethane = 12.5 µmol, oxygen = 400 µmol
Dioxane experiment
Ethane experiment
Oxygen experiment
Dioxane modeling
Ethane modeling
Oxygen modeling
Biomass experiment
Biomass modeling
Concentration (mg COD/L)
Biomass (mg COD/L)
Time (days)

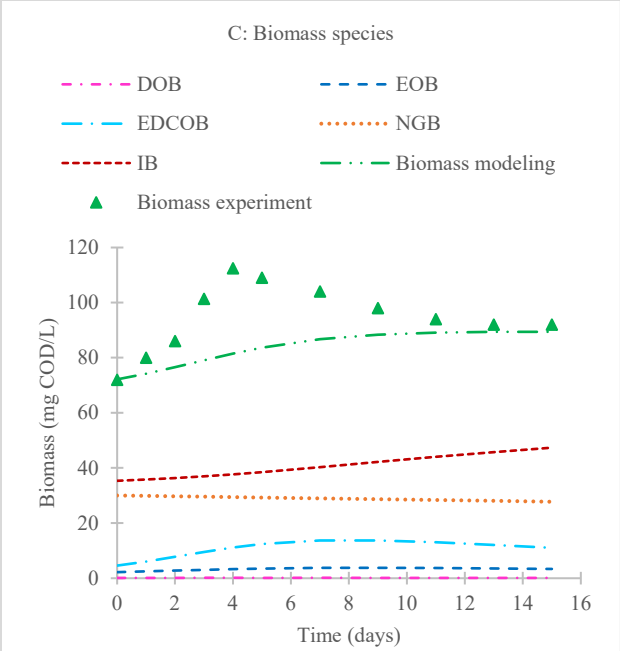
C: Biomass species
DOB
EOB
EDCOB
NGB
IB
Biomass modeling
Biomass experiment
Biomass (mg COD/L)
Time (days)

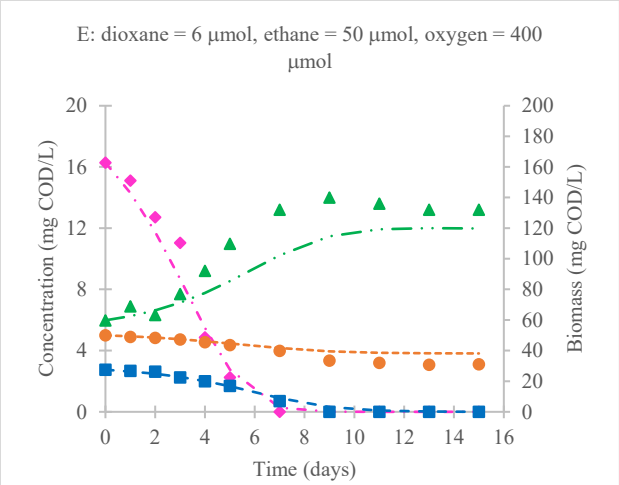
E: dioxane = 6 µmol, ethane = 50 µmol, oxygen = 400 µmol
Concentration (mg COD/L)
Biomass (mg COD/L)
Time (days)

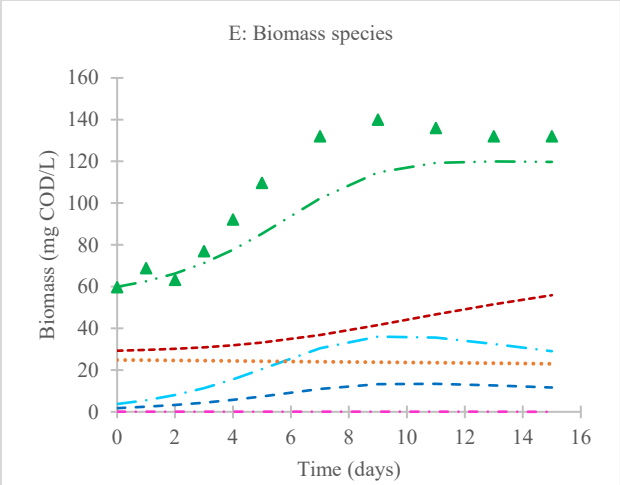
E: Biomass species
Biomass (mg COD/L)
Time (days)

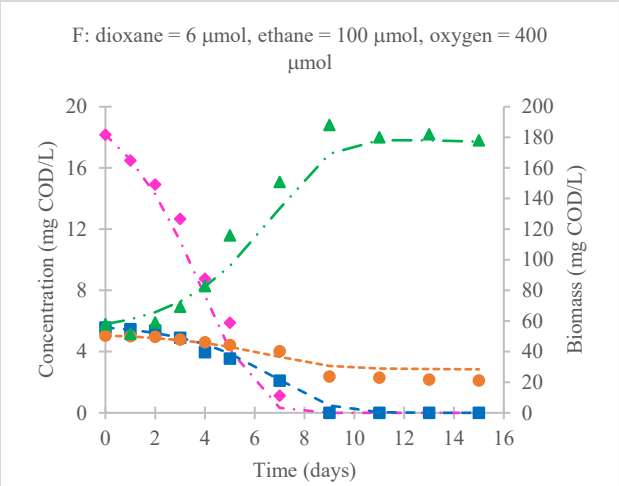
F: dioxane = 6 µmol, ethane = 100 µmol, oxygen = 400 µmol
Concentration (mg COD/L)
Biomass (mg COD/L)
Time (days)

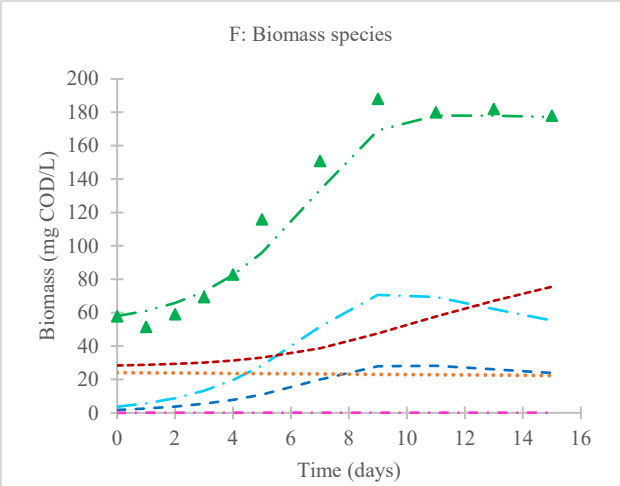
F: Biomass species
Biomass (mg COD/L)
Time (days)

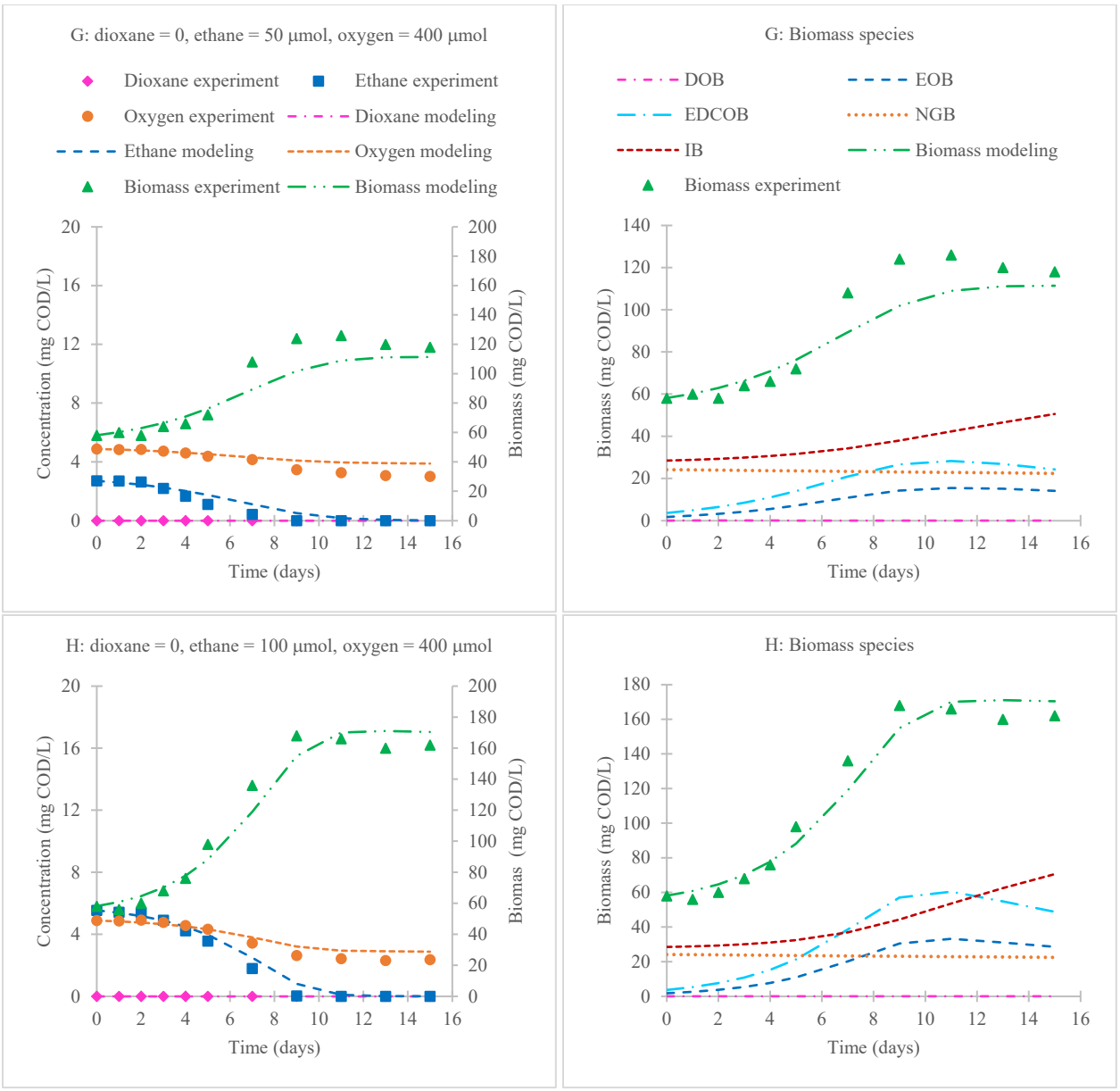

Figure 9: Comparison of modeling simulations and experimentally measured results for 1,4-D and ethane in kinetic batch experiments A – H. The concentrations of ethane and oxygen shown in the graphs are dissolved concentrations. Simulation use the best-fit parameters in Table 10.

The estimated parameters in Table 10 were evaluated by comparing the model-simulated results with an independent set of experimental values, shown in Figure 10. The parameterized model again captured all the major trends, and the mean sum of the squares of the relative residuals (MSRR) for D, I, and J were 0.06, 0.05, and 0.28, respectively.

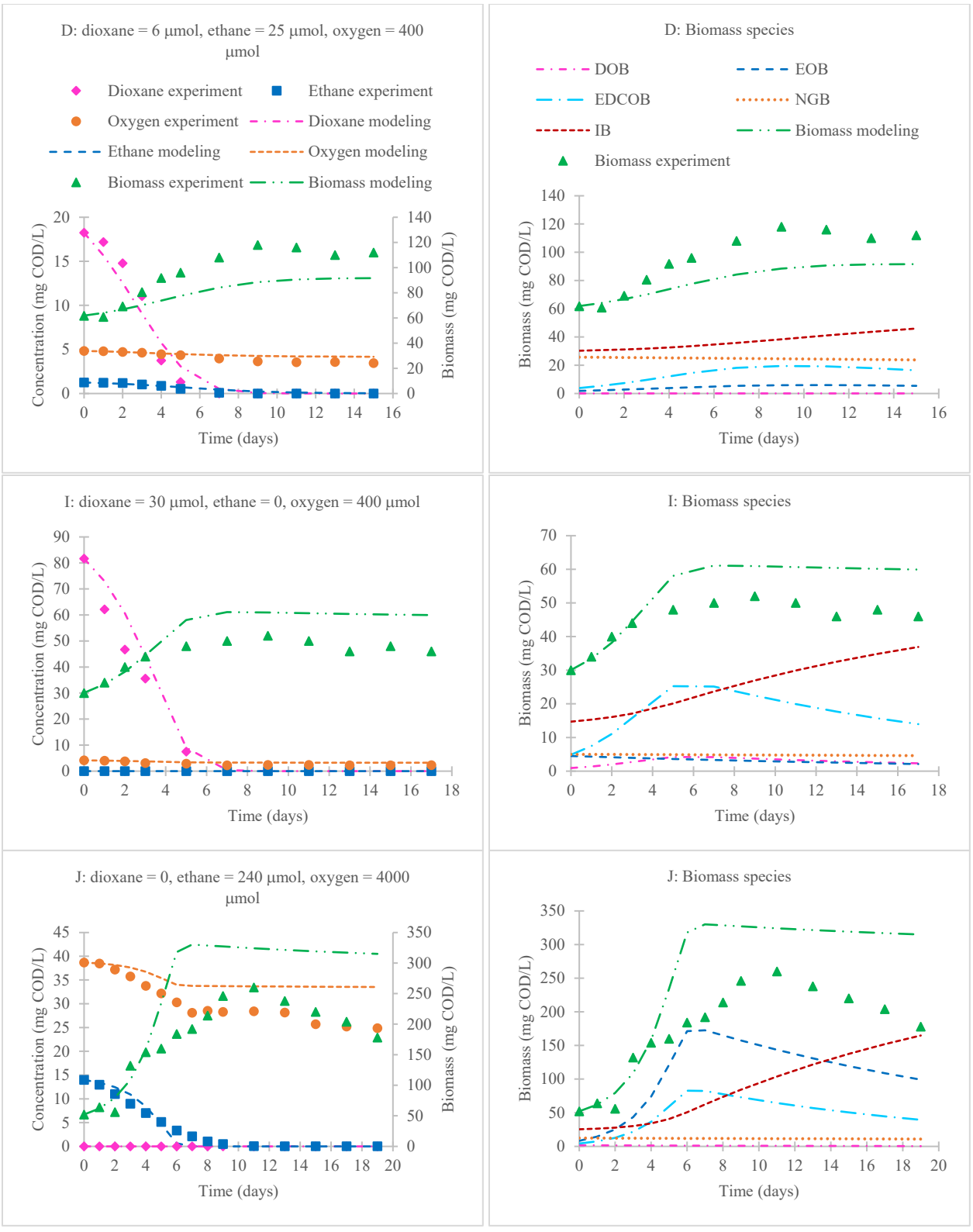

Figure 10: Model evaluation for 1,4-D and ethane kinetics using experiments D, I, and J, which were not used for parameter fitting.

4.4.2. Modeling of ethane and 1,4-dioxane biodegradation in the O_2-MBfR

The MBfR was modeled for the operating conditions used in the experiments at ASU and FSU. Figure 11 shows the progression of model-predicted biofilm thickness. During the start-up stage, the influent concentrations of 1,4-D and ethane were 1000 µg/L (11.35 µM) and 36000 µg/L (1200 µM), respectively. A hydraulic retention time of 8 hours was used to supply a discharge of 210 cm^3/d into the 70-cm^3 reactors.

In the simulations, the biofilm reached a steady-state condition with a biofilm thickness of 56 µm in 20 days. The boundary conditions at the interfaces between the membrane/biofilm and the biofilm/diffusion layers were satisfied for all the six solid biomass species. Similarly, the mass balance of the dissolved chemical species was checked by comparing the mass flux into the biofilm with the difference of the mass inflow and outflow in the reactor.

During the model-testing stages I-VI, the 1,4-D influent concentrations were 100 µg/L in MBfRs1&3 and 10 µg/L in MBfRs2&4, while the influent ethane concentrations varied from 0 to 3600 µg/L. Hydraulic retention times of 8 hours and 4 hours were used for MBfRs1&3 and MBfRs2&4, respectively. By the time that the model reached steady-state conditions in Stage I, significant biofilm losses had occurred, because the loading of ethane supplied had been greatly reduced (Figure 11). As a result of the biofilm losses, the removal efficiencies of 1,4-D declined.

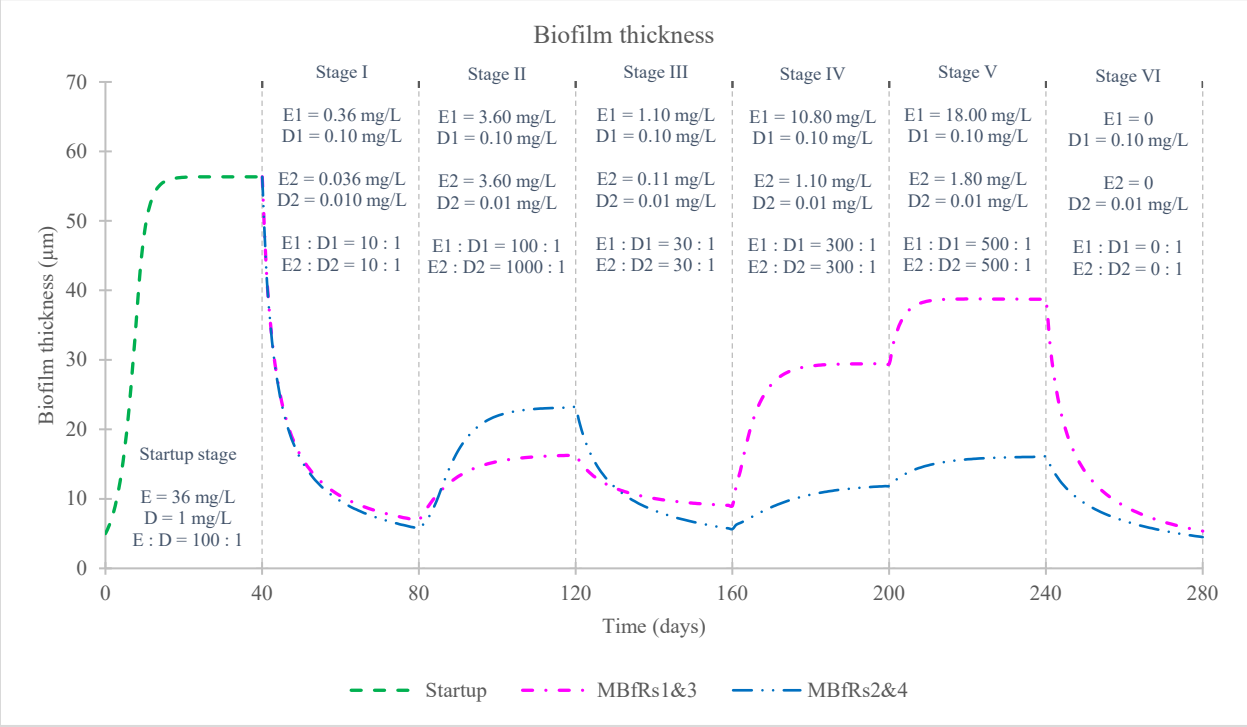

Figure 11: Biofilm thickness during the startup and testing stages of the O_2-MBfRs1&3 and MBfRs2&4. Startup, stage I, stage II, stage IV, and stage were operated by both MBfRs at ASU and FSU. Stage III was operated at FSU only while stage V was operated at ASU only. The E:D ratios are ethane: 1,4-D mole ratios.

After Stage I, the biofilm thickness responded to changes in the influent ethane concentration, particularly for MBfRs1&3, which had the higher influent concentrations of ethane and 1,4-D. Thus, the accumulation of biofilm and the consequent removal capacity for 1,4-D depended on the influent loading of ethane.

Table 12 shows a summary of the operating conditions and steady-state results for the O_2-MBfRs1&3 and MBfRs2&4. When the ethane-to-1,4-D mole ratio was 10 in stage I, the removal efficiencies of 1,4-D were about 29% in MBfRs1&3 and 10% in MBfRs2&4. After increasing the ethane concentration to 3600 µg/L in all MBfRs (stage II), the 1,4-D degradation efficiencies improved to 65% and 56% in MBfRs1&3 and MBfRs2&4, respectively. Similarly for stages III to V, the MBfRs performed better in removing 1,4-D when the ethane-to-1,4-D molar ratios were higher. In stage VI, the four MBfRs were simulated for 1,4-D removal with no ethane supply, the effluent 1,4-D concentrations increased to about 80 µg/L in MBfRs1&3 and to 9.1 µg/L in MBfRs2&4. These findings underscore the need to provide ethane as a primary substrate to maintain sufficient biofilm growth for 1,4-D biodegradation.

Table 12: Summary of simulated performance of the O_2-based MBfRs for the startup and testing stages

Model stage	ASU stage in experiment	FSU stage in experiment	HRT (hrs)	Mole ratio (E:D)	Influent ethane (µg/L)	Influent 1,4-D (µg/L)	Effluent ethane (µg/L)	Effluent 1,4-D (µg/L)	Ethane removed (%)	1,4-D removed (%)
Startup	Startup	Startup	8	100 : 1	36000	1000	1160	190	97	81
MBfRs1&3										
I	I	I	8	10 : 1	360	100	50	71	86	29
II	II	II	8	100 : 1	3600	100	168	35	95	65
III	-	III	8	30 : 1	1100	100	92	53	92	47
IV	III	IV	8	300 : 1	10800	100	365	21	97	80
V	IV	-	8	500 : 1	18000	100	569	17	97	83
VI	V	V	8	0 : 1	-	100	-	80	-	20
MBfRs2&4										
I	I	I	4	10 : 1	36	10	12	9.0	66	10
II	II	II	4	1000 : 1	3600	10	262	4.4	93	56
III	-	III	4	30 : 1	110	10	35	8.8	68	12
IV	III	IV	4	300 : 1	1100	10	126	6.1	89	40
V	IV	-	4	500 : 1	1830	10	167	5.1	91	49
VI	V	V	4	0 : 1	-	10	-	9.1	-	9.3

The simulated results were consistent with the experimental values in terms of the 1,4-D removal trends at various ethane-to-1,4-D molar ratios; this is shown in Figure 12. However, the model underestimated the performances of MBfRs2&4. The reason could be differences in kinetic parameters of biomass species that were able to degrade low concentrations of 1,4-D in MBfRs2&4 experiments versus those that were present during the kinetics batch experiments. The microbial community analysis showed that *P. dioxanivorans*, which is known to utilize 1,4-D as the only carbon source and electron donor (Mahendra and Alvarez-Cohen, 2005; Sales et al., 2013), was dominant during the enrichment and startup stages when the 1,4-D concentrations were high in the ASU experiments. However, during the testing stages, *Mycobacterium*, which can grow on 1,4-D (Deng et al., 2018a; He et al., 2017a, 2017b) and ethane (Lopes Ferreira et al., 2007; Ohkubo, 2009), dominated the biofilm. The relatively low 1,4-D influent concentrations may have selectively enriched bacteria with lower half-maximum-rate concentrations for 1,4-D, and those would have allowed greater removals when the 1,4-D concentration was lower in MBfRs2&4.

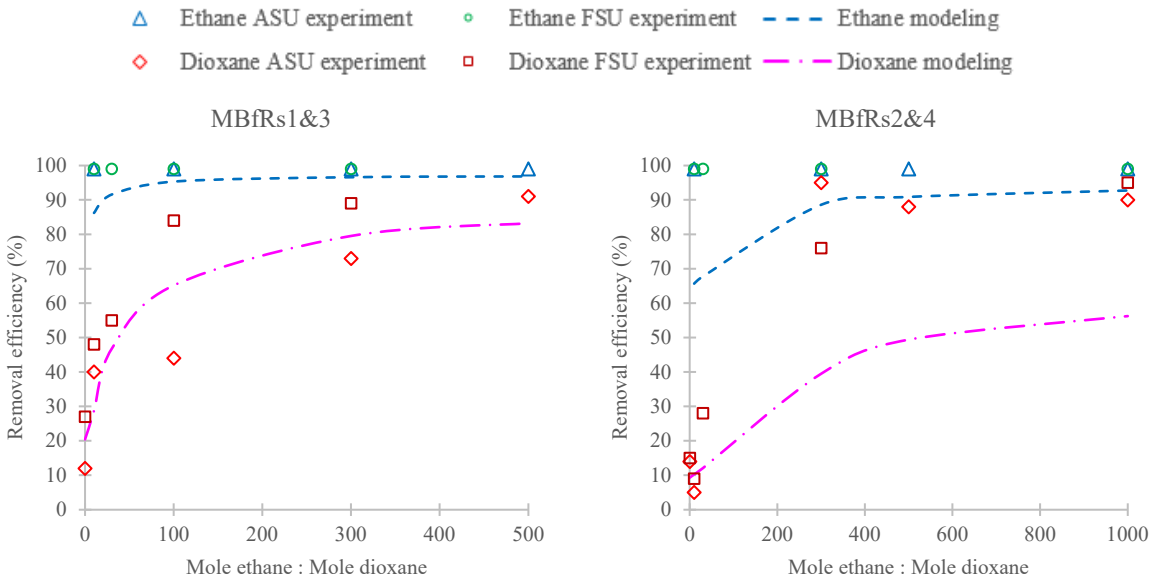

Figure 12: Comparison of the experimental and modeling results for ethane and 1,4-dioxane biodegradation in the O_2-MBfRs1&3 and O_2-MBfRs2&4

Figure 13 presents the simulated spatial distributions of the six biomass species in the biofilm for the various ethane and 1,4-D concentrations. In general, the biofilm's active biomass was dominated by EDCOB, as they can grow on ethane and 1,4-D. SMPOB and DOB fractions were minimal. When the ethane and 1,4-D influent concentrations decreased, the fraction of the active biomass groups decreased, while the fraction of the inert biomass (IB) increased and was almost all of the biomass for no ethane in the influent. These trends reinforce the need to have a sufficient supply of ethane as the primary substrate to support an active biofilm. IB was less than 50% of the biofilm only for E:D $\geq$ 300 mole ethane per mole 1,4-D.

Figure 14 presents profiles of the five chemical species in the biofilm at various ethane and 1,4-D concentrations. The concentrations of ethane and 1,4-D were higher on the liquid side, since they diffuse from the bulk water into the biofilm. O_2 was delivered from the fibers, and its

concentration decreased from the membrane side to the liquid side of the biofilm. UAP and BAP were produced in the biofilm and diffuse into the bulk water; hence, their concentrations are higher on the membrane side. When the ethane and 1,4-D influent concentrations decreased, the concentrations of UAP and BAP decreased due to lower microbial activity and loss of active biomass.

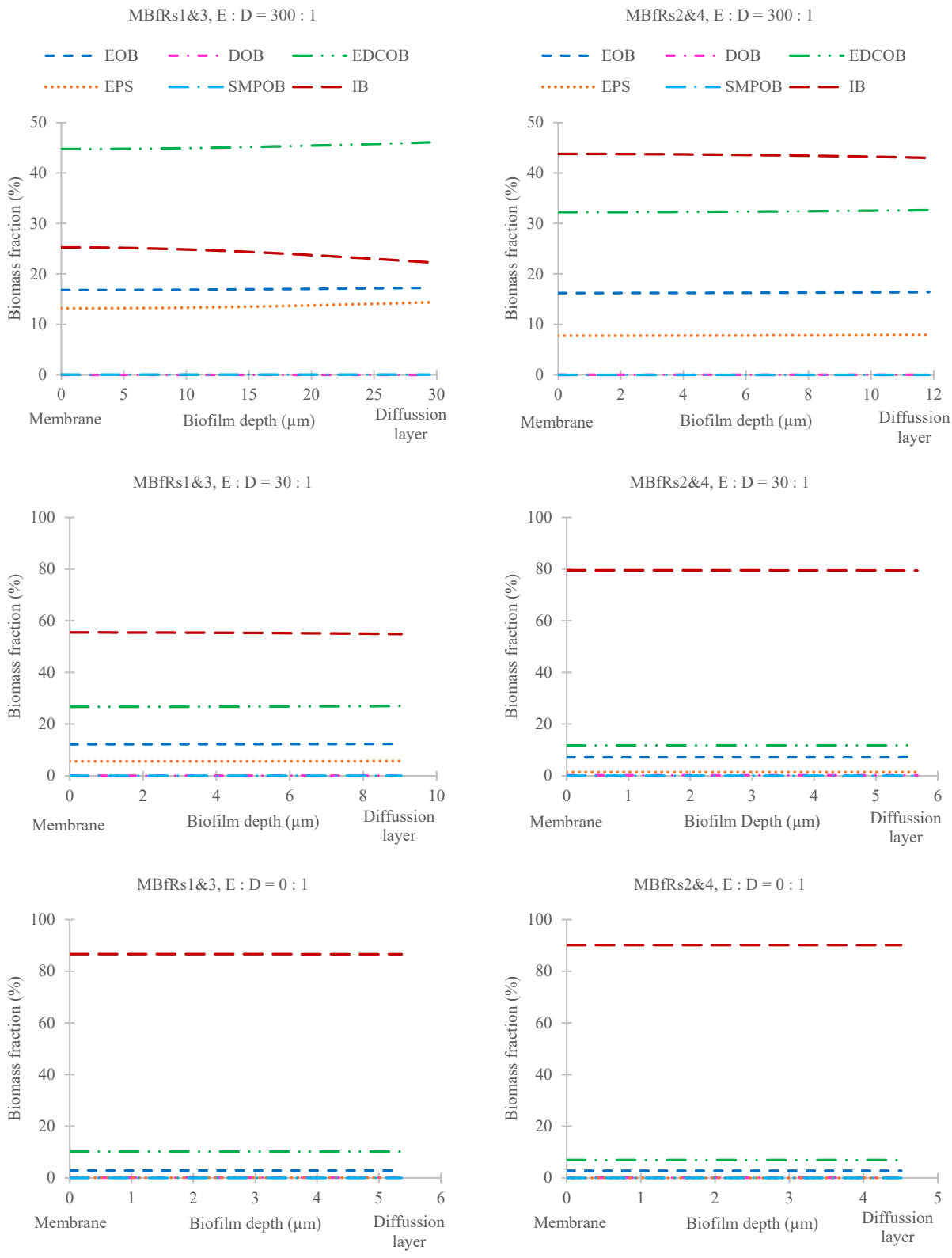

Figure 13: Simulated fractions of solid (biomass) species within the biofilm at different ethane-to-1,4-D mole ratios

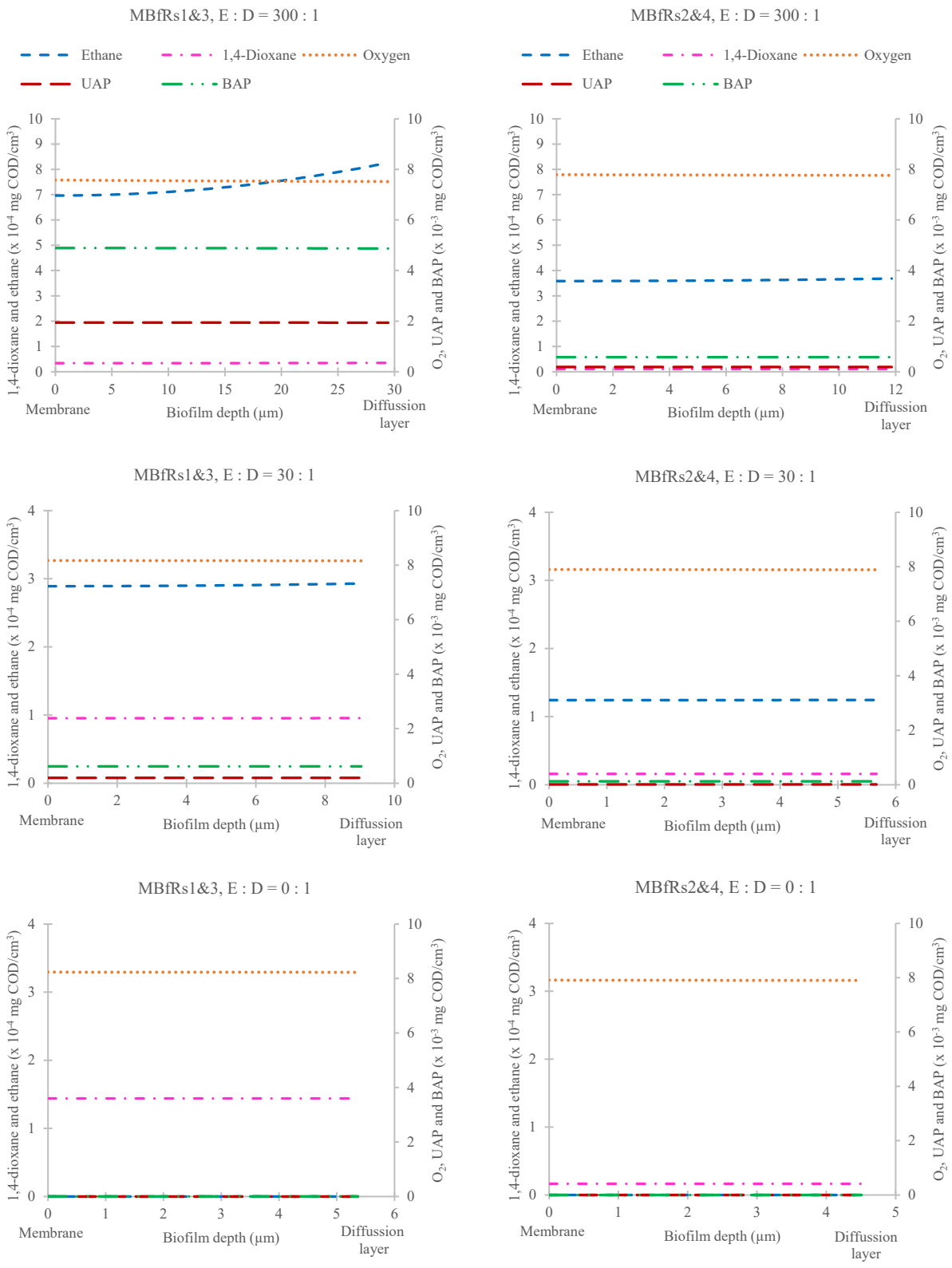

Figure 14: Simulated concentration of the soluble species at different ethane-to-1,4-D mole ratios

4.5. Task 5: Cost analysis

APTwater, LLC, which has developed and launched a commercial scale H_2-based MBfR for nitrate treatment (called ARoNITE), has programs for equipment sizing and capital and operating cost estimation for H_2-based MBfR systems. APTwater modified the design programs for using O_2 in place of H_2. Two separate cases were chosen for cost analyses. The first case is based on the best experimental results obtained thus far (denoted as "Optimum Experimental Case"). Since large improvements are likely for any early-stage technology, a second case of five times higher loading was chosen as an "Optimistic Case."

For both cases, a full-scale system is for a flow rate of 100 gallon/minute (100 gpm) and a typical 1,4-D concentration of 100 μg/L. Co-contamination with TCE and TCA is not considered. Thus, all ethane is supplied from an external source. The design for 1,4-D removal involves a two-stage system: stage one to lower the 1,4-D concentration from 100 to 10 μg/L, and stage two to lower the concentration to ≤ 0.5 μg/L. Should the groundwater concentration be ~ 10 μg/L, only the second stage would be required.

For the "Optimum Experimental Case," the design loading from operating stage III of Tables 4 and 5 was used. At this design loading and applying APTwater's MBfR module containing 170 m^2 membrane area, approximately 226 modules would be required in Stage 1 and 112 modules in Stage 2. The expected capital and operating costs of this system are shown in Table 13. Power was assumed to cost \$0.10/kw-hr and liquid oxygen to cost \$1.80/CCF. The total oxygen requirement was estimated at 14.6 kg/day. Ethane cost was based on a verbal quote from a commercial supplier, Airgas, Inc., of \$2,166 for a bulk size "Y" cylinder containing 161 kg of technical grade ethane (>99% purity) with ethane usage of 5.9 kg/day.

For the "Optimistic Case," using five-times larger design loading, and thus one-fifth the required membrane area, approximately 46 full-scale modules would be required in Stage 1 and 22 modules in Stage 2. The estimated capital and operating expense for the Optimistic Case is shown in Table 14. The capital cost of a system with one-fifth the membrane area is about one-half of the first case, because some system costs (e.g., process instrumentation and controls, safety systems, and forwarding pumps) do not scale down linearly with the membrane module number. Some operating costs for the "Optimistic Case," like power (primarily MBfR recirculation energy) and module replacements, are significantly lower, but ethane and oxygen requirements do not change, as they are related to the kg/d input rates of 1,4-D and ethane.

The preliminary cost analyses in Table 13 and 14 are based solely on experimental results obtained in the limited-scope project. They do not reflect any optimization based on systematic experimentation or model simulations. Both strategies are promising areas for future research.

Table 13: Estimated Capital and Operating Expense for a two-stage O_2-Based MBfR (100 gpm flow, 100 µg 1,4-D/L, 19.9 kg 1,4-dioxane/yr) for the "Optimum Experimental Case"

Budgetary Capital Cost		
	Equipment	$2,600,000
	Site improvements and design	$370,000
	Start-up costs	$75,000
	Contingency	$560,000
	Total installed cost	$3,605,000
	Installed cost per kg 1,4-D/yr	$181,000
Annual Operating Cost		
	Labor	$26,700
	Consumables (ethane)	$33,000
	Consumables (oxygen)	$4,500
	Parts and maintenance	$44,000
	Module replacement	$92,000
	Power	$18,000
	Total annual costs	$218,200
	Total operating cost per kg 1,4-D	$11,000

Table 14: Estimated Capital and Operating Expense for a two-stage O_2-Based MBfR (100 gpm flow, 19.9 kg 1,4-dioxane/yr) for the Optimistic Case

Budgetary Capital Cost		
	Equipment	$1.300,000
	Site improvements and design	$150,000
	Start-up costs	$75,000
	Contingency	$250,000
	Total installed cost	$1,775,000
	Installed cost per kg 1,4-D/yr	$89,200
Annual Operating Cost		
	Labor	$26,700
	Consumables (ethane)	$33,000
	Consumables (oxygen)	$4,500
	Parts and maintenance	$21,000
	Module replacement	$19,000
	Power	$3,600
	Total annual costs	$107,800
	Total operating cost per kg 1,4-D	$5,400

5. Implications for Future Research and Benefits

5.1. Minimum required ethane concentrations and their availability at the contaminated sites

The team completed two phases of the limited scope project. In Phase I, the results demonstrated the concept of a platform for synergistic treatment of TCE, TCA, and 1,4-D: a TCE/TCA-reducing H_2-MCfR followed by a 1,4-dioxane-oxidizing O_2-MBfR. The ethane produced from TCE and TCA reduction in the H_2-MPfR was used as the primary electron donor for microbially co-oxidizing 1,4-D in the O_2-MBfR. The other minor by-products from TCE and TCA reduction, including DCA and MCA, were also degraded in the O_2-MBfR.

Phase II of the project focused on the 1,4-dioxane-oxidizing O_2-MBfR and determined that the mole ratio of ethane: 1,4-dioxane = ~300:1 is the minimum ratio for removing 1,4-D to below the detection limit of 0.5 µg/L, which is only slightly above the health-based reference level of 0.35 µg/L and below the groundwater and drinking-water guideline levels established by most states. The conclusion is based on >500-day continuous operation of four O_2-MBfRs: Two O_2-MBfRs were operated by the ASU team with a mixed culture and the other two identical O_2-MBfRs were operated by the FSU team with a different mixed culture. One practical implication is that the minimum ethane:1,4-dioxane ratio probably does not significantly depend on the culture.

The two O_2-MBfRs operated by each team had two different influent 1,4-D concentrations: 100 and 10 µg/L. In the O_2-MBfRs fed with 10 µg/L of 1,4-D, an ethane: 1,4-dioxane ratio of ≥300 was able to remove 1,4-D to below the detection limit in a single-stage reactor. In the O_2-MBfRs fed with 100 µg/L of 1,4-D, an ethane: 1,4-dioxane ratio ≥300 was able to remove 1,4-D to ~10 µg/L in a single-stage reactor. The practical implication is that a two-stage O_2-MBfR may be the best strategy to treat a water containing 100 µg/L of 1,4-D.

We reviewed reported mole ratio range of TCE:1,4-D in the groundwater (Anderson et al., 2012). If TCA also is present, the TCE+TCE:1,4-D ratio will be larger. As shown in Figure 15, the ratio ranges from 1:1 to 1:1000, with many locations exceeding 1:300. Assuming all TCE is converted to ethane, external ethane addition for these groundwater with high TCE:1,4-dioxane ratios would not be needed, although a preceding MCfR would be required to convert TCE and TCA to ethane.

Table 15 lists suggested ethane concentrations based on the 300:1 mole ratio. As shown in Figure 15, most 1,4-dioxane concentrations are in the range of 1 to 100 µg/L (10^0 – 10^2 ppb). Table 15 lists needed ethane concentrations for input 1,4-dioxane concentrations of ≤ 10, 50, and 100 µg/L. The needed ethane concentrations for 50 and 100 µg/L 1,4-dioxane were set based directly on the 300:1 mole ratio. It is computed from the 300:1 mole ratio of higher 1,4-dioxane concentrations: added ethane concentration in mg/L = influent 1,4-dioxane concentration x 0.1. For example, an influent concentration of 100 µg/L requires added ethane of 10 mg/L.

The ethane concentration for ≤ 10 µg/L 1,4-dioxane was set based on accumulating sufficient biofilm, which is based on having an influent concentration of ethane about 10-fold larger than its

minimum concentration to support a steady-state biofilm, or S_e^{min}. We estimated $S_e^{min} \sim 0.1$ mg/L using Equation 14 (Rittmann & McCarty, 2001).

$$S_e^{min} = K_{ec} \frac{b'}{Y_e q_{ec} - b'} \tag{144}$$

in which K_{ec} is the half-maximum-rate concentration of ethane oxidation by EDCOB (1.45 mg COD · L^{-1}), Y_e is the biomass yield of ethane (0.50 mg COD · mg COD^{-1}), q_{ec} is the maximum specific ethane utilization rate of EDCOB (1.39 mg COD · mg COD^{-1} · d^{-1}), b' is the total biomass loss rate coefficient (d^{-1}), which is comprised of biomass decay coefficient of EDCOB (0.04 d^{-1}) and specific biofilm-detachment rate, b_{det} (d^{-1}) estimated from the biofilm detachment coefficient of 36 cm^{-1} d^{-1} (Tang et al., 2012) and a steady-state biofilm thickness (L_f) that varies from 10 µm to 30 µm based on the biofilm model developed through this project. We used the EDCOB for the calculation of S_e^{min}, as they are the dominant biomass species in the biofilm. Thus, the lowest input concentration of ethane is approximately 1 mg/L, which also corresponds to 3.7 mg COD/L.

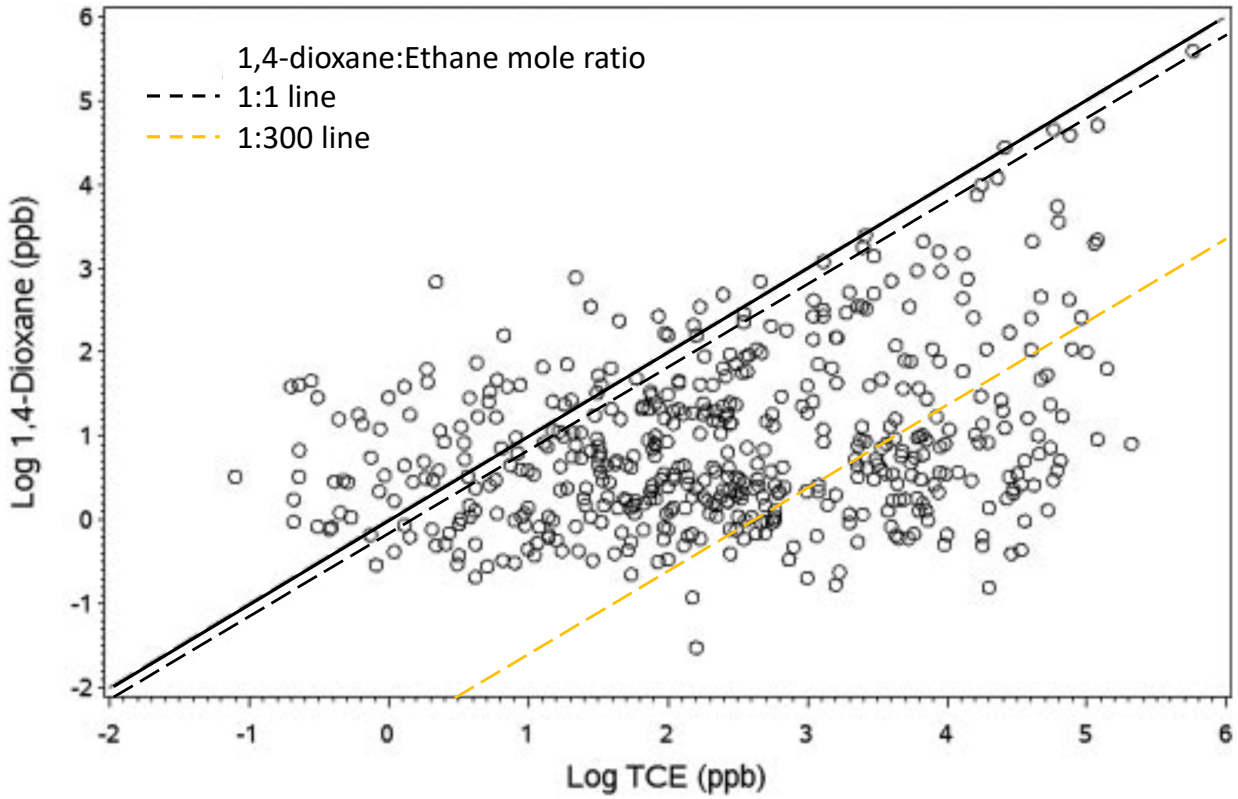

Figure 15: Co-contamination of TCE and 1,4-dioxane in the groundwater. The yellow dashed line highlights the 300:1 mole ratio. The figure was adapted from Anderson et al., (2012).

Table 15: Suggested minimum ethane concentrations for removing various concentrations of 1,4-dioxane in exemplary scenarios. 1 mg/L of ethane = 3.7 mg COD/L.

1,4-dioxane concentration (µg/L)	Suggested minimum ethane concentration (mg/L)
≤ 10	1.0
30	3.0
50	5.0
100	10

5.2. Biodegradation kinetics summary and implications for future research

We adapted the MBfR model framework developed in Phase I to simulate the O_2-MBfRs in Phase II. The ethane and 1,4-D degradation kinetic parameters were determined through batch tests combined with kinetics modeling, and then were input into the O_2-MBfR model. The adapted model simulated well all measured trends of 1,4-D and ethane removal in the tested O_2-MBfRs. For example, a higher ethane: 1,4-D ratio led to greater biofilm accumulation and more removal of 1,4-D. The model simulations deviated from experimental MBfR results for low influent concentration of 1,4-D, which also corresponded to lower influent concentration of ethane: the model simulated less 1,4-D removal than occurred experimentally in MBfRs2&4. This deviation may be explained by significant differences in the microbial communities between MBfRs2&4, which had low ethane and 1,4-D concentrations, and the batch kinetic experiments based on cultures enriched with and tested with higher concentrations.

The hypothesis of different microbial communities is supported by our phylogenetic analyses. The dominant genera dramatically shifted from *Pseudonocardia* in the inoculum and startup stage to *Mycobacterium* and *Methylibium* through the long-term operation of the O_2-MBfRs. The relative abundances of monooxygenases also changed in parallel to the trends of community structure: shifted from PMO dominant to TMO, PMO and MMO coexist. The microbial communities were significantly different between the two MBfRs fed with a low 1,4-dioxane concentration (i.e., 10 µg/L in MBfRs2&4) and the two MBfRs fed with a high 1,4-dioxane concentration (i.e., 100 µg/L in MBfRs1&3).

5.3. Microbial-community summary and its implications for future research

The microbial community results also indicate a transfer from metabolic oxidation of 1,4-D to co-oxidation of ethane and 1,4-D once the 1,4-D influent concentrations were decreased to 10 and 100 µg/L. Eventually, the biofilm microbial communities in the O_2-MBfRs were dominated by the genera *Mycobacterium*, which is a co-oxidizer. This points to a need to study the biodegradation kinetics of 1,4-D and ethane at low concentrations (i.e., µg/L level); this has not been reported in the literature.

Understanding better the role of the 1,4-D-biodegrading bacteria detected in our MBfRs is key, as we now have only circumstantial (albeit strong) evidence that they are involved in the co-oxidation of 1,4-D. Given the low 1,4-D concentrations used and that most other reported studies are with bacteria growing in suspension, not in biofilms, assigning specific function to bacteria thriving in the biofilms will advance the field in a major way. Further community analysis -- including metagenomic and metatranscriptomic analyses with changing conditions and appropriate controls -- will help us define which monooxygenases and which bacteria are involved in 1,4-D and ethane co0oxidation in the biofilms in our MBfRs.

5.4. Cost summary and implications for future research

A typical case of 100 gallons/min flow at a 1,4-D concentration of 100 μg/L was chosen as a basis for preliminary design and cost analysis. This flow and concentration provide a 1,4-D loading that could be used, along with the experimental MBfR performance data, to determine a system size. This design loading and applying APTwater's MBfR module containing 170 m^2 membrane area would require approximately 226 modules in Stage 1 and 112 modules in Stage 2. The expected capital and operating costs of this system per kg 1,4-D/yr are $181,000 and $11,000 respectively. An "Optimistic Case" using five-fold larger design loading would require one-fifth required membrane area, or approximately 46 full-scale modules in Stage 1 and 22 modules in Stage 2. The estimated capital and operating expenses per kg 1,4-D/yr are $89,200 and $5,400 respectively.

This cost summary was based only on the experimental MBfR performance data that correspond to only one fixed flow rate for each MBfR. The experiments were designed to evaluate fundamental kinetics and mechanisms; they were not set up to optimize performance. Likewise, the mathematical modeling was designed and implemented to quantify basic mechanisms and kinetics, not optimize performance. Since the flow rate, which is proportional to the 1,4-D loading, is the major factor that determines the costs, finding the maximum flow rate (i.e., maximum loading rate) that gives satisfactory 1,4-D removal is key to reducing costs. Future research (experimental and modeling) should focus on determining the maximum flow rate that achieved satisfactory 1,4-D removal (i.e., a true maximum loading rate).

5.5. Summary of future research needs

In Phase I, we demonstrated the synergistic platform. In Phase II, we determined that the minimum ethane:1,4-D mole ratio is around 300 to drive the 1,4-D concentration to below the detection limit, generated kinetic and stoichiometric parameters for ethane and 1,4-biodegradation, and showed that a diverse group of bacteria can co-oxidize ethane and 1,4-D. We also uncovered the following fundamental and practical knowledge gaps that need to be filled to ensure that the platform performs reliably and cost-effectively at the pilot or field scale:

1) The kinetics of 1,4-D and ethane biodegradation at relatively high concentrations were well-determined in Phase II, but our experimental results in the O_2-MBfR, combined with modeling results, suggest that continual enrichment with low concentrations altered the microbial community in ways that affected the kinetic and stoichiometry parameters. Determining the

kinetic and stoichiometry parameters for microbial communities truly representative of MBfR biofilms is necessary to ensure that model prediction are accurate.

2) Inputting the most reliable parameters into the already developed O_2-MBfR model will allow us to optimize design and operating strategies in advance of a pilot study. For example, we can evaluate how a pilot-scale system will respond to changes in flow rate and influent concentrations, and then we can truly determine the maximum 1,4-D loading rate that gives an effluent of 1,4-D below 0.5 μg/L.

3) Because only synthetic groundwater was used in Phases I and II, any impacts of real-world groundwater chemistry are unknown. A platform demonstration with actual contaminated groundwater is needed to ensure the reliable performance of the platform. It is better to test this with a laboratory-scale two-stage platform at the maximum 1,4-D loading rate determined by the model with improved parameter values.

4) When the above three knowledge gaps are filled, we will be ready to design, build, and operate a pilot-scale reactor in cooperation with APTwater, LLC.

5.6. Future research plan

We envision a follow-on project occurring in two phases. The first phase will focus on addressing the first three knowledge gaps over two years. The following three tasks are proposed to address the three knowledge gaps.

Task 1 (in the first eight months): Determine the kinetic and stoichiometry parameters for microbial communities truly representative of O_2-MBfR biofilms. The methods are similar to Phase II batch experiments and modeling, but the ethane and 1,4-D concentrations used in the batch tests will be much lower (at μg/L level).

Task 2 (in the second eight months): Use the kinetic and stoichiometry parameters determined in Task 1 to predict (using the existing model of the O_2-MBfR biofilm) the maximum 1,4-D loading rate that gives an effluent 1,4-D concentration of <0.5 μg/L.

Task 3 (in the third eight months): Use the maximum flow rate determined in Task 2 to test the two-stage platform fed with a real groundwater. The two-stage platform includes a H_2-based MPfR to reduce TCE and 1,1,1-TCA to ethane, followed by an O_2-based MBfR to co-oxidize ethane and 1,4-D.

The second-phase research, lasting for an additional two years, will adapt APTwater's H_2-based MBfR modules to become an H_2-MPfR (first stage) and O_2-based MBfR (second stage). The two-stage platform will be evaluated at a field site using the optimum operating conditions predicted by the model.

Literature Cited

Adamson, D.T., Anderson, R.H., Mahendra, S., Newell, C.J., 2015. Evidence of 1,4-Dioxane Attenuation at Groundwater Sites Contaminated with Chlorinated Solvents and 1,4-Dioxane. Environ. Sci. Technol. 49, 6510–6518. https://doi.org/10.1021/acs.est.5b00964

Ahmed, T., Semmens, M.J., Voss, M.A., 2004. Oxygen transfer characteristics of hollow-fiber, composite membranes. Adv. Environ. Res. 8, 637–646. https://doi.org/10.1016/S1093-0191(03)00036-4

Anderson, R.H., Anderson, J.K., Bower, P.A., 2012. Co-Occurrence of 1,4-Dioxane with Trichloroethylene in Chlorinated Solvent Groundwater Plumes at US Air Force Installations: Fact or Fiction. Integr. Environ. Assess. Manag. 8, 731–737. https://doi.org/10.1002/ieam.1306

APHA, 2012. Standard Methods for the Examination of Water and Waste Water, American Public Health Association, American Water Works Association, Water Environment Federation. https://doi.org/10.4236/jmmce.2020.84016

Barajas-Rodriguez, F.J., Freedman, D.L., 2018. Aerobic biodegradation kinetics for 1,4-dioxane under metabolic and cometabolic conditions. J. Hazard. Mater. 350, 180–188. https://doi.org/10.1016/j.jhazmat.2018.02.030

Bernhardt, D., Diekmann, H., 1991. Degradation of dioxane, tetrahydrofuran and other cyclic ethers by an environmental Rhodococcus strain. Appl. Microbiol. Biotechnol. 36, 120–123.

Bolger, A.M., Lohse, M., Usadel, B., 2014. Trimmomatic: a flexible trimmer for Illumina sequence data. Bioinformatics 30, 2114–2120.

Buswell, J.A., Eriksson, K.-E., 1988. Vanillate hydroxylase from *Sporotrichum pulverulentum*. Methods Enzymol. 161, 274–281.

Butler, C., Boltz, J., 2014. Biofilm Processes and Control in Water and Wastewater Treatment, in: Comprehensive Water Quality and Purification. pp. 90–107. https://doi.org/10.1016/B978-0-12-382182-9.00083-9

Chaumeil, P.-A., Mussig, A.J., Hugenholtz, P., Parks, D.H., 2020. GTDB-Tk: a toolkit to classify genomes with the Genome Taxonomy Database.

Chen, D., Jin, X., Chen, Jing, Ye, J., Jiang, N., Chen, Jian-meng, 2016. International Biodeterioration & Biodegradation Intermediates and substrate interaction of 1,4-dioxane degradation by the effective metabolizer *Xanthobacter flavus* DT8. Int. Biodeterior. Biodegradation 106, 133–140. https://doi.org/10.1016/j.ibiod.2015.09.018

Choi, J.Y., Lee, Y.-J., Shin, J., Yang, J.-W., 2010. Anodic oxidation of 1, 4-dioxane on boron-doped diamond electrodes for wastewater treatment. J. Hazard. Mater. 179, 762–768.

Coleman, N. V, Yau, S., Wilson, N.L., Nolan, L.M., Migocki, M.D., Ly, M., Crossett, B., Holmes, A.J., 2011. Untangling the multiple monooxygenases of *Mycobacterium chubuense* strain NBB4, a versatile hydrocarbon degrader. Environ. Microbiol. Rep. 3, 297–307.

Cussler, E.L., 2009. Diffusion Mass Transfer in Fluid Systems, Third. ed. Cambridge University Press.

Deng, D., Li, F., Li, M., 2018a. A novel propane monooxygenase initiating degradation of 1, 4-

dioxane by *Mycobacterium dioxanotrophicus* PH-06. Environ. Sci. Technol. Lett. 5, 86–91.

Deng, D., Li, F., Wu, C., Li, M., 2018b. Synchronic biotransformation of 1, 4-dioxane and 1, 1-dichloroethylene by a gram-negative propanotroph *Azoarcus* sp. DD4. Environ. Sci. Technol. Lett. 5, 526–532.

Deng, D., Pham, D.N., Li, F., Li, M., 2020. Discovery of an inducible toluene monooxygenase that cooxidizes 1, 4-dioxane and 1, 1-dichloroethylene in propanotrophic *Azoarcus* sp. strain DD4. Appl. Environ. Microbiol. 86, e01163-20.

Dourson, M.L., Higginbotham, J., Crum, J., Burleigh-Flayer, H., Nance, P., Forsberg, N.D., Lafranconi, M., Reichard, J., 2017. Update: mode of action (MOA) for liver tumors induced by oral exposure to 1, 4-dioxane. Regul. Toxicol. Pharmacol. 88, 45–55.

EPA, 2017. Technical Fact Sheet – 1,4-Dioxane. United States Environmental Protection Agency Office.

Gou, Z., Xing, X.-H., Luo, M., Jiang, H., Han, B., Wu, H., Wang, L., Zhang, F., 2006. Functional expression of the particulate methane mono-oxygenase gene in recombinant *Rhodococcus erythropolis*. FEMS Microbiol. Lett. 263, 136–141.

Han, P., Bartels, D.M., 1996. Temperature Dependence of Oxygen Diffusion in H2O and D2O. J. Phys. Chem. 100, 5597–5602. https://doi.org/10.1021/jp952903y

He, Y., Mathieu, J., Yang, Y., Yu, P., da Silva, M.L.B., Alvarez, P.J.J., 2017a. 1, 4-Dioxane biodegradation by *Mycobacterium dioxanotrophicus* PH-06 is associated with a group-6 soluble di-iron monooxygenase. Environ. Sci. Technol. Lett. 4, 494–499.

He, Y., Wei, K., Si, K., Mathieu, J., Li, M., Alvarez, P.J.J., 2017b. Whole-genome sequence of the 1, 4-dioxane-degrading bacterium *Mycobacterium dioxanotrophicus* PH-06. Genome Announc. 5.

Huang, H., Shen, D., Li, N., Shan, D., Shentu, J., Zhou, Y., 2014. Biodegradation of 1, 4-dioxane by a novel strain and its biodegradation pathway. Water, Air, Soil Pollut. 225, 1–11.

Inoue, D., Tsunoda, T., Sawada, K., Yamamoto, N., Saito, Y., Sei, K., Ike, M., 2016. 1,4-Dioxane degradation potential of members of the genera *Pseudonocardia* and *Rhodococcus*. Biodegradation 27, 277–286. https://doi.org/10.1007/s10532-016-9772-7

Isaka, K., Udagawa, M., Kimura, Y., Sei, K., Ike, M., 2016. Biological wastewater treatment of 1, 4-dioxane using polyethylene glycol gel carriers entrapping Afipia sp. D1. J. Biosci. Bioeng. 121, 203–208.

Kane, S.R., Chakicherla, A.Y., Chain, P.S.G., Schmidt, R., Shin, M.W., Legler, T.C., Scow, K.M., Larimer, F.W., Lucas, S.M., Richardson, P.M., 2007. Whole-genome analysis of the methyl tert-butyl ether-degrading beta-proteobacterium *Methylibium petroleiphilum* PM1. J. Bacteriol. 189, 1931–1945.

Karges, U., Becker, J., Püttmann, W., 2018. 1,4-Dioxane pollution at contaminated groundwater sites in western Germany and its distribution within a TCE plume. Sci. Total Environ. 619–620, 712–720. https://doi.org/10.1016/j.scitotenv.2017.11.043

Kim, Y.S., Roh, S.G., Kim, S.B., 2020. *Gordonia insulae* sp. Nov., isolated from an island soil. Int. J. Syst. Evol. Microbiol. 70, 2079–2083. https://doi.org/10.1099/ijsem.0.004023

Kotani, T., Kawashima, Y., Yurimoto, H., Kato, N., Sakai, Y., 2006. Gene structure and

regulation of alkane monooxygenases in propane-utilizing *Mycobacterium* sp. TY-6 and *Pseudonocardia* sp. TY-7. J. Biosci. Bioeng. 102, 184–192.

Laspidou, C.S., Rittmann, B.E., 2002. Non-steady state modeling of extracellular polymeric substances, soluble microbial products, and active and inert biomass. Water Res. 36, 1983–1992.

Leaist, D.G., MacEwan, K., Stefan, A., Zamari, M., 2000. Binary Mutual Diffusion Coefficients of Aqueous Cyclic Ethers at 25 °C. Tetrahydrofuran, 1,3-Dioxolane, 1,4-Dioxane, 1,3-Dioxane, Tetrahydropyran, and Trioxane. J. Chem. Eng. Data 45, 815–818. https://doi.org/10.1021/je000079n

Li, F., Deng, D., Li, M., 2020. Distinct Catalytic Behaviors between Two 1,4-Dioxane-Degrading Monooxygenases: Kinetics, Inhibition, and Substrate Range. https://doi.org/10.1021/acs.est.9b05671

Li, M., Mathieu, J., Liu, Y., Van Orden, E.T., Yang, Y., Fiorenza, S., Alvarez, P.J.J., 2013. The Abundance of Tetrahydrofuran/Dioxane Monooxygenase Genes (*thmA*/*dxmA*) and 1,4-Dioxane Degradation Activity Are Significantly Correlated at Various Impacted Aquifers. Environ. Sci. Technol. Lett. 1, 122–127. https://doi.org/10.1021/ez400176h

Lien, H.L., Zhang, W.X., 2007. Nanoscale Pd/Fe bimetallic particles: Catalytic effects of palladium on hydrodechlorination. Appl. Catal. B Environ. 77, 110–116. https://doi.org/10.1016/j.apcatb.2007.07.014

Lopes Ferreira, N., Mathis, H., Labbé, D., Monot, F., Greer, C.W., Fayolle-Guichard, F., 2007. n-Alkane assimilation and tert-butyl alcohol (TBA) oxidation capacity in *Mycobacterium austroafricanum* strains. Appl. Microbiol. Biotechnol. 75, 909–919. https://doi.org/10.1007/s00253-007-0892-1

Luo, Y.-H., Long, X., Wang, B., Zhou, C., Tang, Y., Krajmalnik-Brown, R., Rittmann, B.E., 2021. A Synergistic Platform for Continuous Co-removal of 1, 1, 1-Trichloroethane, Trichloroethene, and 1, 4-Dioxane via Catalytic Dechlorination Followed by Biodegradation. Environ. Sci. Technol.

Ma, F., Wang, Y., Yang, J., Guo, H., Su, D., Yu, L., 2021. Degradation of 1, 4-dioxane by *Xanthobacter* sp. YN2. Curr. Microbiol. 78, 992–1005.

Mahendra, S., Alvarez-cohen, L., 2006. Kinetics of 1,4-Dioxane Biodegradation by Monooxygenase-Expressing Bacteria. Environ. Sci. Technol. 40, 5435–5442.

Mahendra, S., Alvarez-Cohen, L., 2005. *Pseudonocardia dioxanivorans* sp. nov., a novel actinomycete that grows on 1,4-dioxane. Int. J. Syst. Evol. Microbiol. 55, 593–598. https://doi.org/10.1099/ijs.0.63085-0

Mahendra, S., Petzold, C.J., Baidoo, E.E., Keasling, J.D., Alvarez-Cohen, L., 2007. Identification of the intermediates of in vivo oxidation of 1, 4-dioxane by monooxygenase-containing bacteria. Environ. Sci. Technol. 41, 7330–7336.

Manzini, G., 2001. An analysis of the Burrows—Wheeler transform. J. ACM 48, 407–430.

Martin, K.E., Ozsvar, J., Coleman, N. V, 2014. SmoXYB1C1Z of *Mycobacterium* sp. strain NBB4: a soluble methane monooxygenase (sMMO)-like enzyme, active on C2 to C4 alkanes and alkenes. Appl. Environ. Microbiol. 80, 5801–5806.

Masuda, H., 2009. Identification and characterization of monooxygenase enzymes involved in 1, 4-dioxane degradation in *Pseudonocardia* sp. strain ENV478, *Mycobacterium* sp. strain ENV421, and *Nocardia* sp. strain ENV425.

Meinicke, J., Thüm, T., Schröter, R., Benduhn, F., Saake, G., 2014. An overview on analysis tools for software product lines. pp. 94–101.

Meinicke, P., 2015. UProC: tools for ultra-fast protein domain classification. Bioinformatics 31, 1382–1388.

Menzel, P., Ng, K.L., Krogh, A., 2016. Fast and sensitive taxonomic classification for metagenomics with Kaiju. Nat. Commun. 7, 1–9.

Merkey, B.V., 2008. Biofilm Modeling for Wastewater Treatment: Multiple Species and Multiple Components. NORTHWESTERN UNIVERSITY.

Miao, Y., Heintz, M.B., Bell, C.H., Johnson, N.W., Polasko, A.L., Favero, D., Mahendra, S., 2021. Profiling microbial community structures and functions in bioremediation strategies for treating 1, 4-dioxane-contaminated groundwater. J. Hazard. Mater. 408, 124457.

Miao, Y., Johnson, N.W., Phan, T., Heck, K., Gedalanga, P.B., Zheng, X., Adamson, D., Newell, C., Wong, M.S., Mahendra, S., 2020. Monitoring, assessment, and prediction of microbial shifts in coupled catalysis and biodegradation of 1, 4-dioxane and co-contaminants. Water Res. 173, 115540.

Murnane, R.A., Chen, W., Hyman, M., Semprini, L., 2021. Long-term cometabolic transformation of 1,1,1-trichloroethane and 1,4-dioxane by *Rhodococcus rhodochrous* ATCC 21198 grown on alcohols slowly produced by orthosilicates. J. Contam. Hydrol. 240, 103796. https://doi.org/10.1016/j.jconhyd.2021.103796

Nakatsu, C.H., Hristova, K., Hanada, S., Meng, X.-Y., Hanson, J.R., Scow, K.M., Kamagata, Y., 2006. *Methylibium petroleiphilum* gen. nov., sp. nov., a novel methyl tert-butyl ether-degrading methylotroph of the Betaproteobacteria. Int. J. Syst. Evol. Microbiol. 56, 983–989.

Nam, J.-H., Ventura, J.-R.S., Yeom, I.T., Lee, Y., Jahng, D., 2016. Structural and Kinetic Characteristics of 1,4-Dioxane-Degrading Bacterial Consortia Containing the Phylum TM7. J. Microbiol. Biotechnol. 26, 1951–1964.

Oh, S.H., Hwang, I.Y., Lee, O.K., Won, W., Lee, E.Y., 2019. Development and optimization of the biological conversion of ethane to ethanol using whole-cell methanotrophs possessing methane monooxygenase. Molecules 24, 591.

Ohkubo, N., 2009. Biodegradation of Methyl tert - Butyl Ether by *Mycobacterium* spp . 9, 113–122.

Parales, R.E., Adamus, J.E., White, N., May, H.D., 1994. Degradation of 1,4-dioxane by an actinomycete in pure culture. Appl. Environ. Microbiol. 60, 4527–4530. https://doi.org/10.1128/aem.60.12.4527-4530.1994

Parks, D.H., Chuvochina, M., Chaumeil, P.-A., Rinke, C., Mussig, A.J., Hugenholtz, P., 2020. A complete domain-to-species taxonomy for Bacteria and Archaea. Nat. Biotechnol. 38, 1079–1086.

PEST, 2019. PEST Model-Independent Parameter Estimation. User Manual Part I: PEST,

SENSAN and Global Optimisers.

Picone, N., Mohammadi, S.S., Waajen, A.C., van Alen, T.A., Jetten, M.S.M., Pol, A., Op den Camp, H.J.M., 2020. More Than a Methanotroph: A Broader Substrate Spectrum for *Methylacidiphilum fumariolicum* SolV. Front. Microbiol. 11, 1–10. https://doi.org/10.3389/fmicb.2020.604485

Ramalingam, V., Cupples, A.M., 2020. Enrichment of novel Actinomycetales and the detection of monooxygenases during aerobic 1,4-dioxane biodegradation with uncontaminated and contaminated inocula. Appl. Microbiol. Biotechnol. 104, 2255–2269. https://doi.org/10.1007/s00253-020-10376-7

Redmond, M.C., Valentine, D.L., Sessions, A.L., 2010. Identification of novel methane-, ethane-, and propane-oxidizing bacteria at marine hydrocarbon seeps by stable isotope probing. Appl. Environ. Microbiol. 76, 6412–6422. https://doi.org/10.1128/AEM.00271-10

Rittmann, B.E., 2007. The Membrane Biofilm Reactor is a Versatile Platform for Water and Wastewater Treatment. Environ. Eng. Res. 12, 157–175.

Rittmann, B.E., McCarty, P.L., 2001. Environmental Biotechnology: Principles and Applications. McGraw-Hill.

Rittmann, B.E., Tang, Y., Krajmalnik-Brown, R., Luo, Y., Wang, B., 2019. Synergistic Reductive Dechlorination of 1,1,1-Trichloroethane and Trichloroethene and Aerobic Biodegradation of 1,4-Dioxane. SERDP Project ER-2721.

Rochman, F., 2016. Aerobic hydrocarbon-degrading microbial communities in oilsands tailings ponds.

Rolston, H.M., Hyman, M.R., Semprini, L., 2019. Aerobic cometabolism of 1, 4-dioxane by isobutane-utilizing microorganisms including Rhodococcus rhodochrous strain 21198 in aquifer microcosms: Experimental and modeling study. Sci. Total Environ. 694, 133688.

Sales, C.M., Grostern, A., Parales, J. V., Parales, R.E., Alvarez-Cohen, L., 2013. Oxidation of the cyclic ethers 1,4-dioxane and tetrahydrofuran by a monooxygenase in two Pseudonocardia species. Appl. Environ. Microbiol. 79, 7702–7708. https://doi.org/10.1128/AEM.02418-13

Sander, R., 2015. Compilation of Henry's law constants (version 4.0) for water as solvent. Atmos. Chem. Phys. 15, 4399–4981. https://doi.org/10.5194/acp-15-4399-2015

Scheutz, C., Durant, N.D., Hansen, M.H., Bjerg, P.L., 2011. Natural and enhanced anaerobic degradation of 1,1,1-trichloroethane and its degradation products in the subsurface - A critical review. Water Res. 45, 2701–2723. https://doi.org/10.1016/j.watres.2011.02.027

Sei, K., Miyagaki, K., Kakinoki, T., Fukugasako, K., Inoue, D., Ike, M., 2013. Isolation and characterization of bacterial strains that have high ability to degrade 1,4-dioxane as a sole carbon and energy source. Biodegradation 24, 665–674. https://doi.org/10.1007/s10532-012-9614-1

Shin, D., Sung, D.Y., Moon, H.S., Nam, K., 2010. Microbial succession in response to 1, 4-dioxane exposure in activated sludge reactors: effect of inoculum source and extra carbon addition. J. Environ. Sci. Heal. Part A 45, 674–681.

Stewart, P.S., 2003. Diffusion in Biofilms. J. Bacteriol. 185, 1485–1491.

https://doi.org/10.1128/JB.185.5.1485

Stickney, J.A., Sager, S.L., Clarkson, J.R., Smith, L.A., Locey, B.J., Bock, M.J., Hartung, R., Olp, S.F., 2003. An updated evaluation of the carcinogenic potential of 1, 4-dioxane. Regul. Toxicol. Pharmacol. 38, 183–195.

Strand, S.E., Bjelland, M.D., Stensel, H.D., 1990. Kinetics of chlorinated hydrocarbon degradation by suspended cultures of methane-oxidizing bacteria. Res. J. Water Pollut. Control Fed. 62, 124–129.

Suthersan, S., Quinnan, J., Horst, J., Ross, I., Kalve, E., Bell, C., Pancras, T., 2016. Making strides in the management of "emerging contaminants." Groundw. Monit. Remediat. 36, 15–25.

Szabó, Z., Gyula, P., Robotka, H., Bató, E., Gálik, B., Pach, P., Pekker, P., Papp, I., Bihari, Z., 2015. Draft genome sequence of *Methylibium* sp. strain T29, a novel fuel oxygenate-degrading bacterial isolate from Hungary. Stand. Genomic Sci. 10, 1–10.

Tang, Y., Krajmalnik-Brown, R., Rittmann, B.E., 2013a. Modeling trichloroethene reduction in a hydrogen-based biofilm. Water Sci. Technol. 68, 1158–1163. https://doi.org/10.2166/wst.2013.362

Tang, Y., Ontiveros-valencia, A., Feng, L., Zhou, C., Krajmalnik-brown, R., Rittmann, B.E., 2013b. A Biofilm Model to Understand the Onset of Sulfate Reduction in Denitrifying Membrane Biofilm Reactors. Biotechnol. Bioeng. 110, 763–772. https://doi.org/10.1002/bit.24755

Tang, Y., Ontiveros-Valencia, A., Feng, L., Zhou, C., Krajmalnik-Brown, R., Rittmann, B.E., 2013c. A biofilm model to understand the onset of sulfate reduction in denitrifying membrane biofilm reactors. Biotechnol. Bioeng. 110, 763–772. https://doi.org/10.1002/bit.24755

Tang, Y., Valocchi, A.J., 2013. An Improved Cellular Automaton Method to Model Multispecies Biofilms. Water Res. 47, 5729–5742. https://doi.org/10.1016/j.watres.2013.06.055

Tang, Y., Zhao, H., Marcus, A.K., Krajmalnik-brown, R., Rittmann, B.E., 2012a. A Steady-State Biofilm Model for Simultaneous Reduction of Nitrate and Perchlorate, Part 2: Parameter Optimization and Results and Discussion. Environ. Sci. Technol. 46, 1615.

Tang, Y., Zhao, H., Marcus, A.K., Krajmalnik-brown, R., Rittmann, B.E., 2012b. A Steady-State Biofilm Model for Simultaneous Reduction of Nitrate and Perchlorate, Part 1: Model Development and Numerical Solution. Environ. Sci. Technol. 46, 1598–1607.

Tang, Y., Zhou, C., Van Ginkel, S.W., Ontiveros-Valencia, A., Shin, J., Rittmann, B.E., 2012c. Hydrogen permeability of the hollow fibers used in H2-based membrane biofilm reactors. J. Memb. Sci. 407–408, 176–183. https://doi.org/10.1016/j.memsci.2012.03.040

Taquino, K.E., 2001. Ability of Rhodococcus rhodochrous cells grown on ethane, n-propane, n-butane, and isobutane to degrade trichloroethylene. Mississippi State University.

Tusher, T.R., Shimizu, T., Inoue, C., Chien, M.-F., 2021. Isolation and Characterization of Novel Bacteria Capable of Degrading 1, 4-Dioxane in the Presence of Diverse Co-Occurring Compounds. Microorganisms 9, 887.

US-EPA, 2018. 2018 Edition of the Drinking Water Standards and Health Advisories Tables.

USEPA, 2018. Contaminant Information Sheets (CISs) for the Final Fourth Contaminant Candidate List (CCL 4).

Wagner, G.P., Kin, K., Lynch, V.J., 2012. Measurement of mRNA abundance using RNA-seq data: RPKM measure is inconsistent among samples. Theory Biosci. 131, 281–285.

Wang, B., Krajmalnik-brown, R., Zhou, C., Luo, Y., Rittmann, B.E., Tang, Y., 2020. Modeling Trichloroethene Reduction, Methanogenesis, and Homoacetogenesis in a H2-Based Biofilm. J. Environ. Eng. 146, 1–10. https://doi.org/10.1061/(ASCE)EE.1943-7870.0001642

Wang, Q., Zhang, T., 2010. Review of mathematical models for biofilms. Solid State Commun. 150, 1009–1022. https://doi.org/10.1016/j.ssc.2010.01.021

Wanner, O., Gujer, W., 1986. A Multispecies Biofilm Model. Biotechnol. Bioeng. 28, 314–328.

Watschinger, K., Keller, M.A., Golderer, G., Hermann, M., Maglione, M., Sarg, B., Lindner, H.H., Hermetter, A., Werner-Felmayer, G., Konrat, R., 2010. Identification of the gene encoding alkylglycerol monooxygenase defines a third class of tetrahydrobiopterin-dependent enzymes. Proc. Natl. Acad. Sci. 107, 13672–13677.

Wilkinson, B., Zhu, M., Priestley, N.D., Nguyen, H.-H.T., Morimoto, H., Williams, P.G., Chan, S.I., Floss, H.G., 1996. A concerted mechanism for ethane hydroxylation by the particulate methane monooxygenase from Methylococcus capsulatus (Bath). J. Am. Chem. Soc. 118, 921–922.

Winkelmann, J., 2018. Diffusion in Gases, Liquids and Electrolytes, Journal of Chemical Information and Modeling. Springer-Verlag GmbH Germany. https://doi.org/10.1017/CBO9781107415324.004

Xiong, Y., Mason, O.U., Lowe, A., Zhang, Z., Zhou, C., Chen, G., Villalonga, M.J., Tang, Y., 2020. Investigating promising substrates for promoting 1,4-dioxane biodegradation: effects of ethane and tetrahydrofuran on microbial consortia. Biodegradation 31, 171–182. https://doi.org/10.1007/s10532-020-09901-2

Xiong, Y., Mason, O.U., Lowe, A., Zhou, C., Chen, G., Tang, Y., 2019. Microbial Community Analysis Provides Insights into the Effects of Tetrahydrofuran on 1,4-Dioxane Biodegradation. Appl. Environ. Microbiol. 85, 1–11.

Xu, F., Bell, S.G., Lednik, J., Insley, A., Rao, Z., Wong, L., 2005. The heme monooxygenase cytochrome P450cam can be engineered to oxidize ethane to ethanol. Angew. Chemie 117, 4097–4100.

Yamamoto, N., Saito, Y., Inoue, D., Sei, K., Ike, M., 2018. Characterization of newly isolated *Pseudonocardia* sp. N23 with high 1,4-dioxane-degrading ability. J. Biosci. Bioeng. 125, 552–558. https://doi.org/10.1016/j.jbiosc.2017.12.005

Yanık-Yıldırım, K.C., Vardar-Schara, G., 2014. Saturation mutagenesis of *Bradyrhizobium* sp. BTAi1 toluene 4-monooxygenase at alpha-subunit residues proline 101, proline 103, and histidine 214 for regiospecific oxidation of aromatics. Appl. Microbiol. Biotechnol. 98, 8975–8986. https://doi.org/10.1007/s00253-014-5913-2

Yu, H., Kashima, H., Regan, J.M., Hussain, A., Elbeshbishy, E., Lee, H.S., 2017. Kinetic study on anaerobic oxidation of methane coupled to denitrification. Enzyme Microb. Technol. 104, 47–55. https://doi.org/10.1016/j.enzmictec.2017.05.005

Zhang, S., Gedalanga, P.B., Mahendra, S., 2017. Advances in bioremediation of 1,4-dioxane-contaminated waters. J. Environ. Manage. 204, 765–774. https://doi.org/10.1016/j.jenvman.2017.05.033

Zou, B., Huang, Y., Zhang, P.-P., Ding, X.-M., Op den Camp, H.J.M., Quan, Z.-X., 2021. Horizontal gene transfer of copper-containing membrane-bound monooxygenase (CuMMO) and di-iron soluble monooxygenase (SDIMO) in ethane-and propane-oxidizing Rhodococcus. Appl. Environ. Microbiol. AEM-00227.

Appendices

A. Supporting Data

Table A 1: Parameters used in the kinetics modeling

Parameter	Description
	I. Constants
K_H	Dimensionless Henry's law constant for ethane or oxygen
K_{He}	Dimensionless Henry's law constant for ethane (4.71×10^{-2})
K_{Ho}	Dimensionless Henry's law constant for oxygen (3.22×10^{-2})
ρ	Density of ethane (1219 mg/L) or oxygen (1291 mg/L) at 25 °C and 1 atm pressure
	II. Parameters obtained from experiments
M_{eT}	Total mass of ethane in the serum bottle (mg_{COD})
M_{oT}	Total mass of oxygen in the serum bottle (mg_{COD})
M_T	Total mass of ethane or oxygen (mg)
n	Number of measurements for each chemical or type of biomass
N	Total number of measurements made in the experiment
S_d	Concentrations of 1,4-dioxane (mg_{COD} L^{-1})
$S_{d,i}^{e}$	1,4-Dioxane concentrations in the experiment (mg_{COD} L^{-1})
$S_{d,i}^{m}$	1,4-Dioxane concentrations in the model (mg_{COD} L^{-1})
$S_{e,i}^{e}$	Ethane concentration in the experiment (mg_{COD} L^{-1})
$S_{e,i}^{m}$	Ethane concentration in the model (mg_{COD} L^{-1})
S_{eL}	Concentration of ethane in the liquid sample (mg_{COD} L^{-1})
S_G	Concentration of ethane or oxygen in the headspace (mg/L)
S_L	Concentration of ethane or oxygen in the liquid samples (mg/L)
$S_{o,i}^{e}$	Oxygen concentrations in the experiment (mg_{COD} L^{-1})
$S_{o,i}^{m}$	Oxygen concentrations in the model (mg_{COD} L^{-1})
S_{oL}	Concentration of oxygen in the liquid sample (mg_{COD} L^{-1})
t	Time (d)
V_G	Volume of the headspace (L)
V_L	Volume of the liquid sample (L)
V_s	Volume of the gas supplied (L)
X	Concentration of biomass (mg_{COD} L^{-1})
X_0	Initial biomass concentration (mg_{COD} L^{-1})
X_i^e	Biomass concentrations in the experiment (mg_{COD} L^{-1})

Parameter	Description
X_i^m	Biomass concentrations in the model (mg_{COD} L^{-1})
	III. Unknown parameters obtained from model simulation
b_c	Biomass decay coefficient for EDCOB (d^{-1})
b_d	Biomass decay coefficient for DOB (d^{-1})
b_e	Biomass decay coefficient for EOB (d^{-1})
b_n	Biomass decay coefficient for NGB (d^{-1})
f_b	Initial percentage of inert biomass
f_c	Initial percentage of EDCOB
f_d	Initial percentage of DOB
f_e	Initial percentage of EOB
f_n	Initial percentage of NGB
K_d	Half-maximum-rate concentration of 1,4-dioxane oxidation by DOB (mg_{COD} L^{-1})
K_{dc}	Half-maximum-rate concentration of 1,4-dioxane oxidation by EDCOB (mg_{COD} L^{-1})
K_e	Half-maximum-rate concentration of ethane oxidation by EOB (mg_{COD} L^{-1})
K_{ec}	Half-maximum-rate concentration of ethane oxidation by EDCOB (mg_{COD} L^{-1})
K_{id}	Inhibition coefficient of 1,4-dioxane on ethane (mg_{COD} L^{-1})
K_{ie}	Inhibition coefficient of ethane on 1,4-dioxane (mg_{COD} L^{-1})
K_o	Half-maximum-rate concentration of O_2 (mg_{COD} L^{-1})
p_c	Endogenous respiration rate for EDCOB (d^{-1})
p_d	Endogenous respiration rate for DOB (d^{-1})
p_e	Endogenous respiration rate for EOB (d^{-1})
p_n	Endogenous respiration rate for NGB (d^{-1})
q_d	Maximum specific 1,4-dioxane utilization rate of DOB (mg_{COD} mg_{COD}^{-1} d^{-1})
q_{dc}	Maximum specific 1,4-dioxane utilization rate of EDCOB (mg_{COD} mg_{COD}^{-1} d^{-1})
q_e	Maximum specific ethane utilization rate of EOB (mg_{COD} mg_{COD}^{-1} d^{-1})
q_{ec}	Maximum specific ethane utilization rate of EDCOB (mg_{COD} mg_{COD}^{-1} d^{-1})
X_b	Concentration of inert biomass (mg_{COD} L^{-1})
X_c	Concentration of EDCOB (mg_{COD} L^{-1})
X_d	Concentration of DOB (mg_{COD} L^{-1})
X_e	Concentration of EOB (mg_{COD} L^{-1})
X_n	Concentration of NGB (mg_{COD} L^{-1})
Y_d	Biomass yield of 1,4-dioxane (mg_{COD} mg_{COD}^{-1})
Y_e	Biomass yield of ethane (mg_{COD} mg_{COD}^{-1})

Table A 2: Model inputs used in the O_2-based MBfR modeling

Symbol	*Description*	*Value*	*Unit*	*References*
k_1	Coefficient of electrons used for biomass production	0.77	-	(Merkey, 2008; Rittmann et al., 2019; Rittmann and McCarty, 2001; Tang et al., 2013b, 2012b)
k_2	Coefficient for electrons going to UAP	0.05	-	
k_3	Coefficient for electrons going to EPS	0.18	-	
Y_1	Yield of ethane oxidation for cell synthesis	0.50	*mg-COD/ mg-COD*	Kinetics experiment
Y_2	Yield of 1,4-dioxane oxidation for cell synthesis	0.39	*mg-COD/ mg-COD*	Kinetics experiment
Y_3	Yield of UAP oxidation for cell synthesis	0.60	*mg-COD/ mg-COD*	(Rittmann and McCarty, 2001; Tang et al., 2012b)
Y_4	Yield of BAP oxidation for cell synthesis	0.60	*mg-COD/ mg-COD*	
p_1	Endogenous respiration of EOB	0.009	d^{-1}	Kinetics experiment
p_2	Endogenous respiration of DOB	0.012	d^{-1}	Kinetics experiment
p_3	Endogenous respiration of EDCOB	0.007	d^{-1}	Kinetics experiment
p_5	Endogenous respiration of SMPOB	0.05	d^{-1}	(Wanner and Gujer, 1986)
b_1	Decay coefficient for EOB	0.04	d^{-1}	Kinetics experiment
b_2	Decay coefficient for DOB	0.05	d^{-1}	Kinetics experiment
b_3	Decay coefficient for EDCOB	0.04	d^{-1}	Kinetics experiment
b_5	Decay coefficient for SMPOB	0.10	d^{-1}	(Rittmann and McCarty, 2001; Wanner and Gujer, 1986)
k_{hyd}	Hydrolysis rate of EPS	0.22	d^{-1}	(Rittmann et al., 2019; Rittmann and McCarty, 2001; Tang et al., 2013b, 2012b)
k_d	Biofilm detachment coefficient	36	$cm^{-1}\ d^{-1}$	(Rittmann et al., 2019; Tang et al., 2012b)
X_f	Biomass density	79	$mg\text{-}COD/cm^3$	(Rittmann et al., 2019; Tang et al., 2012b)
f_{bd}	Fraction of biomass that is Biodegradable	0.8	-	(Merkey, 2008; Rittmann et al., 2019; Rittmann

Symbol	*Description*	*Value*	*Unit*	*References*
				and McCarty, 2001; Tang et al., 2012b)
$\hat{q}_1$	Maximum specific ethane utilization rate of EOB	1.39	$\frac{mg\ COD}{mg\ COD \times d}$	Kinetics experiment
$\hat{q}_4$	Maximum specific 1,4-dioxane utilization rate of DOB	2.00	$\frac{mg\ COD}{mg\ COD \times d}$	Kinetics experiment
$\hat{q}_7$	Maximum specific ethane utilization rate of EDCOB	1.39	$\frac{mg\ COD}{mg\ COD \times d}$	Kinetics experiment
$\hat{q}_8$	Maximum specific 1,4-dioxane utilization rate of EDCOB	2.14	$\frac{mg\ COD}{mg\ COD \times d}$	Kinetics experiment
$\hat{q}_{12}$	Maximum specific UAP utilization rate of SMPOB	1.27	$\frac{mg\ COD}{mg\ COD \times d}$	(Laspidou and Rittmann, 2002; Rittmann and McCarty, 2001)
$\hat{q}_{13}$	Maximum specific BAP utilization rate of SMPOB	0.07	$\frac{mg\ COD}{mg\ COD \times d}$	
k_{11}	Half-maximum-rate concentration of O_2 for ethane oxidation by EOB	1.39×10^{-3}	*mg-COD/cm³*	Kinetics experiment
k_{12}	Half-maximum-rate concentration of O_2 for endogenous respiration of EOB	1.39×10^{-3}	*mg-COD/cm³*	Kinetics experiment
k_{21}	Half-maximum-rate concentration of ethane oxidation by EOB	1.48×10^{-3}	*mg-COD/cm³*	Kinetics experiment
k_{14}	Half-maximum-rate concentration of O_2 for 1,4-dioxane oxidation by DOB	1.39×10^{-3}	*mg-COD/cm³*	Kinetics experiment
k_{15}	Half-maximum-rate concentration of O_2 for endogenous respiration of DOB	1.39×10^{-3}	*mg-COD/cm³*	Kinetics experiment
k_{34}	Half-maximum-rate concentration of 1,4-dioxane oxidation by DOB	2.50×10^{-2}	*mg-COD/cm³*	Kinetics experiment
k_{17}	Half-maximum-rate concentration of O_2 for ethane oxidation by EDCOB	1.39×10^{-3}	*mg-COD/cm³*	Kinetics experiment
k_{18}	Half-maximum-rate concentration of O_2 for 1,4-dioxane oxidation EDCOB	1.39×10^{-3}	*mg-COD/cm³*	Kinetics experiment
k_{19}	Half-maximum-rate concentration of O_2 for endogenous respiration of EDCOB	1.39×10^{-3}	*mg-COD/cm³*	Kinetics experiment
k_{27}	Half-maximum-rate concentration of ethane oxidation by EDCOB	1.45×10^{-3}	*mg-COD/cm³*	Kinetics experiment
k_{38}	Half-maximum-rate concentration of 1,4-dioxane oxidation by EDCOB	2.49×10^{-2}	*mg-COD/cm³*	Kinetics experiment
k_{28i}	Inhibition coefficient of ethane on 1,4-dioxane oxidation by EDCOB	3.21×10^{-3}	*mg-COD/cm³*	Kinetics experiment

Symbol	*Description*	*Value*	*Unit*	*References*
k_{37i}	Inhibition coefficient of 1,4-dioxane on ethane oxidation by EDCOB	2.10×10^{-2}	*mg-COD/cm³*	Kinetics experiment
$k_{1\text{-}12}$	Half-maximum-rate concentration of O_2 for UAP oxidation by SMPOB	1.39×10^{-3}	*mg-COD/cm³*	Kinetics experiment
$k_{1\text{-}13}$	Half-maximum-rate concentration of O_2 for BAP oxidation by SMPOB	1.39×10^{-3}	*mg-COD/cm³*	Kinetics experiment
$k_{1\text{-}14}$	Half-maximum-rate concentration of O_2 for endogenous respiration of SMPOB	1.39×10^{-3}	*mg-COD/cm³*	Kinetics experiment
$k_{4\text{-}12}$	Half-maximum-rate concentration of UAP oxidation by SMPOB	5.0×10^{-3}	*mg-COD/cm³*	(Tang et al., 2013b, 2012b; Wanner and Gujer, 1986)
$k_{5\text{-}13}$	Half-maximum-rate concentration of BAP oxidation by SMPOB	5.0×10^{-3}	*mg-COD/cm³*	
D_1	Diffusion coefficient of O_2 in the diffusion layer	1.81	*cm²/d*	(Cussler, 2009; Han and Bartels, 1996; Stewart, 2003)
D_2	Diffusion coefficient of ethane in the diffusion layer	1.04	*cm²/d*	(Cussler, 2009; Stewart, 2003)
D_3	Diffusion coefficient of 1,4-dioxane in the diffusion layer	0.95	*cm²/d*	(Leaist et al., 2000; Winkelmann, 2018)
D_4	Diffusion coefficient of UAP in the diffusion layer	1.00	*cm²/d*	(Tang et al., 2013b, 2012b)
D_5	Diffusion coefficient of BAP in the diffusion layer	0.60	*cm²/d*	
D_{f1}	Diffusion coefficient of O_2 in the biofilm	1.09	*cm²/d*	(Stewart, 2003)
D_{f2}	Diffusion coefficient of ethane in the biofilm	0.62	*cm²/d*	(Stewart, 2003)
D_{f3}	Diffusion coefficient of 1,4-dioxane in the biofilm	0.29	*cm²/d*	(Leaist et al., 2000; Stewart, 2003; Winkelmann, 2018)
D_{f4}	Diffusion coefficient of UAP in the biofilm	0.80	*cm²/d*	(Tang et al., 2013b, 2012b)
D_{f5}	Diffusion coefficient of BAP in the biofilm	0.50	*cm²/d*	
D_m	Diffusion coefficient of O_2 in the membrane	$5.75\ x\ 10^{-3}$	*cm²/d*	(Ahmed et al., 2004; Tang et al., 2012c) [1]

[1] $D_m = \frac{K_m \rho_O R T (D_O - L_m)}{M_O d_m} = \frac{1\times10^{-9}\frac{cm^3 cm}{cm^2 - s - cm\ Hg}\times\frac{1\ cm\ Hg}{1334.16\ pa}\times1428\ {}^{g}/_{m^3}\times8.314\ \frac{J}{K\ mol}\times298\ K\ (280-55)\ \mu m}{32\ {}^{g}/_{mol}\times280\ \mu m}\times\frac{24\times3600\ s}{d}$

$= 5.75 \times 10^{-3}\ {}^{cm^2}/_{d}$

Symbol	*Description*	*Value*	*Unit*	*References*
K_H	Dimensionless Henry's law constant for O_2	0.0322	-	(Sander, 2015)
L_d	Thickness of effective diffusion layer	0.01	*cm*	(Rittmann et al., 2019; Tang et al., 2012b)
L_m	Thickness of membrane	0.0055	*cm*	MBfR experiment
A	Total membrane surface area	146.37	cm^2	MBfR experiment [2]
V	Volume of MBfR	70	cm^3	MBfR experiment
Q	Flow rate	210, 420	cm^3/d	MBfR experiment [3]
S_{1g}	O_2 concentration in the bulk gas	0.267	*mg-COD/cm³*	MBfR experiment [4]
S_{1i}	O_2 concentration in the influent	0	*mg-COD/cm³*	MBfR experiment
S_2	Ethane concentration in the influent	0 to 0.1344	*mg-COD/cm³*	MBfR experiment [5]
S_3	1,4-Dioxane concentration in the influent	1.818, 18.18, 181.818	*x 10⁻⁵ mg-COD/cm³*	MBfR experiment [6]

[2] *Fiber length, L = 26 cm, outer diameter, D_o = 280 μm, and number of fibers, n = 64. Total membrane surface area,* $A = \pi\, D_o\, L\, n = \ 0.028\pi \times 26 \times 64 = 146.37\ cm^2$

[3] *Experiment set for hydraulic retention times (HRT) of 4 and 8 hours.* $Q = \frac{V}{HRT} \times 24\ cm^3/d$

[4] *O_2 concentration in the bulk gas is calculated from the pressure of O_2 in the membrane based on the ideal gas law.*

$$S_{1g} = \frac{P}{RT} = \frac{3\ Psig \times 6894.76 {}^{Pa}/_{Psig} \times (4\times8)\ {}^{g\ COD}/_{mol} \times 1000\ {}^{mg}/_{g}}{8.314\ {}^{J}/_{K\ mol} \times 298\ K \times 10^6\ {}^{cm^3}/_{m^3}} = 0.267\ \frac{mg\ COD}{cm^3}$$

[5] *Experiment set for ethane influent rates of 0 to 36,000 μg/l.* $1\ \frac{\mu g\ ethane}{l} = \frac{14\times8\ mg\ COD}{30\ mg\ ethane} \times \frac{1\ mg}{1000\ \mu g} \times \frac{1\ l}{1000\ cm^3}$

[6] *Experiment set for 1,4-Dioxane influent rates of 10, 100, and 1000 μg/l.*

$$1\ \frac{\mu g\ dioxane}{l} = \frac{20\times8\ mg\ COD}{88\ mg\ dioxane} \times \frac{1\ mg}{1000\ \mu g} \times \frac{1\ l}{1000\ cm^3}$$

Table A 3: Model outputs of the O_2-based MBfR modeling

Symbol	*Description*	*Unit*
S_{f1}	O_2 concentration in the biofilm	*mg-COD/cm³*
S_{f2}	Ethane concentration in the biofilm	*mg-COD/cm³*
S_{f3}	1,4-Dioxane concentration in the biofilm	*mg-COD/cm³*
S_{f4}	UAP concentration in the biofilm	*mg-COD/cm³*
S_{f5}	BAP concentration in the biofilm	*mg-COD/cm³*
f_1	Fraction of EOB	-
f_2	Fraction of DOB	-
f_3	Fraction of EDCOB	-
f_4	Fraction of EPS	-
f_5	Fraction of SMPOB	-
S_{b1}	O_2 Concentration in the bulk liquid (effluent)	*mg-COD/cm³*
S_{b2}	Ethane Concentration in the bulk liquid (effluent)	*mg-COD/cm³*
S_{b3}	1,4-Dioxane Concentration in the bulk liquid (effluent)	*mg-COD/cm³*
S_{b4}	UAP Concentration in the bulk liquid (effluent)	*mg-COD/cm³*
S_{b5}	BAP Concentration in the bulk liquid (effluent)	*mg-COD/cm³*
J_{1m}	O_2 flux out across the membrane	*mg-COD/(cm²d)*
J_1	O_2 flux in to or out of the biofilm	*mg-COD/(cm²d)*
J_2	Ethane flux in to or out of the biofilm	*mg-COD/(cm²d)*
J_3	1,4-Dioxane flux in to or out of the biofilm	*mg-COD/(cm²d)*
J_4	UAP flux out of the biofilm	*mg-COD/(cm²d)*
J_5	BAP flux out of the biofilm	*mg-COD/(cm²d)*
L_f	Thickness of biofilm	*cm*
L	Distance from the attachment surface to position z in the biofilm	*cm*
U_L	Moving speed of the biofilm at position z	*cm/d*
μ_1	The growth rate of EOB	d^{-1}
μ_2	The growth rate of DOB	d^{-1}
μ_3	The growth rate of EDCOB	d^{-1}
μ_4	The growth rate of EPS	d^{-1}
μ_5	The growth rate of SMPOB	d^{-1}
μ_6	The growth rate of IB	d^{-1}
$\bar{\mu}$	Average growth rate of all solid biomass species in the biofilm	d^{-1}
t	Time	*d*

Symbol	*Description*	*Unit*
dt	Time step	d
R_i	Reaction rate of chemical species i	$mg\text{-}COD/(cm^3\ d)$
$C_{R\text{-}pr}$	Conversion rate in process pr	$mg\text{-}COD/(cm^3\ d)$
z	Biofilm depth	cm
z_m	Membrane thickness	cm
η_{ip}	Coefficient of chemical species i in process p	-
η_{jp}	Coefficient of biomass species j in process p	-

Table A 4: Shallow metagenomic sample information before and after quality control

Reactor	Sample	Before QC				After QC	
		sequence	base	Q20(%)	Q30(%)	sequence	base
Bottle	**Ethane**	2424485	732194470	97.33	91.85	2128751	599793215
MBfR1	**Enrichment**	2702925	816283350	97.47	92.41	2383131	677634665
	Start-up	2485407	750592914	97.34	92.09	2169596	614795814
	I	2794288	843874976	97.36	92.13	2430632	689886073
	II	3743196	1130445192	98.19	94.43	3148629	937121242
	III	4527480	1367298960	98.11	94.22	3845758	1143767531
	IV	3315945	1001415390	98.18	94.37	2887392	859141607
MBfR2	**Enrichment**	3811315	1151017130	97.56	92.60	3398421	969895767
	Start-up	3332427	1006392954	97.55	92.58	2973354	848828448
	I	2108664	636816528	97.26	91.84	1813804	512100387
	II	3656280	1104196560	98.23	94.45	3108983	926762099
	III	2554808	771552016	97.84	93.57	2344729	694891142
	IV	3380942	1021044484	98.19	94.41	3039469	904728174